https://doi.org/10.5194/egusphere-2023-1458
Preprint. Discussion started: 3 August 2023

What Drives Plate Motion?

Yongfeng Yang

Bureau of Water Resources of Shandong Province, No. 127, Lishan Road, Jinan, China

Correspondence to: Yongfeng Yang (roufeng_yang@outlook.com)

Abstract. Plate motion is a remarkable Earth process that is widely ascribed to two primary driving forces: ridge push and slab pull. With the release of the first- and second-order stress fields in 1989, it was found that the observed stresses are mainly distributed on the uppermost brittle part of the lithosphere. A modeling analysis, however, reveals that the stress produced by ridge push is mainly distributed in the lower part of the lithosphere. Doglioni and Panza recently showed that slab pull was inconsistent with the geometry and kinematics of plate. These findings suggest that other force is possibly responsible for plate motion and the observed stress. Here, we propose that the pressure of deep ocean water against the continental wall exerts enormous force (i.e., ocean-generated force) on the continent. The continent is fixed on top of the lithosphere, this attachment allows the ocean-generated force to laterally transfer to the lithospheric plate. We show that this force may combine the ridge push, collisional, and shearing forces to form force balances for the lithospheric plate; the calculated movements for the South American, African, North American, Eurasian, Australian, and Pacific plates are well consistent with the observed movements in both speed and azimuth, the RMS of the calculated speed against the observed speed for these plates is 0.91, 3.76, 2.77, 2.31, 7.43, and 1.95 mm/yr, respectively.

1 Introduction

One of the most significant achievements in the 20th century was the establishment of plate tectonics, which developed from the previous concept of continental drift (Wegener, 1915 and 1924). Plate tectonics mainly describes the motion of a dozen different-sized plates that connect with each other to form a giant "jigsaw puzzle" over the Earth's surface. The evidence supporting this motion includes shape fitting of the African and American continents, a coal belt crossing from North America to Eurasia, identical directions of ice sheet movement in southern Africa and India, and Global Positioning System (GPS) speed measurements. In addition, paleomagnetic reversals in oceans (Hess, 1962; Vine and Matthews, 1963) reflect seafloor spreading, and studies of the Hawaii-Emperor seamount chain have shown that the chain is actually a trace of the lithosphere rapidly moving over relatively motionless hotspots (Wilson, 1963; Raymond et al., 2000), which further confirms the Earth's surface motion. During the past 50 years, the understanding of plate motion has expanded greatly. Plates were found to have been periodically dispersed and aggregated in the Mesozoic period, accompanied by 5-6 significant astronomical events (Cande and Kent, 1992; Cande et al., 1989; Ma et al., 1996; Wan, 1993; Hibsch et al., 1995). The speed and direction of plate

https://doi.org/10.5194/egusphere-2023-1458
Preprint. Discussion started: 3 August 2023

motion supported by paleomagnetism and deformation in the intraplate regions exhibited various styles over geological time (Wan, 2018). Global measurements of tectonic stresses reveal a strong correlation with plate motion, and the observed stresses may be used to constrain the forces that act on the plates (Zoback et al., 1989; Zoback, 1992; Bott and Kusznir, 1984; Zoback& Magee, 1991; Richards, 1992; Sperner et al., 2003; Heidbach et al., 2016; Heidbach et al., 2007; Heidbach et al., 2010; Heidbach et al., 2018).

Exploring the plate driving forces is important because it provides the first insights into the processes that yield plate tectonics. Throughout the history of plate tectonics, a large number of forces have been postulated to account for plate motion. Forces include centrifugal and tidal forces, ridge push, slab pull, basal drag, slab suction, mantle plume, geoid deformation, and the Coriolis force (Wegener, 1915; Hales, 1936; Holmes, 1931; Pekeris, 1935; Runcorn, 1962a,b; Wilson, 1963; McKenzie, 1968; McKenzie, 1969; Morgan, 1971; Morgan, 1972; Turcotte and Oxburgh, 1972; Forsyth & Uyeda, 1975; Oxburgh and Turcotte, 1978; Spence, 1987; White & McKenzie, 1989; Richards, 1992; Vigny et al., 1992; Bott, 1993; Tanimoto& Lay, 2000; Conrad & Lithgow-Bertelloni, 2002; Turcotte and Schubert, 2014). Slab pull is derived from a cold and dense sinking plate that uses its weight to pull the remaining plate to which it is attached. Ridge push is usually treated either as a boundary force or a body force. As a boundary force, ridge push is derived from a "gravity wedging" effect of a warm, buoyant mantle upwelling beneath the ridge crest and acts at the edge of the lithospheric plate. In contrast, as a body force, ridge push is derived from the horizontal pressure gradient of the cooling and thickening of the oceanic lithosphere and acts over the area of the oceanic portion of a given plate. As these two forces act on the edges of plates, they are often termed boundary forces. Basal drag (i.e., basal shear traction) is thought to be caused by the viscous moving asthenosphere along the bottom of the lithosphere, the moving asthenosphere originates from the mantle convection. Mantle plume represents the rising hot mantle flow that originates from the core-mantle boundary (Morgan, 1971; Morgan, 1972; Wilson, 1963).

Early studies on deformation modeling and torque balance analysis tended to agree that ridge push and slab pull are important for plate motion, whereas basal drag provides resistance instead of a driving force (Forsyth & Uyeda, 1975; Solomon et al., 1975; Chapple and Tullis, 1977; Richardson et al., 1979; Wortel and Cloetingh, 1981; Cloetingh and Wortel, 1986; Richardson and Cox, 1984; Richardson and Reding, 1991; Stefanick and Jurdy, 1992). Subsequent studies with complicated physical models yielded an improved understanding: buoyancy anomalies within the lithosphere, crust, and mantle act as the principal drivers, whereas viscous dissipation within the lithosphere and at its base and shear along thrust faults at collision zones resist plate motion (Conrad and Hager, 1999;Conrad and Lithgow-Bertelloni, 2002; Stadler et al., 2010; Lithgow-Bertelloni and Richards, 1995; Becker and O'Connell, 2001; Zhong, 2001; Bird et al., 2008; Becker and Faccenna, 2011; Ghosh et al., 2013; Coltice et al., 2017). That is, in addition to slab pull and ridge push, the lithosphere and mantle feed plate move in some way. For example, the lithosphere's density variation forms a lateral pressure gradient by which plate motion is driven. The sinking slab inserts into the deeper mantle, while the hot mantle flows (i.e., plumes) originating from the core-mantle boundary rise up to the top of the asthenosphere; this process of upwelling and downwelling causes the large-scale circulation of the plate and mantle (i.e., whole mantle convection). A more detailed description of whole mantle convection is discussed in previous

https://doi.org/10.5194/egusphere-2023-1458
Preprint. Discussion started: 3 August 2023

studies (Coltice et al., 2017; Bercovici et al., 2015). On the whole, the research from the past 40 years tends to agree that slab pull and ridge push are the primary plate driving forces, whereas the question of whether mantle plumes act as a driving force remains controversial.

2 What is the problem of the primary driving forces?

2.1 Slab pull

Slab pull is considered as a "negative" buoyancy to drive the oceanic plate (e.g., Conrad & Lithgow-Bertelloni, 2003). However, since this force was proposed, its validity remains debated. Doglioni and Panza (2015) recently carried out an in-depth investigation on slab pull, and some of their findings include the following:

1) As demonstrated by Cruciani et al. (2005), the slab dip is unrelated to the age of the oceanic lithosphere; consequently, the negative buoyancy that increases with age and is determined by the cooling oceanic lithosphere cannot control the slab dip.

2) It is assumed that eclogitization within a slab would increase the density of the lithosphere. Nevertheless, eclogitization is mostly distributed in the oceanic crust at depths of 6~8 km, and this transformation does not occur in the remaining lithospheric mantle at depths of 60~80 km. It is possible that a small part of the slab density can increase, but the majority of the slab density does not change.

3) It is often asked why the lithosphere would subduct. This issue arises when an oceanic hydrated and serpentinized lithosphere is involved (Ulmer & Trommsdorff, 1995). Without being metamorphosed by the subduction process, the oceanic lithosphere would not be denser than the surrounding rocks. As pointed out by Panza et al. (2007), serpentinized LID often occurs along transform faults and ridges; therefore, it is lighter than the asthenospheric mantle and elicits the question of how the plates can be pulled.

4) Most of the slabs are affected by down dip compression, and this influence is limited to depths below 300 km (Isacks& Molnar, 1971). Frepoli et al. (1996) showed that most slabs may appear at shallower depths; this situation requires a slab to be forced to sink rather than to naturally sink.

5) Although there is no slab for continental plates, these plates still move, for example, as shown in the movements of North America, South America, and Africa (Gripp & Gordon, 2002). Trench suction is widely used to account for these movements, but the mantle beneath both South and North America is moving eastward (Russo & Silver, 1994; Bokelmann, 2002). This trend is objective to the kinematics required by the trench suction model.

6) In the hotspot reference frame, the plate velocities seem to be inversely proportional to the low velocity zone's viscosity and not related to both the age of the downgoing lithosphere and the length of the subduction zones. For example, the Pacific Plate is the fastest moving plate, but the viscosity of the asthenosphere beneath this plate is rather low (Pollitz et al., 1998; Gripp & Gordon, 2002).

https://doi.org/10.5194/egusphere-2023-1458
Preprint. Discussion started: 3 August 2023

7) The vertical velocity of plates (subduction-related uplift or subsidence along plate boundaries) is far slower than the horizontal velocity (Kreemer et al., 2002); this situation implies that the vertical motions of plates are rather passive. Additionally, a kinematics analysis reveals that the subduction rate appears to be controlled by horizontal plate motion. For instance, along E- (or NE-) directed slabs, the convergence rate is faster than the subduction rate; therefore, the subduction cannot be the energetic source of plate motion.

8) When the plate motion relative to the underlying mantle is addressed, the slab might move out of the mantle and sink just because there is a faster upper plate overriding it (El Gabryet al., 2013).

9) The strength of the oceanic lithosphere is low (e.g., approximately 8×10^{12} N m^{-1}) (Liu et al., 2004), which means that the oceanic lithosphere is able to resist a force that is smaller than slab pull (approximately 3.3×10^{13} N m^{-1}) (Turcotte & Schubert, 2002). If slab pull is the primary driving force for the Pacific Plate, this argument of strength above would require a stretching for the Pacific Plate before slab pull drives this plate to move.

10) Brandmayr et al. (2011) and El Gabry et al. (2013) recently investigated geodynamics in the Mediterranean region. Their findings of Vs and ρ distributions with depth suggest that the slabs are less dense than the surrounding mantle, and no evidence is found to support slab pull.

These arguments on slab pull lead to the conclusion that this force cannot drive oceanic plate (Doglioni and Panza, 2015). This conclusion is further strengthened by Faccincani et al. (2021). These authors revealed that the lithospheric mantle density structure can be affected by variations in thermal regimes and bulk composition, and their results suggest that the lithospheric mantle is not denser than the underlying asthenospheric mantle. A difference in density between the lithospheric mantle and the underlying asthenospheric mantle means that the oceanic plate, which consists of the lithospheric crust and mantle, is unlikely to sink, forming a "negative" buoyancy to drive plate motion.

2.2 Ridge push

2.2.1 Resultant stress

Tectonic stresses are caused by the forces that act on the plates (Middleton and Wilcock, 1996), and they in turn provide constraints on the plate driving forces. With the first release of the first- and second-order stress fields (Zoback et al., 1989; Zoback, 1992; Zoback & Magee, 1991), it became evident in the World Stress Map (WSM) that the maximum horizontal compressional stress S_H in North America, South America and Europe has an orientation that is predominantly subparallel to either the relative or absolute plate motions (Richardson, 1992; Müller et al., 1992; Zoback, 1992). Due to this coupling of stress orientations and plate motions, the first-order intraplate stress patterns are concluded, mainly by means of torque analysis, to be caused by the same forces that drive plate motion, especially ridge push, slab pull, collisional force, trench suction, and traction at the base of the lithosphere (Richardson, 1992; Zoback, 1992; Grünthal and Stromeyer, 1992; Gölke and Coblentz, 1996; Zoback and Zoback, 1991; Zoback and Burke, 1993; Zoback et al., 1989). Subsequent releases of the stress field (Heidbach et al., 2016; Sperner et al., 2003; Heidbach et al., 2010; Heidbach et al., 2007; Heidbach et al., 2018) and modeling

https://doi.org/10.5194/egusphere-2023-1458
Preprint. Discussion started: 3 August 2023

studies that reproduce plate tectonics (Ghosh et al., 2013; Richards, 1992; Stadler et al., 2010; Becker and O'Connell, 2001; Bird et al., 2008; Ghosh and Holt, 2012; Lithgow-Bertelloni and Guynn, 2004; Alisic et al., 2012) support this conclusion. These modeling studies examined the stress's orientation and style (i.e., compressional or extensional), but they are limited to the lithosphere's surface, i.e., the lithosphere is treated as a thin "shell" that is similar to the membrane, the related forces act at the edges of the lithospheric plates and their base to produce the stresses, the resultant stresses are projected onto the surface of the plate, and then these stresses are compared with the observed stresses in the WSM. Consequently, an examination of the consistency between the modeled stresses and the observed stresses across the entire thickness of the lithosphere is lacking. The first release of the first- and second-order stress fields (Zoback et al., 1989; Zoback, 1992; Zoback & Magee, 1991) revealed another important feature of the tectonic stresses: the observed stresses are mainly concentrated on the uppermost brittle part of the lithosphere (which is ~ 40 km in depth), except for some portions of the continent that are dominated by high topography. This vertical distribution of tectonic stresses is not included in these modeling studies (i.e., Ghosh and Holt, 2012; Lithgow-Bertelloni and Guynn, 2004). As mentioned above, ridge push is treated either as a boundary force or a body force. As a boundary force, it is derived from a "gravity wedging" effect of a warm, buoyant mantle upwelling and acts at the edge of the lithospheric plate. Turcotte and Schubert (2014) suggested that the ridge push force may be outlined in Figure 1(top) and written as $F_{RP} = F_1 - F_2 - F_3$, and $F_1 = F_5$, $F_2 = F_4$. Since each of F_3, F_4, and F_5 relates to pressure P that linearly increases with depth, we would expect that the minimal ridge push force would appear at the uppermost part of the oceanic ridge, whereas the maximal ridge push force would appear at the lowermost part.

https://doi.org/10.5194/egusphere-2023-1458
Preprint. Discussion started: 3 August 2023

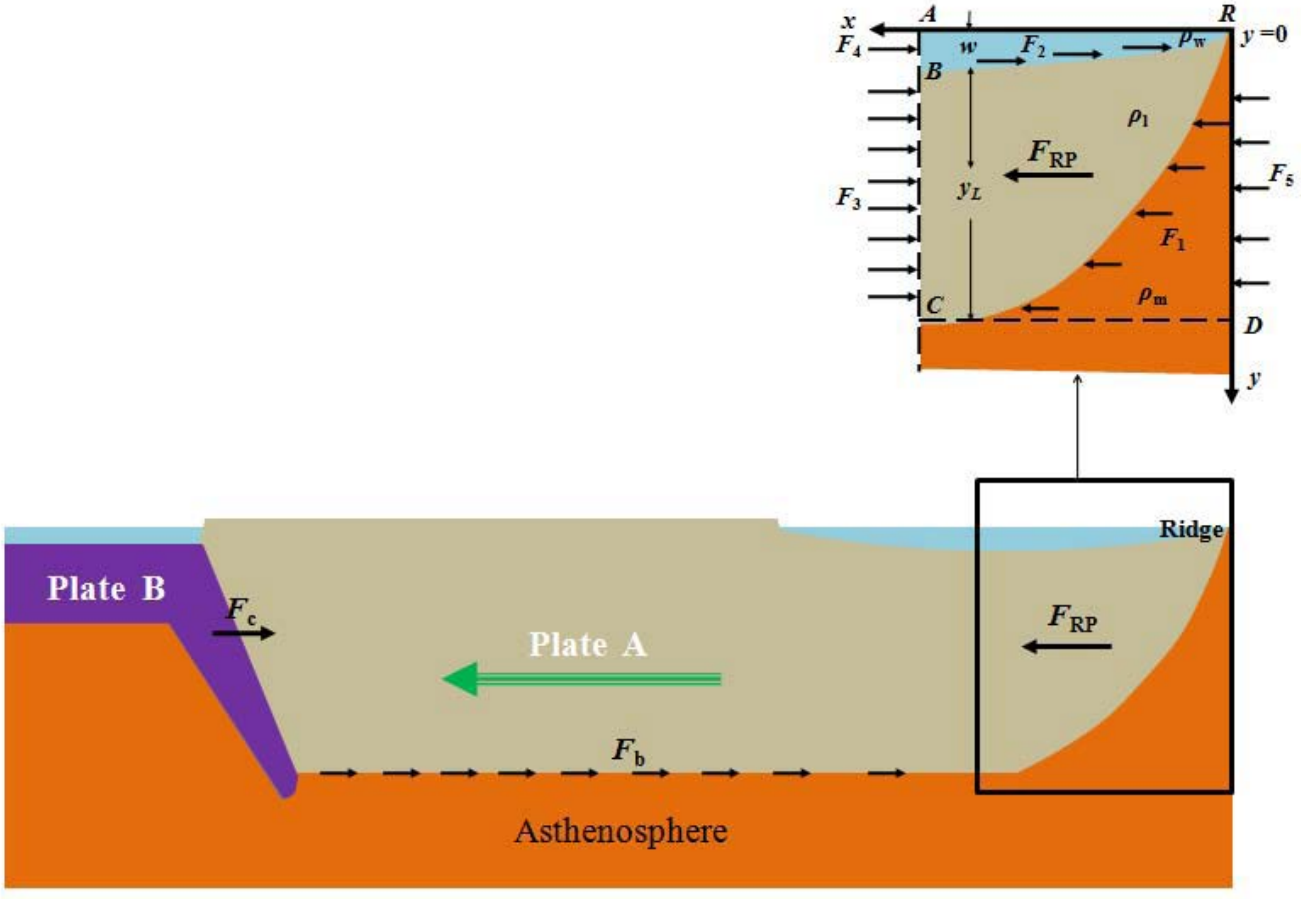

Figure 1: Modeling the distribution of ridge push force F_{RP}, basal friction force F_b, and collisional force F_c around a sample continental plate.

The distribution of ridge push, basal friction, and collisional forces around a continental plate is outlined in Figure 1, in which trench suction is neglected. These forces represent the primary driving forces. It is assumed that Plate A moves towards the left, Plate B exerts a collisional force (i.e., F_c) on its left side, the oceanic ridge exerts a push force (i.e., F_{RP}) on its right side, and the asthenosphere exerts a friction force (i.e., F_b) on its base. This force distribution requires the stress produced by these forces to be distributed mostly in the lowermost part of the plate.

We developed a simplified model to verify this expectation (Figure 2 (top)). The model is made of rocks materials and is straight, meaning that the Earth's curvature is not considered. The model is assumed to be homogeneous and isotropic, and its thickness and length are 100 km and 290 km, respectively. Along the horizontal direction, it receives a collisional force F_c, and this force is resistive and uniformly exerted on its left side; the oceanic ridge exerts a push force F_{RP} on its right side, this force is driving and increases with depth; the mantle exerts a frictional force F_b on its base, and this force is resistive. These

https://doi.org/10.5194/egusphere-2023-1458
Preprint. Discussion started: 3 August 2023

forces realize a horizontal force balance. Along the vertical direction, it is supported by the mantle, and its gravity is balanced out by the supporting from the mantle.

Finite element analysis software (i.e., Abaqus) is used to resolve the stress caused by these forces. The model's bottom is given a remote boundary condition. As the upper part of the lithospheric plate is elastic and brittle, whereas the lower part is plastic and ductile, this requires to assume that the physical property of the model is vertically transited from elasticity to plasticity. The inputs include the vertical pressure caused by the rock's weight and the lateral pressures caused by the loads (i.e., F_{RP}, F_b, and F_c). The outputs include the stress produced by the vertical pressure alone and the stress produced by a combination of the vertical and lateral pressures. The two-dimensional frame allows to know the horizontal stress (i.e., S11) and the vertical stress (i.e., S22).

However, in order to expedite the deduction, we will only discuss the horizontal stress (i.e., S11) in the following. The elastic modulus, Poisson ratio, and rock density of the model are set to 100,000 MPa, 0.3, and 2,690 kg/m^3, respectively. The pressure caused by the rock's weight yields Set I data; The F_{RP} is given as 4.0×10^{12} N m^{-1}, which is generally accepted by the scientific community (Turcotte and Schubert, 2004). It is assumed that F_b and F_c are 80% and 20% of F_{RP}, respectively. The pressures caused by these loads yield Set II data; To test the stress variation when the resistive forces are moderately adjusted, we again assume F_b and F_c to be 50% and 50% of F_{RP}. The pressures caused by these revised loads yield Set III data.

To gain a more accurate understanding of the resultant stress, we cut a rectangular area *GHIJ* to specifically discuss. The stress clouds of this area are compared in Figure 2 (left). Please note that any of these loads (i.e., F_{RP}, F_b, and F_c) is too small relative to the rock's weight. For example, when F_{RP} =4.0×10^{12} N m^{-1} is applied to the model's right side (which is 85 km length), its resultant mean pressure is 47.06 MPa, while the mean lithostatic pressure of the model (which is 100 km depth) is 1318.1 MPa. This reality means that, if we use a stress cloud to compare the stress caused by a combination of the rock's weight and the loads with the stress caused by the rock's weight alone, both of them may be indistinguishable. To create a visual impression, we magnify these loads 50 times, which yields Set II' data and Set III' data (see Figure 2(right)). We find that the horizontal stress caused by these loads is compressional and mainly concentrated on the lower part of section *GHIJ*.

We use three sections (i.e., M_1N_1, M_2N_2, and M_3N_3) from that rectangular area to quantify the comparison. Each section keeps a span of 50 km relative to one another. The stress diagrams for three sections are compared in Figure 3. When we subtract the stress caused by the rock's weight from the stress caused by the rock's weight and these loads, we obtain the stress caused by the loads, which is exhibited in Set II (III) - Set I. These stress diagrams agree the result exhibited in the stress clouds.

Kusznir and Bott (1977) argued that, due to the ductile nature of the lower part of the lithosphere, there would be a redistribution of any stress applied to the whole lithosphere that would result in stress amplification in the upper brittle part of the lithosphere. This view is based on the assumption that force is uniformly exerted on the side of the lithospheric plate, but the reality is that the ridge push force would increase with depth; consequently, the redistribution of the stress and its amplification are not applicable to the ridge push force. In contrast, we have considered this ductile nature in the modeling, but no evidence was

https://doi.org/10.5194/egusphere-2023-1458
Preprint. Discussion started: 3 August 2023

found for stress amplification in the upper part of section *GHIJ*. Our modeling analysis suggests that the stress caused by a combination of the ridge push, collisional, and basal friction forces, cannot be in accordance with the observed stress.

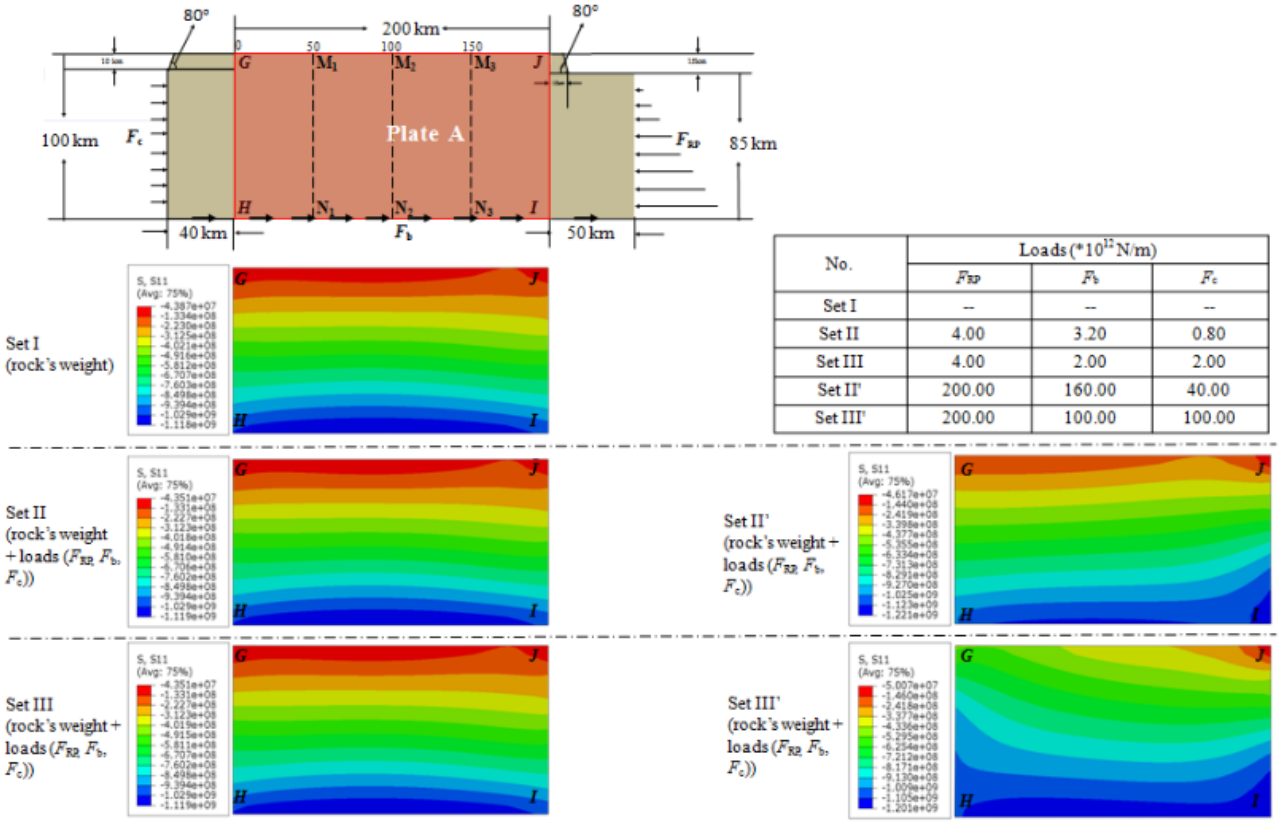

No.	Loads (*10^{12} N/m)		
	F_{RP}	F_b	F_c
Set I	--	--	--
Set II	4.00	3.20	0.80
Set III	4.00	2.00	2.00
Set II'	200.00	160.00	40.00
Set III'	200.00	100.00	100.00

Figure 2: Stress cloud comparison. F_{RP}, F_b, and F_c denote the ridge push force, the basal friction force, and the collisional force.

https://doi.org/10.5194/egusphere-2023-1458
Preprint. Discussion started: 3 August 2023

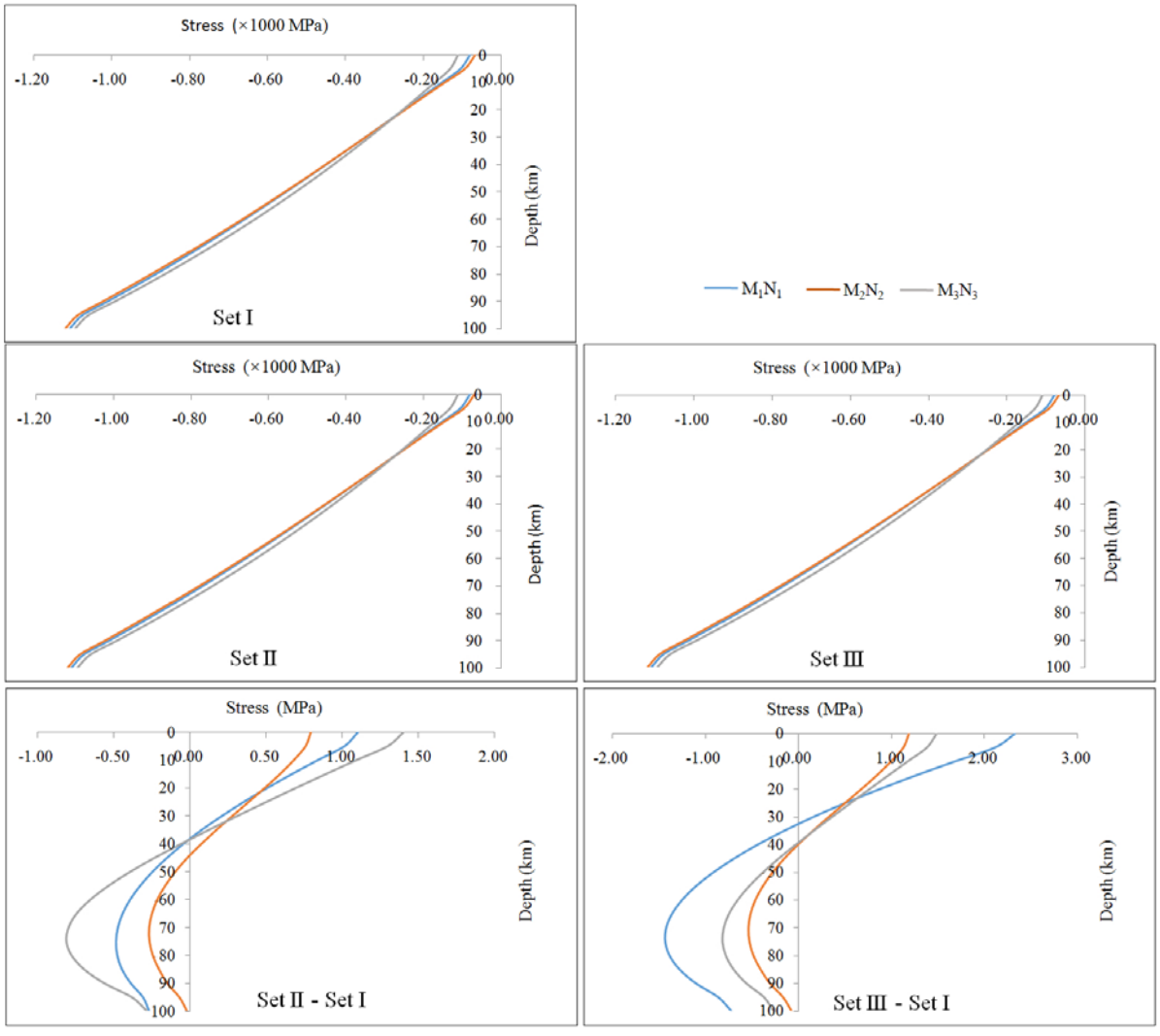

Figure 3: Stress diagram comparison.

2.2.2 Geometry and kinematics of the continental plate

In examining the plate's shape around the globe, we see that the eastern coastline of the American continent is approximately subparallel to the Atlantic ridge at the plate's boundary, and the coastline of Australia's continent is subparallel to the boundary of the Australian Plate. However, the coastline's length of the American continent is greater than that of the Atlantic ridge, whereas the coastline's length of the Australian continent is less than that of its boundary. This feature is also clear for the Indian Plate. Such fashion implies that the driving force of continental plate is likely related to the coastline.

All plates are steadily moving over the Earth's surface, this means that there would be separations and approaches between plates. Separations would result in a gap between two plates. The gap would allow magma to erupt and form a mid-ocean ridge

https://doi.org/10.5194/egusphere-2023-1458
Preprint. Discussion started: 3 August 2023

(MOR). In this respect, the MOR may be the result of plate motion. Currently, the MOR is treated as the cause of the plate driving force. This treatment leads to a chicken-or-egg question: which came first? In physics, the object that exerts force must be clearly differentiated from the object that accepts this force. Some argue that once subduction and spreading are initiated, plates may drive themselves as part of the large circulation of the mantle and lithosphere, which resolves the chicken-or-egg question. However, this view cannot be convincing. Ridge push force contributes to not only the oceanic plates but also the continental plates. The oceanic plates are subducting into the trenches, they take part in the large circulation. Instead, the continental plates never sink, they wouldn't take part in the large circulation, therefore, the chicken-or-egg question remains for the continental plates.

As mentioned in section 1, the latest understanding of plate dynamics is that the lithosphere, crust, and mantle compose the large-scale circulation, and that the plate itself is an integral part of this circulation. Consequently, the dynamic source of plate motion is traced back to the Earth's interior. The terrestrial planets (Venus, Mercury, and Mars) share similar formation procession and interior structure (i.e., crust, mantle, and core) with the Earth, they also have the same spatial surroundings (i.e., asteroid impact) as the Earth does. Therefore, the question remains of why there is plate motion on Earth but not on the other terrestrial planets. This discrepancy of plate motion distribution, together with the above mentioned problems of slab pull and ridge push, implies that some key factor of the Earth, which is still currently unknown, is more likely to cause plate motion.

3 An ocean-generating force driving mechanism for plate motion

3.1 Ocean-generating force

Ocean water covers approximately 71% of the Earth's surface, and its total volume is almost 1.35 billion km^3, with an average depth of nearly 3,700 meters. Geochemical study of zircons suggests that liquid water has existed for more than 4 Gy ago (Mojzsis et al., 2001; Bercovici et al., 2015; Valley et al., 2002). Ocean water is supported by the upper part of the lithosphere, this loading allows the weight of the ocean water to be vertically transferred to the lithosphere. The impact of ocean water on the isostatic balance and heat process of the lithosphere has been widely discussed (Bercovici et al., 2015; Fleitout and Froidevaux, 1983; Osei Tutu et al., 2018; Ricard et al., 1984; Steinberger et al., 2001; Lithgow-Bertelloni, 2014; Ghosh and Holt, 2012; Naliboff et al., 2012). The absence of plate tectonics on the other terrestrial planets (e.g., Mars and Venus) is already recognized; this absence is typically ascribed to the lack of liquid water because the water on Mars possibly appeared in liquid form in the planet's early history and water on Venus has disappeared through a runaway greenhouse (Squyres et al., 2004). Nevertheless, the mechanism by which liquid water contributes to plate tectonics remains enigmatic (Bercovici et al., 2015). A view is that the Earth's surface is cooled by liquid water since the Earth's temperature needs to be stabilized by a negative feedback in the formation of plate tectonics (Bercovici et al., 2015; Walker et al., 1981; Berner, 2004).

Liquid exerts pressure on the wall of a container that holds it. The pressure generated on the wall of a cubic container may be written as $P=\rho gy/2$, and the application of this pressure across the wall yields a force. This force may be expressed as

https://doi.org/10.5194/egusphere-2023-1458
Preprint. Discussion started: 3 August 2023

$F=PS=\rho g y^2 x/2$, where S is the wall area, g and ρ are the gravitational acceleration and liquid density, respectively, and x and y are the liquid width and depth, respectively, in the container. Referring to the real world, ocean basins are naturally gigantic containers, and their depths are often more than a few kilometers and vary from one place to another. All of these factors imply that oceans can generate enormous pressure everywhere and that this pressure is unequal among oceans. Furthermore, the application of pressure against oceanic basin walls, which consist of the continents, can yield enormous unequal forces on the continents. Geometrically, ocean pressure is always exerted vertically to the continental slope, by which a normal force is formed. This normal force is called the ocean-generated force, which may be further decomposed into a horizontal force and a vertical force. The horizontal force may be further written as $F = 0.5\rho g L h^2$, where ρ, g, L, and h are the density of water, gravitational acceleration, ocean width that fits the continent's width, and ocean depth, respectively.

In practice, the continent's side is not flat, and the continent's base is generally wider than its top, making the continent appear more like a circular truncated cone standing in the ocean. As the horizontal force is related to the ocean's width (i.e., the continent side's width), we need to horizontally project the continent onto a polygonal column, dissect the whole side of this column into a series of smaller rectangular sides connecting one to another and subsequently calculate the horizontal force generated at each of these rectangular sides. Figure 4 exhibits the horizontal forces generated on the continents. The horizontal forces and the parameters for calculating them are listed in Table 1. Figure 4 exhibits the horizontal forces generated on the continents. The horizontal forces and the parameters for calculating them are listed in Table 1.

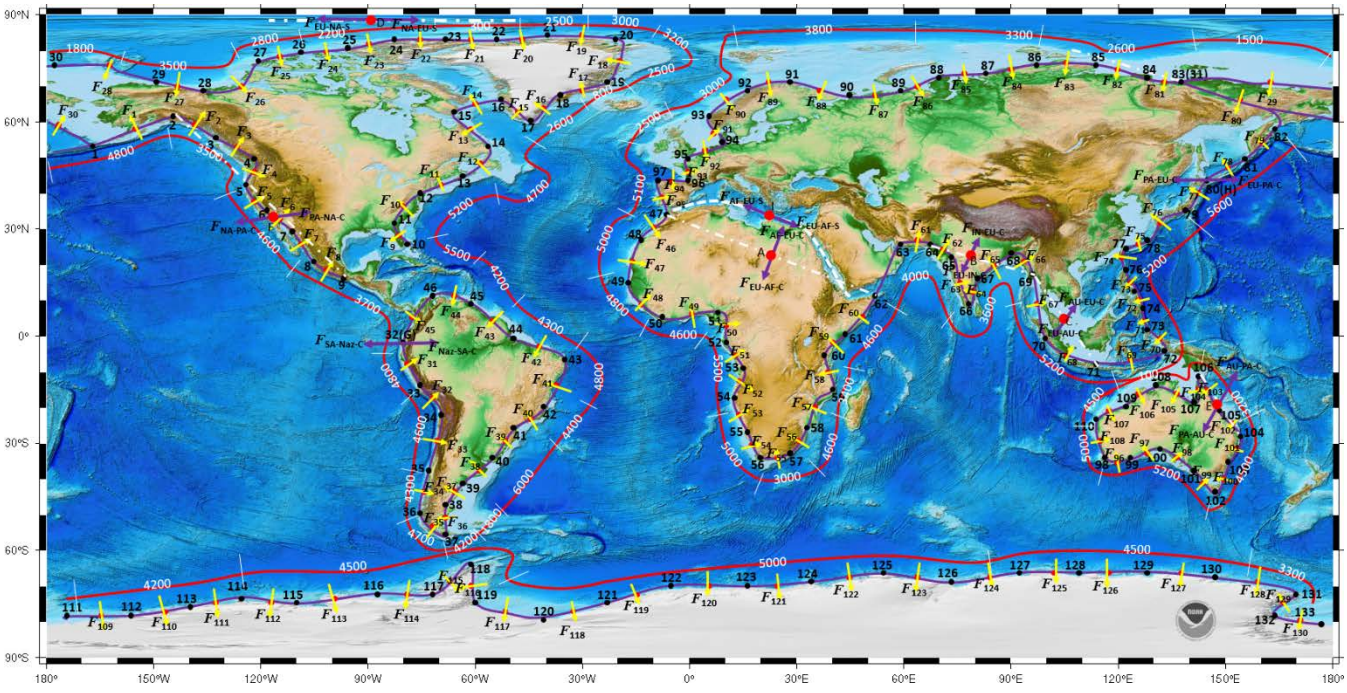

Figure 4: Geographic treatment of the control sites on the continents and the horizontal forces generated on them. F (yellow arrows) denotes the horizontal force. The red lines depict the ocean depths. The black dots denote the control sites;

https://doi.org/10.5194/egusphere-2023-1458
Preprint. Discussion started: 3 August 2023

the small red dots denote the geometric centers of the sides. The large red dots denote the exerting centers of the collisional and shearing forces (large purple arrows) between plates. The background map is ETOPO1 Global Relief Model (Amanteand Eakins, 2009)**.** Note that the ocean depths were artificially resolved through the NOAA bathymetric data viewer.

https://doi.org/10.5194/egusphere-2023-1458
Preprint. Discussion started: 3 August 2023

Table 1(A). Basic information for the horizontal forces

Control site			Side						
				Length	Hypothetical geocentric center		Ocean depth	Horizontal force	
j	d_j	q_j	i	L_i	α_i	β_i	$h_{i\text{-ocean}}$	F_i	Inclination to latitude, east (γi)
	Longitude	Latitude		km	Longitude	Latitude	m	N (*10^{17})	Degrees (°)
1	194.09°	54.23°	1	1747.90	204.23°	60.39°	4,800	1.9733	140.74°
2	214.37°	66.55°	2	1071.92	220.79°	62.71°	4,800	1.2102	127.52°
3	227.21°	58.86°	3	1190.03	232.02°	54.29°	3,500	0.7143	121.53°
4	236.82°	49.71°	4	931.50	236.29°	45.54°	3,500	0.5591	354.92°
5	235.76°	41.36°	5	921.16	238.93°	38.05°	4,600	0.9551	36.94°
6	242.09°	34.73°	6	1319.66	246.74°	30.35°	4,600	1.3683	42.46°
7	251.39°	25.96°	7	662.22	253.02°	23.38°	4,000	0.5192	30.03°
8	254.64°	20.80°	8	1092.31	259.13°	18.34°	3,700	0.7327	59.98°
9	263.61°	15.88°							
10	280.94°	25.22°	9	700.05	279.36°	28.05°	5,500	1.0377	206.26°
11	277.78°	30.87°	10	1125.90	281.21°	35.10°	5,200	1.4918	146.46°
12	284.63°	39.32°	11	1126.57	290.39°	42.06°	5,200	1.4927	122.57°
13	296.15°	44.79°	12	1032.68	300.23°	48.58°	5,200	1.3683	144.54°
14	304.31°	52.37°	13	1254.00	299.14°	57.29°	3,000	0.5530	209.60°
15	293.97°	62.21°	14	701.87	300.48°	63.47°	4,700	0.7597	113.29°
16	306.98°	64.72°	15	708.93	311.51°	62.32°	3,000	0.3126	41.23°
17	316.04°	59.91°	16	870.41	320.23°	63.36°	2,600	0.2883	151.37°
18	324.42°	66.80°	17	662.56	330.75°	68.72°	800	0.0208	129.72°
19	337.08°	70.63°	18	1360.30	337.57°	76.75°	3,200	0.6825	178.95°
20	338.06°	82.87°	19	275.43	327.87°	83.08°	2,800	0.1058	260.40°
21	317.67°	83.29°	20	198.31	311.52°	82.83°	2,500	0.0607	239.16°
22	305.37°	82.37°	21	231.66	297.64°	82.75°	300	0.0010	249.11°
23	289.90°	83.12°	22	238.55	281.92°	82.74°	2,200	0.0566	249.47°
24	273.94°	82.36°	23	336.45	267.96°	81.15°	2,200	0.0798	322.66°
25	261.98°	79.94°	24	294.67	255.30°	79.43°	2,200	0.0699	292.70°

https://doi.org/10.5194/egusphere-2023-1458
Preprint. Discussion started: 3 August 2023

26	248.62°	78.91°	25	313.81	244.23°	77.84°	2,800	0.1206	319.08°
27	239.83°	76.77°	26	997.49	229.64°	73.31°	3,500	0.5987	319.52°
28	219.44°	69.84°	27	523.95	212.59°	70.37°	3,500	0.3145	257.09°
29	205.73°	70.90°	28	753.32	195.39°	72.17°	3,500	0.4522	291.66°
30	185.05°	73.44°	29	1601.37	171.87°	68.03°	1,500	0.1766	317.22°
31	158.68°	62.61°	30	2225.18	176.39°	58.42°	50	0.0003	293.80°

Notes: all geographic sites refer to Figure 4.

285

Table 1(B). Basic information for the horizontal forces (continued)

Control site			Side						
				Length	Hypothetical geocentric center		Ocean depth	Horizontal force	
j	d_j	q_j	i	L_i	α_i	β_i	$h_{i\text{-ocean}}$	F_i	Inclination to latitude, east (γi)
	Longitude	Latitude		km	Longitude	Latitude	m	N (*10^{17})	Degrees
32	278.96°	-2.20°	31	1290.88	281.25°	-7.55°	4,800	1.4573	22.92°
33	283.53°	-12.90°	32	1163.08	286.57°	-17.26°	4,600	1.2059	33.59°
34	289.60°	-21.62°	33	1737.42	287.89°	-29.30°	4,600	1.8014	349.01°
35	286.17°	-36.97°	34	1405.78	284.78°	-43.22°	4,300	1.2737	350.81°
36	283.39°	-49.46°	35	876.16	287.57°	-52.48°	4,700	0.9484	40.11°
37	291.74°	-55.50°	36	977.06	291.92°	-51.11°	1,800	0.1551	181.43°
38	292.09°	-46.71°	37	731.33	294.03°	-43.73°	1,800	0.1161	154.87°
39	295.96°	-40.75°	38	1014.55	300.13°	-37.59°	6,000	1.7897	133.75°
40	304.29°	-34.43°	39	1161.02	307.71°	-30.12°	6,000	2.0480	145.55°
41	311.13°	-25.81°	40	1086.71	315.40°	-22.90°	5,200	1.4398	126.58°
42	319.66°	-19.98°	41	1571.58	322.47°	-13.46°	4,600	1.6295	157.31°
43	325.28°	-6.93°	42	1744.37	318.22°	-3.48°	4,300	1.5804	243.89°
44	311.15°	-0.02°	43	1602.67	305.40°	4.36°	4,200	1.3853	232.65°
45	299.64°	8.73°	44	292.31	300.11°	7.50°	4,800	0.3300	200.75°
46	300.58°	6.27°	45	2576.75	289.77°	2.04°	3,700	1.7285	291.42°
47	353.22°	34.24°	46	908.04	350.19°	31.09°	5,000	1.1123	320.52°

https://doi.org/10.5194/egusphere-2023-1458
Preprint. Discussion started: 3 August 2023

48	347.15°	27.93°	47	1462.59	345.17°	21.61°	5,000	1.7917	343.79°
49	343.19°	15.29°	48	1482.74	347.41°	10.07°	4,800	1.6739	38.46°
50	351.63°	4.84°	49	1689.12	359.25°	5.29°	4,600	1.7514	93.36°
51	6.87°	5.73°	50	898.57	8.32°	1.96°	4,600	0.9317	20.99°
52	9.77°	-1.82°	51	1051.19	11.94°	-6.03°	5,500	1.5581	27.12°
53	14.11°	-10.24°	52	887.15	13.10°	-14.11°	5,500	1.3150	345.81°
54	12.09°	-17.98°	53	1157.53	14.03°	-22.88°	5,000	1.4180	19.99°
55	15.96°	-27.77°	54	779.24	17.82°	-30.90°	5,000	0.9546	26.98°
56	19.67°	-34.02°	55	669.59	23.27°	-33.69°	3,000	0.2953	83.72°
57	26.87°	-33.36°	56	1010.77	29.68°	-29.52°	4,600	1.0480	147.57°
58	32.48°	-25.68°	57	1416.91	36.40°	-20.46°	4,000	1.1109	144.93°
59	40.31°	-15.24°	58	1063.87	39.56°	-10.51°	3,400	0.6026	188.85°
60	38.81°	-5.78°	59	880.15	41.14°	-2.58°	4,600	0.9126	144.02°
61	43.47°	0.63°	60	1479.88	47.38°	6.04°	4,600	1.5344	144.34°
62	51.29°	11.45°							

Notes: all geographic sites refer to Figure 4.

Table 1(C). Basic information for the horizontal forces (continued)

Control site			Side						
				Length	Hypothetical geocentric center		Ocean depth	Horizontal force	
j	d_j	q_j	i	L_i	α_i	β_i	$h_{i\text{-ocean}}$	F_i	Inclination to latitude, east (γi)
	Longitude	Latitude		km	Longitude	Latitude	m	N (*10^{17})	Degrees
69	95.41°	16.55°	67	1802.58	97.12°	8.62°	5,000	2.2082	11.96°
70	98.82°	0.68°	68	1806.5	105.79°	-3.54°	5,200	2.3935	60.27°
71	112.76°	-7.75°	69	2151.54	122.43°	-6.51°	100	0.0011	97.36°
72	132.09°	-5.27°	70	1075.97	130.03°	-0.89°	5,200	1.4256	204.11°
73	127.96°	3.49°	71	485.05	127.35°	5.59°	5,200	0.6427	196.28°
74	126.73°	7.68°	72	435.29	126.29°	9.59°	5,200	0.5767	167.20°
75	125.85°	11.5°	73	947.45	123.79°	15.27°	5,200	1.2553	152.16°

https://doi.org/10.5194/egusphere-2023-1458
Preprint. Discussion started: 3 August 2023

76	121.72°	19.04°	74	554.03	121.85°	21.53°	5,200	0.7341	177.22°
77	121.98°	24.02°	75	614.22	124.74°	25.22°	5,200	0.8138	115.61
78	127.49°	26.41°	76	1399.63	132.94°	30.63°	5,200	1.8545	131.96°
79	138.39°	34.84°	77	1133.3	141.69°	39.26°	5,600	1.7415	150.02°
80	144.98°	43.68°	78	954.18	149.84°	46.38°	5,600	1.4662	128.80°
81	154.69°	49.07°	79	1196.64	159.22°	53.76°	5,600	1.8388	150.27°
82	163.74°	58.44°	80	1136.53	161.21°	60.53°	3,800	0.8042	266.56°
83	158.68°	62.61°	81	1393.86	143.60°	67.44°	1,500	0.1537	254.05°
84	128.51°	72.26°	82	603.43	120.52°	73.84°	2,600	0.1999	234.78°
85	112.52°	75.42°	83	469.11	104.03°	75.62°	2,600	0.1554	275.25°
86	95.54°	75.81°	84	440.81	89.21°	74.73°	3,300	0.2352	302.95°
87	82.88°	73.64°	85	490.57	75.85°	72.86°	3,300	0.2618	290.54°
88	68.82°	72.08°	86	529.37	63.55°	70.47°	3,800	0.3746	312.33°
89	58.27°	68.86°	87	603.56	51.38°	68.00°	3,800	0.4271	288.45°
90	44.49°	67.13°	88	546.62	38.16°	67.67°	3,800	0.3868	257.5°
91	31.83°	68.20°	89	753.91	23.04°	67.60°	3,800	0.5334	280.17°
92	14.25°	66.99°	90	733.5	9.68°	64.34°	300	0.0032	323.21°
93	5.11°	61.69°	91	926.31	6.17°	57.56°	5,100	1.1806	7.80°
94	7.22°	53.43°	92	708.24	183.36°	51.35°	3,000	0.3123	310.79°
95	359.49°	49.26°	93	591.35	359.14°	46.61°	5,100	0.7537	5.18°
96	358.79°	43.96°	94	761.67	354.04°	43.83°	5,100	0.9707	267.83°
97	349.29°	43.70°	95	1104.32	351.26°	38.97°	5,100	1.4074	17.89°
98	133.29°	-38.42°	96	1032.06	128.33°	-36.08°	5,200	1.3674	120.28°
99	123.36°	-33.73°	97	774.89	127.27°	-32.59°	5,200	1.0267	109.16°
100	131.18°	-31.44°	98	1089.81	135.80°	-34.55°	5,200	1.444	50.76°
101	140.41°	-37.65°	99	875.86	143.60°	-40.77°	5,200	1.1605	37.70°
102	146.78°	-43.89°	100	958.73	148.49°	-39.78°	4,500	0.9513	162.28°
103	150.20°	-35.67°	101	877.51	152.09°	-32.06°	4,500	0.8707	156.08°
104	153.98°	-28.45°	102	943.16	151.56°	-24.82°	3,200	0.4732	211.22°

Notes: all geographic sites refer to Figure 4.

https://doi.org/10.5194/egusphere-2023-1458
Preprint. Discussion started: 3 August 2023

Table 1(D). Basic information for the horizontal forces (continued)

Control site			Side						
				Length	Hypothetical geocentric center		Ocean depth	Horizontal force	
j	d_j	q_j	i	L_i	α_i	β_i	$h_{i\text{-ocean}}$	F_i	Inclination to latitude, east (γ_i)
	Longitude	Latitude		km	Longitude	Latitude	m	N ($*10^{17}$)	Degrees
105	149.13°	-21.19°	103	1359.76	145.75°	-16.01°	3,200	0.6823	212.08°
106	142.36°	-10.82°	104	802.72	141.57°	-14.35°	100	0.0004	347.77°
107	140.78°	-17.88°	105	1216.8	135.51°	-15.81°	100	0.0006	247.79°
108	130.24°	-13.74°	106	1109.61	125.89°	-16.48°	100	0.0005	303.28°
109	121.53°	-19.22°	107	864.63	117.80°	-20.95°	4,500	0.8579	296.31°
110	114.06°	-22.67°	108	2529.37	123.68°	-30.55°	5,000	3.0985	46.39°
111	188.47°	-78.56°	109	391.5	196.72°	-78.09°	4,200	0.3384	285.48°
112	204.97°	-77.61°	110	519.06	213.35°	-76.35°	4,200	0.4487	302.42°
113	221.73°	-75.08	111	461.58	229.17°	-74.47°	4,200	0.399	286.94°
114	236.61°	-73.86°	112	401.97	243.06°	-74.38°	4,500	0.3989	253.39°
115	249.51°	-74.90°	113	780.47	261.99°	-74.03°	4,500	0.7744	284.02°
116	274.46°	-73.16°	114	477.75	281.74°	-72.91°	4,500	0.4741	263.24°
117	289.02°	-72.65°	115	1595.2	298.54°	-66.48°	4,500	1.5828	328.21°
118	308.06°	-60.30°	116	1702.14	305.75°	-67.92°	5,000	2.0851	186.49°
119	303.40°	-75.53°	117	418.96	309.48°	-76.83°	5,000	0.5132	226.90°
120	315.53°	-78.12°	118	850.21	327.66°	-75.67°	5,000	1.0415	308.82°
121	339.79°	-73.22°	119	644.56	347.35°	-71.56°	5,000	0.7896	304.72°
122	354.90°	-69.89°	120	919.54	186.86°	-69.65°	5,000	1.1264	266.74°
123	18.81°	-69.41°	121	674.24	26.90°	-68.64°	5,000	0.8259	284.57°
124	34.98°	-67.87°	122	819.5	44.05°	-66.87°	5,000	1.0039	285.64°
125	53.12°	-65.86°	123	838.69	62.26°	-67.22°	5,000	1.0274	249.11°
126	71.40°	-68.58°	124	983.34	82.48°	-67.32°	5,000	1.2046	286.27°
127	93.55°	-66.06°	125	675.92	101.11°	-66.29°	4,500	0.6707	265.79°
128	108.67°	-66.51°	126	908.21	119.04°	-66.82°	4,500	0.9012	267.30°

https://doi.org/10.5194/egusphere-2023-1458
Preprint. Discussion started: 3 August 2023

129	129.41°	-66.90°	127	654.62	136.97°	-67.01°	4,500	0.6495	267.88°
130	144.52°	-67.12°	128	1098.65	157.08°	-69.49°	3,900	0.8188	242.07°
131	169.63°	-71.85°	129	631.15	166.64°	-74.58°	3,300	0.3368	163.76°
132	163.65°	-77.31°	130	645.18	177.36°	-78.01°	3,300	0.3443	256.53°
133	191.07°	-78.70°							
A	26.50°	22.40°	AF-EU-C (EU-AF-C)					4.2000	66.13° (246.13°)
B	21.05°	80.92°	IN-EU-C (EU-IN-C)					1.3000	71.47° (251.47°)
C	12.15°	104.09°	AU-EU-C (EU-AU-C)					1.5000	54.74° (234.74°)
D	88.00°	84.59°	NA-EU-S (EU-NS-S)					4.0000	0.00° (180.00°)
E	-19.64°	148.17°	AU-PA-C (PA-AU-C)					1.0000	55.00° (235.00°)
F	41.22°	238.99°	NA-PA-C (PA-NA-C)					3.0000	185.00° (5.00°)
G	-2.20°	278.96°	Naz-SA-C (SA-Naz-C)					0.2000	0.00° (180.00°)
H	43.68°	144.98°	PA-EU-C (EU-PA-C)					0.1000	180.00° (0.00°)
I	20.68°	35.70°	AF-EU-S (EU-AF-S)					0.8000	170.00° (350.00°)

Notes: all geographic sites refer to Figure 4.

https://doi.org/10.5194/egusphere-2023-1458
Preprint. Discussion started: 3 August 2023

3.2 Resultant movements of plates

The continents are fixed on the top of the lithosphere, and the lithospheric plates connect to each other, this relationship allows the ocean-generated force to be laterally transferred to the lithospheric plates. Subsequently, we list the plausible forces that act on a sample continental plate (Figure 5) and discuss the physical nature of these forces.

These forces can be classified into two categories: the forces acting on the parts of the continent that connect to the oceans and those acting at both the bottom surface of the continental plate and the parts of the continental plate that connect to adjacent plates. The forces acting on the parts of the continent that connect to the ocean derive from ocean pressure and are treated as ocean-generated forces, denoted as F_R on the right and F_L on the left. The horizontal forces decomposed from these forces are denoted as F_R' on the right and F_L' on the left. The force acting on the bottom surface of the continental plate arises from a coupling between the plate and underlying viscous asthenosphere. This force is called the basal friction force and is denoted as f_{base}. According to Forsyth & Uyeda (1975), if there is thermal convection in the asthenosphere, f_{base} would be a driving force (Runcorn, 1962a, b; Turcotte & Oxburgh, 1972; Morgan, 1972). If, instead, the asthenosphere is passive relative to plate motion, f_{base} would be a resistive force. Here, we assume f_{base} to be a resistive force. Given that the continental plate moves toward the right, the forces acting on the parts of the continental plate that connect to adjacent plates include the collisional force from the plate on the right side and the push force from the ridge on the left side, they are denoted as F_C and F_{ridge}, respectively.

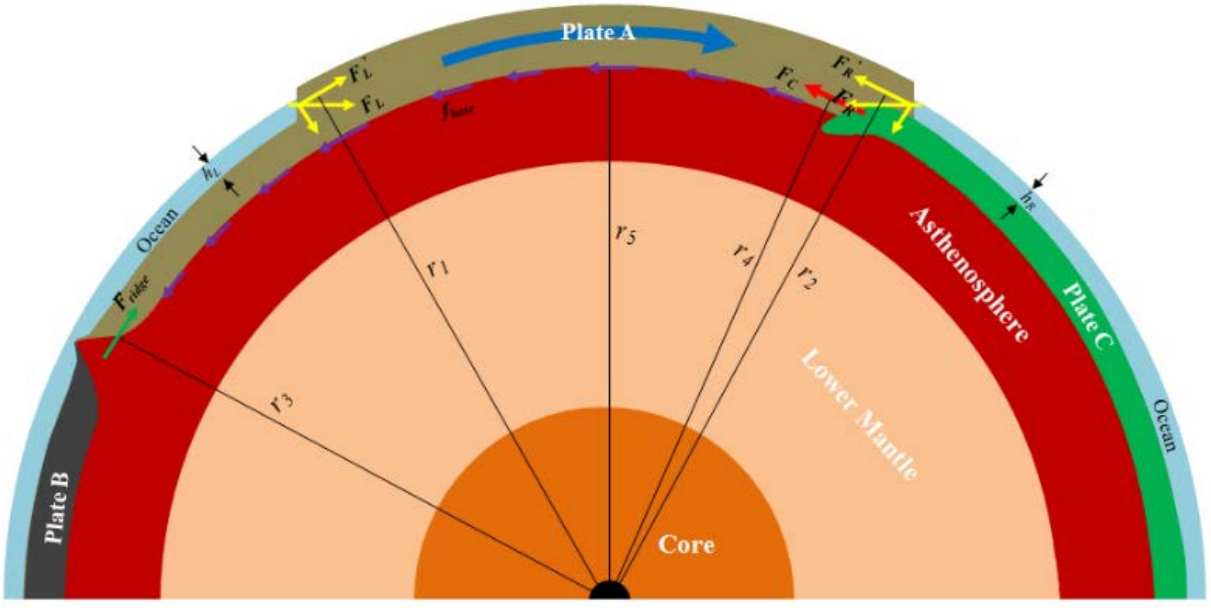

Figure 5: Modeling the dynamics of a continental plate. F_L(F_R) represents the ocean-generated force on the left (right) side of Plate A, while F_L'(F_R') and F_L''(F_R'') denote the horizontal and vertical forces decomposed from the ocean-generated force,

https://doi.org/10.5194/egusphere-2023-1458
Preprint. Discussion started: 3 August 2023

respectively. f_{base} denotes the basal friction force exerted by the underlying asthenosphere, while F_C and F_{ridge} denote the collisional force from Plate C on the right side and the push force from the ridge on the left side, respectively. h_L and h_R are the ocean depths on the left and right, respectively. r_1, r_2, r_3, r_4, and r_5 denote the distances of these forces to the Earth's center. Note that the ocean depth and lithospheric plate thickness are highly exaggerated.

Plate motion is conventionally understood as a rigid plate rotating about an axis that penetrates the Earth's center, and this rotation must be a consequence of the integrated effect of all torques acting on the plate (e.g., Richardson, 1992; Forsyth & Uyeda, 1975). Following this understanding, we use torque balance to discuss the movement caused by these forces. According to Figure 5, a combined torque for Plate A may be written as

$$\tau = (r_1F_L' - r_2F_R') + r_3F_{\text{ridge}} - (r_4F_C + r_5f_{base}) \quad (1)$$

where the first term $(r_1F_L' - r_2F_R')$ denotes the torque yielded by the final horizontal force, the second term r_3F_{ridge} denotes the torque yielded by the ridge push force, both of them represent the driving torque for the continental plate, and the third term $(r_4F_C + r_5f_{base})$ denotes the resisting torque, which hinders the movement of the continental plate. Taking into consideration the reality that the plate is too thin (e.g., less than few hundred kilometers) relative to the Earth's radius (e.g., more than six thousand kilometers), we approximate $r_1 = r_2 = r_3 = r_4 = r_5$. F_L' and F_R' may be further written as $F_L' = 0.5\rho g L h_L^2$ and $F_R' = 0.5\rho g L h_R^2$, where ρ, g, L, h_L, and h_R are the density of water, gravitational acceleration, ocean width that fits the continent's width, ocean depth at the left, and ocean depth at the right, respectively.

Equation (1) provides three possibilities for the continental plate. If the driving torque is greater than the resisting torque, the combined torque is greater than zero, and the continental plate is subjected to an accelerating motion. Practically, it is impossible for the continental plate to undergo such a movement. If the driving torque is equal to the resisting torque, the combined torque is zero, and the continental plate would be subjected to a steady motion. If the driving torque is less than the resisting torque, the combined torque is less than zero, and the continental plate remains motionless.

Plate A's movement exhibited in Figure 5 is parallel to that of Plate B and Plate C, this situation is rather idealized. Practically, the movements of most plates intersect with each other. For instance, the South American Plate moves northwest, the Nazca Plate moves eastward, the African Plate moves northeast, the Eurasian Plate moves eastward. These nonparallel movements would yield additional collisional forces and shearing forces between plates. If two plates are not moving in the opposite direction, the collisional and shearing forces between them may be driving; and if the two plates are moving in the opposite direction, the collisional and shearing forces between them may be resisting. Below, we develop two semi-analytic methods (I and II) to independently resolve plate motion.

Method I

It is assumed that the Earth's surface is covered with Plate A, Plate B, Plate C, Plate D, and others, and that Euler pole of each plate has been established (Figure 6). For Plate A, the horizontal force F_i (i=1, 2, 3, 4, and 5) acts on the side of the continent

https://doi.org/10.5194/egusphere-2023-1458
Preprint. Discussion started: 3 August 2023

that is fixed on top of Plate A. The horizontal force (F_1, for instance) yields a component (F_1', for instance) that is orthogonal to the rotation axis of the plate; this component then yields a torque (τ_1', for instance). The torques yielded by all the components decomposed from the horizontal forces are summed into first driving torque. The ridge push force $F_{r\text{-}i}$ (i=1, 2, 3, and 4) acts on the edge of the plate, this force also yields a component that is orthogonal to the rotation axis; this component also yields a torque. The torques yielded by all the components decomposed from the ridge push forces are summed into second driving torque. Given that Plate A, Plate B, Plate C, and Plate D move eastward, southward, westward, and eastward, respectively, and that Plate D moves faster than Plate A, these make Plate A undergo a collisional driving force $F_{B\text{-}c}$ from Plate B, a shearing driving force $F_{D\text{-}s}$ from Plate D, a collisional resistive force $F_{C\text{-}c}$ from Plate C, a shearing resistive force $F_{B\text{-}s}$ from Plate B, and a basal friction force F_{basal} from the underlying viscous asthenosphere. The collisional driving force $F_{B\text{-}c}$ and the shearing driving force $F_{D\text{-}s}$ also yield two components that are orthogonal to the rotation axis of the plate; these components also yield torques. The torques yielded by these two components are summed into third driving torque. The collisional resistive force $F_{C\text{-}c}$ and the shearing resistive force $F_{B\text{-}s}$ also yield two components that are orthogonal to the rotation axis; these components also yield torques. The torques yielded by these two components are summed into first resistive torque. The basal friction force F_{basal} yields second resistive torque.

Then, we divide these five sets of torques into two exerting parts: one, which includes the second driving torque and a little portion of the first and third driving torque, balances out the first resistive torque, and the other, which including the remaining portion of the first and third driving torque, balances the second resistive torque. Consequently, all these torque balances allow Plate A to be steadily rotated under the assumption that the acceleration and inertia of the plate are neglected. The remaining portion of the first and third driving torque is called the net driving torque, and the second resistive torque is called the net resistive torque. The balance between the net driving torque and the net resistive torque may be written as

$$\tau_{driving} - \tau_{basal} = 0 \quad (2)$$

where $\tau_{driving}$ is the net driving torque, $\tau_{driving} = \varepsilon\tau$, and ε is the ratio of the net driving torque to the first and third driving torque. As shown in Figure 6(A), the component decomposed from a force (the horizontal force, for instance) may be written as $F_{i'} = F_i \cos\eta_i$, and $\eta_i = \gamma_i - \lambda_i$, where γ_i is the inclination of this force to latitude. λ_i is the azimuth of arc P_iE with respect to latitude. This component yields a torque τ_i with respect to the rotation axis, i.e., $\tau_i = r_i F_{i'}$, where r_i denotes the lever arm distance of the component $F_{i'}$, $r_i = R_{earth}\sin\varphi_{Pi}$, R_{earth} is the Earth's radius and R_{earth}=6,371 km, and φ_{Pi} is the angle of site P_i and the Euler pole. A sum of the torques yielded by the components, which are decomposed from the horizontal forces, collisional driving forces, and shearing driving forces, forms the first and third driving torque τ. τ_{basal} denotes the net resistive torque yielded by the basal friction force, it can be written as $\tau_{basal} = r_K F_{basal}$, where r_K denotes the lever arm distance of the basal friction force. According to the principle of viscous fluid mechanics, the basal friction force may be expressed as $F_{basal} = \mu Au/y$, μ, A, u, and y are the viscosity of the asthenosphere, the plate's area, the plate's speed, and the thickness of the asthenosphere, respectively. Therefore, $u = y\tau_{driving}/\mu A$, this speed represents average level of the plate's movement.

https://doi.org/10.5194/egusphere-2023-1458
Preprint. Discussion started: 3 August 2023

In general, the largest speed of a plate occurs at the plate's equator, while the smallest speed occurs at the location whose angle distance to the Euler pole is minimal or maximal. As shown in Figure 6(B), we assume that the geometric center (i.e., location *K*) of Plate A moves at the average speed, namely, u=u_k. And then, the speed of any location *S* within this plate may be expressed with $u_s=u_k\sin\varphi_s/\sin\varphi_k$, where $\varphi_s(\varphi_k)$ is the angle distance of location *S* (*K*) to the Euler pole (i.e., location *E*) relative to the Earth's center. The speed u_s can be further decomposed into the longitudinal speed $u_{s\text{-}lo}$ and latitudinal speed $u_{s\text{-}la}$, and $u_{s\text{-}lo}=u_s\sin(\lambda_s\text{-}90^o)$, $u_{s\text{-}la}=u_s\cos(\lambda_s\text{-}90^o)$, where λ_s is the azimuth of arc *SE* with respect to latitude. The azimuth of the movement is then calculated through the longitudinal and latitudinal speeds. All these angles and distances (i.e., η_i, γ_i, λ_i, λ_s, φ_{Pi}, φ_k, φ_s, r_i, r_K) may be further calculated through the latitudes and longitudes of related locations.

https://doi.org/10.5194/egusphere-2023-1458
Preprint. Discussion started: 3 August 2023

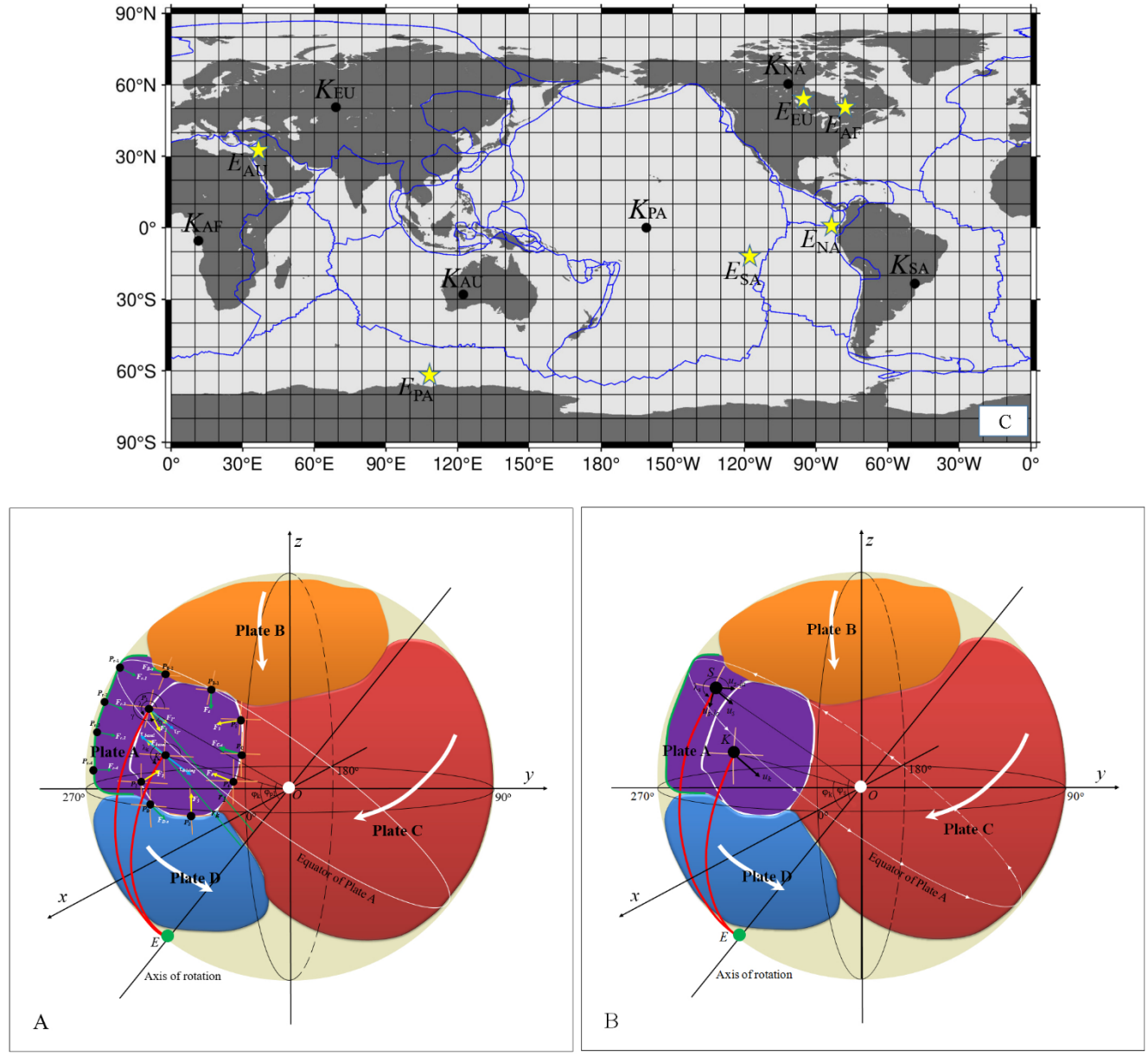

395

Figure 6: Modeling the torque balances for plate motion. (A) Geometry of horizontal forces, ridge push forces, collisional forces, and shearing forces over a spherical frame. The white oval within Plate A represents the scope of the continent. The green line denotes the oceanic ridge. The pink lines beneath the locations (black dots) denote the latitudinal and longitudinal directions. **(B) Decomposing the average movement of the plate into the movement of any location.** The

https://doi.org/10.5194/egusphere-2023-1458
Preprint. Discussion started: 3 August 2023

location K and E are the geometric center of Plate A and its Euler pole, respectively. **(C) Exhibiting the geometric centers (black dots) of the six selected plates and the established Euler pole locations (yellow stars) over a planar frame.**

Here, we use six plates (South American, African, Eurasian, North American, Australian, and Pacific plates) to demonstrate their movements. In order to simplify the following deduction, we plot globally tectonic plates into a grid of $10^{\circ}\times10^{\circ}$ and use these grid nodes, which are within plate, to obtain the geometric center of each plate. The geometric center is approximately calculated through the average of the latitudes and longitudes of these nodes. The Euler pole location of each of these plates is cited from the GSRM v.2.1 (Kreemer et al., 2014). Both the geometric center of each plate and its Euler pole location are exhibited in Figure 6(C).

Besides the horizontal forces, the other possible forces (i.e., collisional and shearing) for these plates must be considered. For example, the African, Indian, and Australian plates provide the collisional driving forces $F_{\text{AF-EU-C}}$, $F_{\text{IN-EU-C}}$, and $F_{\text{AU-EU-C}}$ for the Eurasian Plate, respectively. The Nazca plate provides a collisional driving force $F_{\text{Naz-SA-C}}$ for the South American Plate. The Eurasian Plate provides a shearing resistive force $F_{\text{EU-NA-S}}$ for the North American Plate; vice versa, the North American Plate provides a shearing driving force $F_{\text{NA-EU-S}}$ for the Eurasian Plate. The Australian, North American, and Eurasian Plates provide the collisional driving forces $F_{\text{AU-PA-C}}$, $F_{\text{NA-PA-C}}$, and $F_{\text{EU-PA-C}}$ for the Pacific Plate, respectively. Taking into consideration the long argument of slab pull that is listed in section 2.1, we presently neglect slab pull. And if this force can be confirmed in the future, it can be added into this model. The details of these forces are exhibited in Figure 4 and listed Table 1. The resultant torques from all related forces are listed in Table 2.

https://doi.org/10.5194/egusphere-2023-1458
Preprint. Discussion started: 3 August 2023

Table 2 (A). Parameters for the torques of six selected plates in the method I

Plate	Eule pole		No.	Angle between horizontal force and its decomposed force	Decomposed force	Angle of site P_i and Eule pole	Earth's radius	Lever arm distance	Torque
	E		i	η_i	$F_{i'}$	φ_{pi}	R_{earth}	r_i	τ_i
	Latitude	Longitude		Degrees	N (*10^{17})	Degrees	m (*10^3)	m (*10^3)	N·m (*10^{23})
North America	2.19°	276.25°	1	97.27°	0.2497	79.30°	6371.00	6260.27	-1.5632
			2	92.72°	0.0574	72.92°	6371.00	6089.89	-0.3493
			3	86.94°	0.0381	63.32°	6371.00	5692.78	0.2170
			4	316.47°	0.4054	55.68°	6371.00	5261.94	2.1332
			5	353.88°	0.9497	49.51°	6371.00	4845.13	4.6012
			6	358.11°	1.3675	39.66°	6371.00	4066.52	5.5611
			7	343.60°	0.4981	30.91°	6371.00	3272.51	1.6300
			8	14.05°	0.7108	23.29°	6371.00	2519.47	1.7909
			9	212.77°	0.8725	26.03°	6371.00	2795.38	-2.4389
			10	115.64°	0.6455	33.23°	6371.00	3490.93	-2.2536
			11	129.96°	0.9586	41.83°	6371.00	4249.32	-4.0733
			12	101.72°	0.2780	50.75°	6371.00	4933.75	-1.3715
			13	227.96°	0.3704	58.02°	6371.00	5404.09	-2.0014
			14	129.97°	0.4880	63.81°	6371.00	5717.10	-2.7900
			15	65.38°	0.1302	65.61°	6371.00	5802.46	0.7556
			16	90.08°	0.0004	69.11°	6371.00	5952.09	-0.0023
			17	109.75°	0.0010	75.74°	6371.00	6174.81	-0.0061
			18	207.62°	0.6048	81.54°	6371.00	6301.68	-3.8112
			19	281.86°	0.0218	83.53°	6371.00	6330.41	0.1377
			20	254.21°	0.0165	81.97°	6371.00	6308.49	-0.1042
			21	258.36°	0.0002	81.06°	6371.00	6293.59	-0.0013
			22	251.94°	0.0175	80.59°	6371.00	6285.20	-0.1102

https://doi.org/10.5194/egusphere-2023-1458
Preprint. Discussion started: 3 August 2023

	23	318.90°	0.0601	79.05°	6371.00	6255.08	0.3762
	24	282.85°	0.0155	77.95°	6371.00	6230.53	0.0969
	25	303.63°	0.0668	77.54°	6371.00	6220.87	0.4153
	26	295.24°	0.2553	76.48°	6371.00	6194.44	1.5815
	27	223.62°	0.2277	79.34°	6371.00	6261.13	-1.4256
	28	252.92°	0.1328	85.13°	6371.00	6347.96	-0.8430
	29	268.96°	0.0032	93.29°	6371.00	6360.48	-0.0203
	30	240.52°	0.0001	93.27°	6371.00	6360.61	-0.0009
	EU-NA-S	47.10°	2.7231	89.81°	6371.00	6370.96	-17.3490
	PA-NA-C	35.15°	1.6353	51.43°	6371.00	4981.26	8.1461
						total	-13.0728

Note: the negative symbol "-" beneath torque denotes counterclockwise with respect to the axis of rotation.

Table 2 (B). Parameters for the torques of six selected plates in the method I (continued)

Plate	Eule pole		No.	Angle between horizontal force and its decomposed force	Decomposed force	Angle of site P_i and Eule pole	Earth's radius	Lever arm distance	Torque
	E		i	η_i	$F_{i'}$	φ_{pi}	R_{earth}	r_i	τ_i
	Latitude	Longitude		Degrees	N (*10^{17})	Degrees	m (*10^3)	m (*10^3)	N·m (*10^{23})
South America	-14.10°	242.14°	31	94.63°	0.1175	38.23°	6371.00	3942.62	-0.4635
			32	117.64°	0.5594	40.64°	6371.00	4149.63	-2.3212
			33	75.71°	0.4446	45.73°	6371.00	4561.87	2.0280
			34	68.24°	0.4722	42.53°	6371.00	4306.96	2.0337
			35	107.25°	0.2812	41.10°	6371.00	4188.48	-1.1777
			36	247.03°	0.0605	48.92°	6371.00	4802.51	-0.2907
			37	214.43°	0.0958	50.48°	6371.00	4914.25	-0.4707

https://doi.org/10.5194/egusphere-2023-1458
Preprint. Discussion started: 3 August 2023

			38	188.74°	1.7689	54.93°	6371.00	5214.44	-9.2238
			39	200.24°	1.9216	61.42°	6371.00	5594.69	-10.7506
			40	181.06°	1.4396	66.20°	6371.00	5829.25	-8.3917
			41	212.82°	1.3693	71.37°	6371.00	6037.15	-8.2667
			42	301.17°	0.8180	74.55°	6371.00	6140.76	5.0232
			43	286.96°	0.4041	66.24°	6371.00	5831.18	2.3565
			44	253.52°	0.0936	58.47°	6371.00	5430.40	-0.5084
			45	347.68°	1.6887	58.25°	6371.00	5417.83	9.1491
			Naz-SA-C	71.58°	0.0632	38.26°	6371.00	3945.32	0.2493
								total	-21.0251
Africa	49.66°	281.92°	46	70.14°	0.3779	53.21°	6371.00	5102.38	1.9283
			47	102.95°	0.4016	56.52°	6371.00	5314.13	-2.1344
			48	164.92°	1.6163	66.57°	6371.00	5845.72	-9.4486
			49	218.52°	1.3702	77.78°	6371.00	6226.76	-8.5319
			50	145.39°	0.7668	86.18°	6371.00	6356.85	-4.8747
			51	154.94°	1.4114	94.61°	6371.00	6350.43	-8.9632
			52	117.56°	0.6083	101.46°	6371.00	6243.91	-3.7983
			53	155.92°	1.2945	108.55°	6371.00	6039.87	-7.8188
			54	165.93°	0.9259	116.64°	6371.00	5694.53	-5.2727
			55	137.16°	0.2165	121.92°	6371.00	5407.37	-1.1709
			56	283.40°	0.2429	123.18°	6371.00	5331.97	1.2950
			57	275.06°	0.0979	121.18°	6371.00	5450.79	0.5337
			58	313.40°	0.4141	115.74°	6371.00	5738.80	2.3762
			59	264.22°	0.0918	110.48°	6371.00	5968.21	-0.5481
			60	259.19°	0.2878	107.05°	6371.00	6090.91	-1.7529
			EU-AF-C	7.26°	4.1663	76.43°	6371.00	6193.10	25.8022
			EU-AF-S	81.71°	0.1154	88.57°	6371.00	6369.01	-0.7349
									-23.1140

Note: the negative symbol "-" beneath torque denotes counterclockwise with respect to the axis of rotation.

435

https://doi.org/10.5194/egusphere-2023-1458
Preprint. Discussion started: 3 August 2023

Table 2 (C). Parameters for the torques of six selected plates in the method I (continued)

late	Eule pole		No.	Angle between horizontal force and its decomposed force	Decomposed force	Angle of site P_i and Eule pole	Earth's radius	Length of lever arm	Torque
	E		i	η_i	$F_{i'}$	φ_{pi}	R_{earth}	r_i	τ_i
	Latitude	Longitude		Degrees	N (*10^{17})	Degrees	m (*10^3)	m (*10^3)	N·m (*10^{23})
Eurasia	55.38°	264.59°	67	258.40°	0.4439	115.16°	6371.00	5766.75	-2.5600
			68	149.71°	2.0668	125.41°	6371.00	5192.58	-10.7320
			69	334.71°	0.0010	122.62°	6371.00	5365.89	0.0051
			70	83.52°	0.1608	114.29°	6371.00	5806.87	0.9336
			71	79.27°	0.1196	109.58°	6371.00	6002.67	0.7181
			72	37.66°	0.4566	106.33°	6371.00	6114.00	2.7916
			73	49.55°	0.8144	102.01°	6371.00	6231.63	5.0750
			74	21.11°	0.6848	96.81°	6371.00	6326.02	4.3322
			75	81.02°	0.1270	92.43°	6371.00	6365.29	0.8082
			76	62.48°	0.8568	84.59°	6371.00	6342.61	5.4341
			77	40.27°	1.3288	73.63°	6371.00	6112.77	8.1227
			78	57.60°	0.7856	64.43°	6371.00	5747.16	4.5148
			79	31.07°	1.5750	54.93°	6371.00	5214.08	8.2124
			80	171.95°	0.7962	49.33°	6371.00	4832.06	-3.8475
			81	154.76°	0.1390	49.63°	6371.00	4854.19	-0.6747
			82	133.27°	0.1370	48.52°	6371.00	4772.97	-0.6539
			83	174.32°	0.1546	48.39°	6371.00	4763.58	-0.7366
			84	23.23°	0.2161	49.86°	6371.00	4870.34	-1.0527
			85	11.67°	0.2564	51.62°	6371.00	4994.15	-1.2803
			86	34.19°	0.3098	53.25°	6371.00	5104.74	-1.5816
			87	11.01°	0.4192	54.21°	6371.00	5167.62	-2.1662
			88	175.74°	0.3857	52.24°	6371.00	5036.62	1.9426

https://doi.org/10.5194/egusphere-2023-1458
Preprint. Discussion started: 3 August 2023

	89	0.46°	0.5334	48.88°	6371.00	4799.38	-2.5601
	90	45.07°	0.0023	47.33°	6371.00	4684.66	-0.0107
	91	5.85°	1.1744	50.70°	6371.00	4930.18	-5.7901
	92	44.78°	0.2217	45.84°	6371.00	4570.16	1.0132
	93	102.94°	0.1687	55.45°	6371.00	5247.62	-0.8854
	94	81.57°	0.1424	54.98°	6371.00	5217.66	0.7429
	95	122.84°	0.7633	57.09°	6371.00	5348.90	-4.0826
	AF-EU-C	174.37°	4.1797	82.54°	6371.00	6317.01	-26.4034
	IN-EU-C	178.65°	1.2996	103.51°	6371.00	6194.68	-8.0509
	AU-EU-C	166.77°	1.4602	110.51°	6371.00	5967.18	-8.7133
	NA-EU-S	106.31°	1.1233	36.62°	6371.00	3800.34	-4.2691
	PA-EU-C	97.84°	0.0136	68.57°	6371.00	5930.61	0.0808
	AF-EU-S	29.84°	0.6940	93.37°	6371.00	6359.96	4.4136
						total	-36.9103

Note: the negative symbol "-" beneath torque denotes counterclockwise with respect to the axis of rotation.

Table 2 (D). Parameters for the torques of six selected plates in the method I (continued)

Plate	Eule pole		No.	Angle between horizontal force and its decomposed force	Decomposed force	Angle of site P_i and Eule pole	Earth's radius	Length of lever arm	Torque
	E		i	η_i	$F_{i'}$	φ_{pi}	R_{earth}	r_i	τ_i
	Latitude	Longitude		Degrees	N (*10^{17})	Degrees	m (*10^3)	m (*10^3)	N·m (*10^{23})
			96	254.20°	0.3723	110.26°	6371.00	5976.79	-2.22515
			97	241.45°	0.4908	107.86°	6371.00	6063.97	-2.97597
Australia	33.31°	36.38°	98	182.17°	1.4429	115.09°	6371.00	5769.94	-8.32561
			99	170.88°	1.1458	123.09°	6371.00	5337.79	-6.11606
			100	294.07°	0.3880	126.38°	6371.00	5129.41	1.990312

https://doi.org/10.5194/egusphere-2023-1458
Preprint. Discussion started: 3 August 2023

			101	283.24°	0.1994	126.78°	6371.00	5102.73	1.01746
			102	334.60°	0.4275	123.59°	6371.00	5307.41	2.268856
			103	331.54°	0.5998	114.69°	6371.00	5788.35	3.471845
			104	106.97°	0.0001	110.38°	6371.00	5972.19	-0.0007
			105	261.10°	0.0001	106.09°	6371.00	6121.32	-0.0006
			106	66.81°	0.0002	98.56°	6371.00	6300.01	0.0013
			107	64.56°	0.3686	94.58°	6371.00	6350.68	2.340567
			108	178.47°	3.0974	104.19°	6371.00	6176.62	-19.1313
			EU-AU-C	15.71°	1.4440	64.82°	6371.00	5765.39	8.325007
			PA-AU-C	3.92°	0.9977	118.47°	6371.00	5600.47	5.587377
								total	-13.7727
Pacific	-63.09°	109.63°	AU-PA-C	87.49°	0.0437	50.72°	6371.00	4931.80	0.2157
			NA-PA-C	39.99°	2.2984	143.46°	6371.00	3793.07	-8.7181
			EU-PA-C	12.55°	0.0976	110.42°	6371.00	5970.70	0.5828
								total	-7.9195

Note: the negative symbol "-" beneath torque denotes counterclockwise with respect to the axis of rotation.

https://doi.org/10.5194/egusphere-2023-1458
Preprint. Discussion started: 3 August 2023

The asthenosphere viscosity is not yet exactly determined. Many numerical studies using glacial isostatic adjustment and geoid modeling have shown that asthenospheric viscosity ranges from 10^{17} to 10^{20} Pas (e.g., Steinberger, 2016; Hager and Richards, 1989; Mitrovica, 1996; King, 1995; Kido et al., 1998; James et al., 2009; Pollitz et al., 1998; Berker, 2017; Kaufmann and Lambeck, 2000; Hu et al., 2016). Laboratory experiments, however, suggested that the magnitude of the asthenospheric viscosity could be substantially different from those constrained by numerical studies. The viscosity is variable and likely related to the thermodynamic state, grain size, composition of the medium, and state of stress (Bercovici et al., 2015). Both the melt contents of the asthenosphere and the water in the asthenosphere may greatly affect the viscosity (Mei et al., 2002; Hirth and Kohlstedt, 1996). Hirth and Kohlstedt (1996) reported a variable viscosity profile for a melt-free oceanic lithosphere with a mean value of ~10^{18} Pas. These authors (e.g., Doglioni et al., 2011; Scoppola et al., 2006) concluded that, in consideration of the water- and melt-rich layers characterized by much lower viscosities, a strong vertical variability of viscosity may be more realistic. The asthenosphere's effective viscosity can be greatly lowered to 10^{15} Pas if the water content in the case of both diffusion and dislocation creep is included (Korenaga and Karato, 2008). Scoppola et al. (2006) conducted a more detailed review of asthenospheric viscosity and concluded that the presently accepted values of viscosity might be reduced through a combined experiment including these parameters (i.e., melt content, water content, mechanical anisotropy, and shear localization). A "superweak", low-viscosity asthenosphere supported by recent observations is being accepted by the geophysical community (Kawakatsu et al., 2009; Hawley et al., 2016; Holtzman, 2016; Naif et al., 2013; Freed et al., 2017; Hu et al., 2016; Stern et al., 2015; Bercker, 2017). Jordan (1974) treated the asthenospheric thickness as 300 km.

Taking into account the present status of the viscosity and thickness of the asthenosphere above, we adopt y=300 km for each of the six selected plates, $\mu=10^{18}$ Pas for the South American, African, North American, and Eurasian plates, $\mu=0.6\times10^{18}$ Pas for the Australian Plate, and $\mu=0.12\times10^{18}$ Pas for the Pacific Plate.

The other parameters (i.e., plate area, the ratio of the net driving torque and the first and third driving torque) and the resultant average movements of these six plates are listed in Table 3.

There have been many plate motion models (i.e., GSRM, NUVEL-1, and MORVEL) that include global navigation satellite systems (GNSS) and paleomagnetic data. For instance, GSRM v.2.1 includes more than 6,739 continuous GPS velocity measurements (Kreemer et al., 2014). The movements reproduced by these models may approximately represent observations. Here, the movements of 450 locations (41 for the South American Plate, 70 for the African Plate, 93 for the North American Plate, 95 for the Eurasian Plate, 47 for the Australian Plate, and 104 for the Pacific Plate) are reproduced by GSRM v.2.1. The calculated and reproduced movements are then compared in Figure 7. It can been seen that the calculated movements for these locations are well consistent with the reproduced movements in both speed and azimuth, the RMS of the calculated speed against the reproduced speed for the South American, African, North American, Eurasian, Australian, and Pacific plates is 0.91, 3.76, 2.77, 2.31, 7.43, and 1.95 mm/yr, respectively.

https://doi.org/10.5194/egusphere-2023-1458
Preprint. Discussion started: 3 August 2023

Table 3. The net driving torques and their resultant movements for these six selected plates in the method I

Plate	Area	Ratio	Net driving torque	Geometric center of the plate			Lever arm distance for basal friction force	Movement
	A	ε	$\tau_{driving}$	*K*		φ_k	r_k	u
	km^2		N·m (10^{23})	Latitude	Longitude	Degrees	m (10^3)	mm/yr
South America	43,600,000	0.15	3.18	-24.39°	313.66°	67.63°	5891.49	11.73
Africa	61,300,000	0.64	14.74	-5.57°	13.43°	95.22°	6344.59	35.85
North America	75,900,000	0.79	10.39	59.57°	256.88°	59.31°	5478.57	23.64
Eurasia	67,800,000	0.31	11.51	50.32°	68.84°	73.49°	6108.39	26.29
Australia	47,000,000	0.91	12.55	-28.30°	122.98°	102.51°	6219.65	67.72
Pacific	103,300,000	0.75	5.98	0.10°	198.65°	89.64°	6370.88	71.61

https://doi.org/10.5194/egusphere-2023-1458
Preprint. Discussion started: 3 August 2023

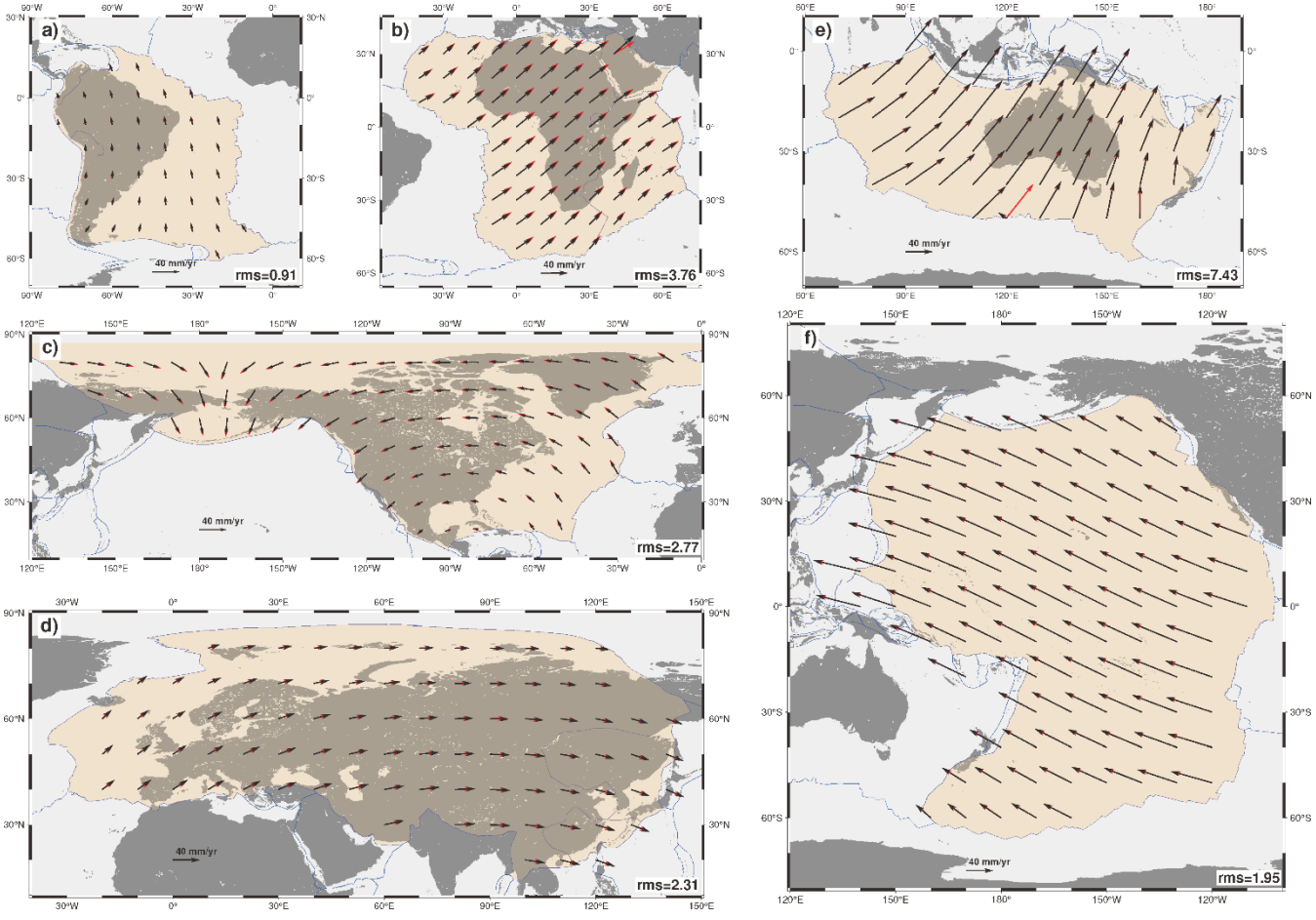

Figure 7: The reproduced movements from GSRM v.2.1 (black arrows) verse the calculated movements from our model (red arrows) in the method I. a), b), c), d), e), and f) are the South American, African, North American, Eurasian, Australian, and Pacific plates, respectively.

https://doi.org/10.5194/egusphere-2023-1458
Preprint. Discussion started: 3 August 2023

Method II

We assume that the Earth's surface is covered with Plate A, Plate B, Plate C, Plate D, and others (Figure 8). For Plate A, it undergoes the horizontal force F_i (i=1, 2, 3, 4, and 5), the ridge push force $F_{r\text{-}i}$ (i=1, 2, 3, and 4), the collisional driving force $F_{B\text{-}c}$, the shearing driving force $F_{D\text{-}s}$, the collisional resistive force $F_{C\text{-}c}$, the shearing resistive force $F_{B\text{-}s}$, and the basal friction force F_{basal}. One horizontal force (F_1, for instance) yields a torque (τ_1, for instance), another horizontal force (F_2, for instance) yields another torque (τ_2, for instance), a combination of these two torques results in a new torque ($\tau_{1\text{-}2}$, for instance), this new torque then combines the torque yielded by third horizontal force to form another new torque. Subsequently, the torques yielded by all the horizontal forces are combined into a final torque. The collisional driving force $F_{B\text{-}c}$ yields a torque, the shearing driving force $F_{D\text{-}s}$ yields a torque, the final torque combines these two torques to firm first driving torque. The collisional resistive force $F_{C\text{-}c}$ and the shearing resistive force $F_{B\text{-}s}$ also yield two torques, they combine to firm first resistive torque. The basal friction force F_{basal} yields second resistive torque. The ridge push force $F_{r\text{-}i}$ (i=1, 2, 3, and 4) also yields a torque, the torques yielded by all the ridge push forces are combined into second driving torque.

Then, we divide these four sets of torques into two exerting parts: one, which includes the second driving torque and a portion of the first driving torque, balances out first the resistive torque, and the other, which including the remaining portion of the first driving torque, balances the second resistive torque. Consequently, all these torque balances allow Plate A to be steadily rotated under the assumption that the acceleration and inertia of the plate are neglected. The remaining portion of the first driving torque is called the net driving torque, and second resistive torque is called the net resistive torque. We assume that the net driving torque exerts on the geometric center (i.e., location K) of Plate A, this makes the plate move along a big circle that represents the equator of this Plate. And then, the balance between the net driving torque and the net resistive torque may be expressed with Equation (2). According to Figure 8(A), a force F_i yields a torque τ_i with respect to the Earth's center, i.e., $\tau_i = R_{\text{earth}} F_i$, where R_{earth} is the Earth's radius and R_{earth}=6,371 km. The combination of two torques follows the trigonometric principle and may be written as

$$\tau_j{}^2 = \tau_i{}^2 + \tau_{i+1}{}^2 + 2\tau_i\tau_{i+1}\cos(\gamma_i - \gamma_{i+1}) \quad (3)$$

where τ_j is the combined torque, τ_i and τ_{i+1} are the torque yielded by the force F_i and F_{i+1}, respectively. γ_i and γ_{i+1} denote the inclination of the forces F_i and F_{i+1} to latitude, respectively. τ_{basal} denotes the net resistive torque yielded by the basal friction force, it can be written as $\tau_{basal} = R_{\text{earth}} F_{basal}$. According to the principle of viscous fluid mechanics, the basal friction force may be expressed as $F_{basal} = \mu Au/y$, μ, A, u, and y are the viscosity of the asthenosphere, the plate's area, the plate's speed, and the thickness of the asthenosphere, respectively. Therefore, $u = y\tau_{driving}/\mu A$, this speed represents average level of the plate's movement.

On the whole, the largest speed of a plate occurs at the plate's equator, while the smallest speed occurs at the location whose angle distance to the Euler pole is minimal or maximal. According to Figure 8(B), we assume that the geometric center (i.e., location K) of Plate A moves at a speed of $u_k = \zeta u$, where ζ is an amplification coefficient of the average speed. And then, the speed of any location S within this plate may be expressed with $u_s = u_k \sin\varphi_s / \sin\varphi_k$, where $\varphi_s(\varphi_k)$ is the angle distance of location

https://doi.org/10.5194/egusphere-2023-1458
Preprint. Discussion started: 3 August 2023

S (*K*) to the Euler pole (i.e., location *E*) relative to the Earth's center. The Euler pole is calculated through the location *K* and the orientation of the first driving torque τ. The speed u_s can be further decomposed into the longitudinal speed $u_{s\text{-}lo}$ and latitudinal speed $u_{s\text{-}la}$, and $u_{s\text{-}lo}=u_s\sin(\lambda_s\text{-}90^o)$, $u_{s\text{-}la}=u_s\cos(\lambda_s\text{-}90^o)$, where λ_s is the azimuth of arc *SE* with respect to latitude. The azimuth of the movement is then calculated through the longitudinal and latitudinal speeds. All these angles and distances (i.e., γ_i, λ_s, φ_k, φ_s) may be calculated through the latitudes and longitudes of related locations.

https://doi.org/10.5194/egusphere-2023-1458
Preprint. Discussion started: 3 August 2023

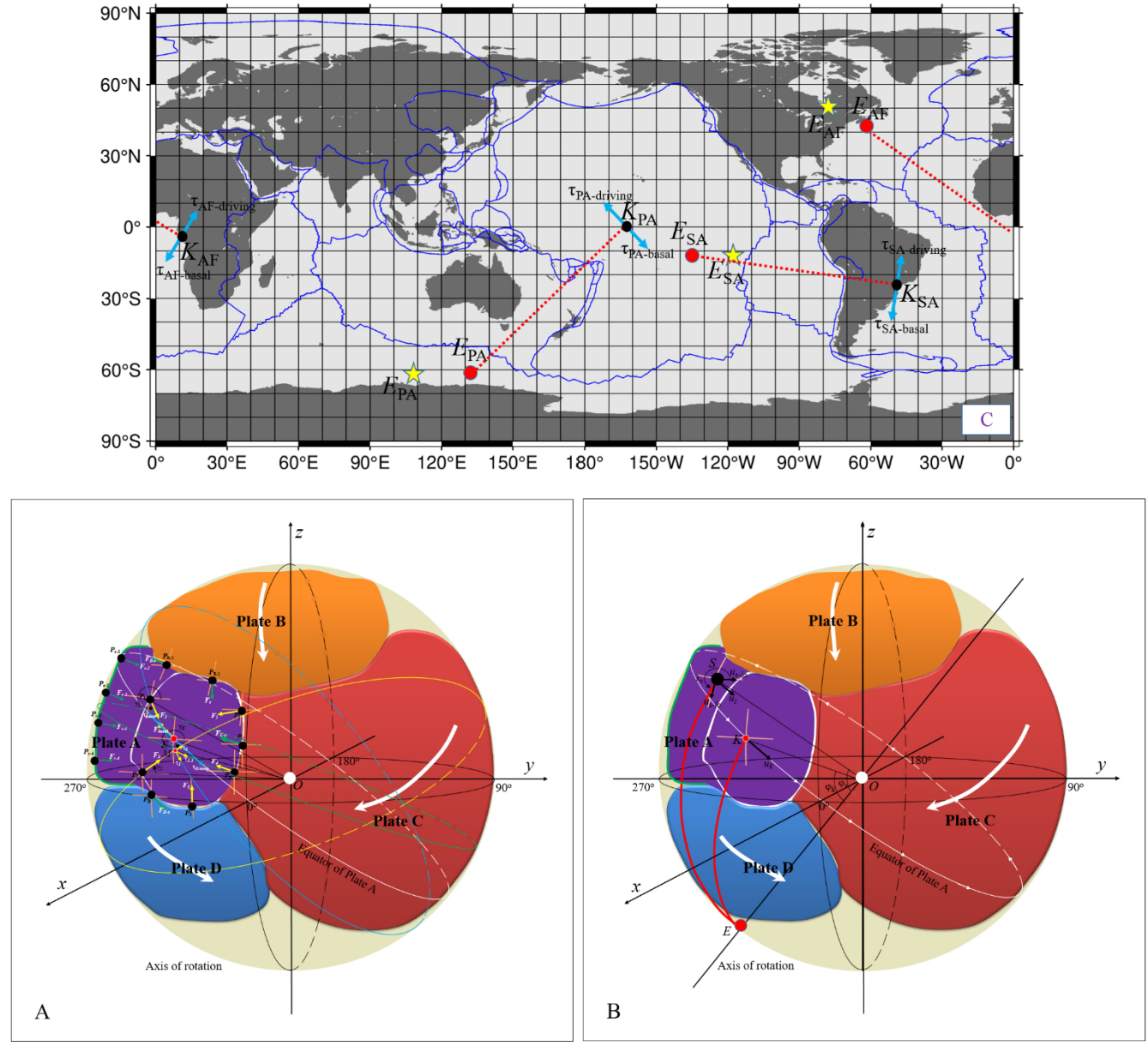

535

Figure 8: Modeling the torque balances for plate motion. (A) Geometry of horizontal forces, ridge push forces, collisional forces, and shearing forces over a spherical frame. The large light blue and yellow circles denote the orientations of the torques yielded by the horizontal force F_1 and F_2, the large green circle denotes the orientation of the combined torque of these two torques, and the large white circle denotes the possible orientation of the first driving torque. **(B) Decomposing**
540 **the average movement of the plate into the movement of any location.** The location K and E are the geometric center of

https://doi.org/10.5194/egusphere-2023-1458
Preprint. Discussion started: 3 August 2023

the plate and its Euler pole, respectively. **(C) Exhibiting the torque balance of the selected plates over a planar frame.** The calculated Euler pole locations (red dots) are compared to the established Euler pole locations (yellow stars).

We here use three plates (South American, African, and Pacific plates) to demonstrate the resultant movements. The geometric centers of these plates, the calculated Euler pole location, and the established Euler pole location cited from GSRM v.2.1 (Kreemer et al., 2014) are exhibited in Figure 8(C). A few other possible forces (i.e., collisional and shearing) are considered for these plates. For example, the Eurasian Plate provides a collisional driving force $F_{\text{EU-AF-C}}$ and a shearing driving force $F_{\text{EU-AF-S}}$ for the African Plate. The Nazca plate provides a collisional driving force $F_{\text{Naz-SA-C}}$ for the South American Plate. The Australian, North American, and Eurasian plates provide the collisional driving force $F_{\text{AU-PA-C}}$, $F_{\text{NA-PA-C}}$, and $F_{\text{EU-PA-C}}$ for the Pacific Plate, respectively. Again, we neglect slab pull. And if this force can be confirmed in the future, it may be added into this model.

The details of these forces have been exhibited in Figure 4 and listed in Table 1. The resultant torques from all related forces are listed in Table 4. The viscosity and thickness of the asthenosphere for these three plates are the same as that listed in the method I. The other parameters (i.e., plate area, the ratio of the net driving torque to the first driving torque, and the amplification coefficient) and the resultant average movements are listed in Table 5.

The movements of 215 locations (41 for the South American Plate, 70 for the African Plate, and 104 for the Pacific Plate) are reproduced by GSRM v.2.1. The calculated and reproduced movements are compared in Figure 9. We find that the calculated movements for these locations are basically consistent with the reproduced movements in both speed and azimuth, the RMS of the calculated speed against the reproduced speed for the South American, African, and Pacific plates is 0.98, 3.18, and 6.51 mm/yr, respectively. This result is not as good as that demonstrated in the method I. One major cause for this is that, in the method II the collisional and/or shearing forces considered are not enough. For example, the Australian, North American, and Eurasian plates collide the Pacific Plate extensively, the three collisional forces $F_{\text{AU-PA-C}}$, $F_{\text{NA-PA-C}}$, and $F_{\text{EU-PA-C}}$ are too spare relative to the long collisional zone; In addition, there may be shearing force between the North American Plate and the Pacific Plate, but we omit this force. As a result, the first driving torque that we calculate is not too accurate in both magnitude and orientation; Another cause for this is that the geometric center of a plate is strictly not calculated through the average of the latitudes and longitudes of those nodes. The less accurate first driving torque adds to the less accurate geometric center, naturally, the calculated Euler pole location and the resultant movement of the plate cannot be accurate. Even so, our goal is realized that a combination of the ocean-generated force, the ridge push force, the collisional force, and the shearing force indeed may be responsible for plate motion.

https://doi.org/10.5194/egusphere-2023-1458
Preprint. Discussion started: 3 August 2023

Table 4 (A). Parameters for the torques of three selected plates in the method II

Plate	Eule pole		No.	Horizontal force	Earth's radius	Torque	No.	Combined torque	
	E		i	F_i	R_{earth}	τ_i	j	τ_j	Inclination to latitude, east (γ_j)
	Latitude	Longitude		N (*10^{17})	m (*10^3)	N·m (*10^{23})		N·m (*10^{23})	Degrees
South America	-14.68°	224.18°	31	1.4573	6371.00	9.2848	31	9.2815	22.92°
			32	1.2059	6371.00	7.6829	31-32	16.8927	27.75°
			33	1.8014	6371.00	11.4769	31-33	26.8242	12.22°
			34	1.2737	6371.00	8.1145	31-34	34.5354	7.29°
			35	0.9484	6371.00	6.0420	31-35	39.7562	12.02°
			36	0.1551	6371.00	0.9883	31-36	39.7462	13.45°
			37	0.1161	6371.00	0.7397	31-37	39.1661	14.12°
			38	1.7897	6371.00	11.4020	31-38	34.9655	30.59°
			39	2.0480	6371.00	13.0480	31-39	31.7450	52.47°
			40	1.4398	6371.00	9.1732	31-40	35.3756	66.91°
			41	1.6295	6371.00	10.3814	31-41	36.7958	83.30°
			42	1.5804	6371.00	10.0688	31-42	27.5043	90.28°
			43	1.3853	6371.00	8.8257	31-43	21.2133	105.00°
			44	0.3300	6371.00	2.1025	31-44	21.1033	110.69°
			45	1.7285	6371.00	11.0123	31-45	10.0916	109.90°
			NA-SA-C	0.2000	6371.00	4.4597	31-NA-SA-C	9.5515	83.84°

https://doi.org/10.5194/egusphere-2023-1458
Preprint. Discussion started: 3 August 2023

Table 4 (B). Parameters for the torques of three selected plates in the method II (continued)

Plate	Eule pole		No.	Horizontal force	Earth's radius	Torque	No.	Combined torque	
	E		i	F_i	R_{earth}	τ_i	j	τ_j	Inclination to latitude, east (γ_j)
	Latitude	Longitude		N (*10^{17})	m (*10^3)	N·m (*10^{23})		N·m (*10^{23})	Degrees
Africa	44.43°	298.60°	46	1.1123	6371.00	7.0867	46	7.0867	320.52°
			47	1.7917	6371.00	11.4148	46-47	18.1425	334.91°
			48	1.6739	6371.00	10.6648	46-48	24.8049	357.55°
			49	1.7514	6371.00	11.1579	46-49	26.1494	22.67°
			50	0.9317	6371.00	5.9357	46-50	32.0830	22.36°
			51	1.5581	6371.00	9.9269	46-51	41.9838	23.48°
			52	1.3150	6371.00	8.3777	46-52	48.8835	17.47°
			53	1.4180	6371.00	9.0339	46-53	57.9100	17.86°
			54	0.9546	6371.00	6.0816	46-54	63.9220	18.73°
			55	0.2953	6371.00	1.8813	46-55	64.7399	20.24°
			56	1.0480	6371.00	6.6768	46-56	60.9224	25.24°
			57	1.1109	6371.00	7.0773	46-57	57.7443	31.35°
			58	0.6026	6371.00	3.8393	46-58	54.2170	32.90°
			59	0.9126	6371.00	5.8140	46-59	52.4030	38.84°
			60	1.5344	6371.00	9.7756	46-60	50.6747	49.55°
			EU-AF-C	4.2000	6371.00	26.7582	46-EU-AF-C	26.1669	66.52°
			EU-AF-S	0.8000	6371.00	5.0968	46-EU-AF-S	27.8008	56.25°
Pacific	-65.25°	136.77°	NA-PA-C	3.0000	6371.00	19.1130	NA-PA-C	19.1130	185.00°
			*AU-PA-C	2.2000	6371.00	14.0162	NA-PA-C-AU-PA-C	14.7433	138.26°
			EU-PA-C	0.1000	6371.00	0.6371	NA-PA-C-EU-PA-C	14.2742	136.56°

https://doi.org/10.5194/egusphere-2023-1458
Preprint. Discussion started: 3 August 2023

Note: * denotes this force is changed from 1.0×10^{17} N listed in Table 1 to 2.2×10^{17} N.

Table 5. The net driving torques and their resultant movements for three selected plates in the method II

Plate	Area	Ratio	Net driving torque	Geometric center of the plate			Earth's radius	Amplification coefficient	Movement
	A		$\tau_{driving}$	K		φ_k	R_{earth}		u
	km^2	ε	N·m (10^{23})	Latitude	Longitude	Degrees	m (10^3)	ζ	mm/yr
South America	43,600,000	0.30	2.8640	-24.39°	313.66°	83.84°	6371.00	1.20	11.71
Africa	61,300,000	0.40	11.1202	-5.57°	13.43°	56.25°	6371.00	1.20	32.33
Pacific	103,300,000	0.35	4.9960	0.10°	198.65°	136.56°	6371.00	1.20	71.82

https://doi.org/10.5194/egusphere-2023-1458
Preprint. Discussion started: 3 August 2023

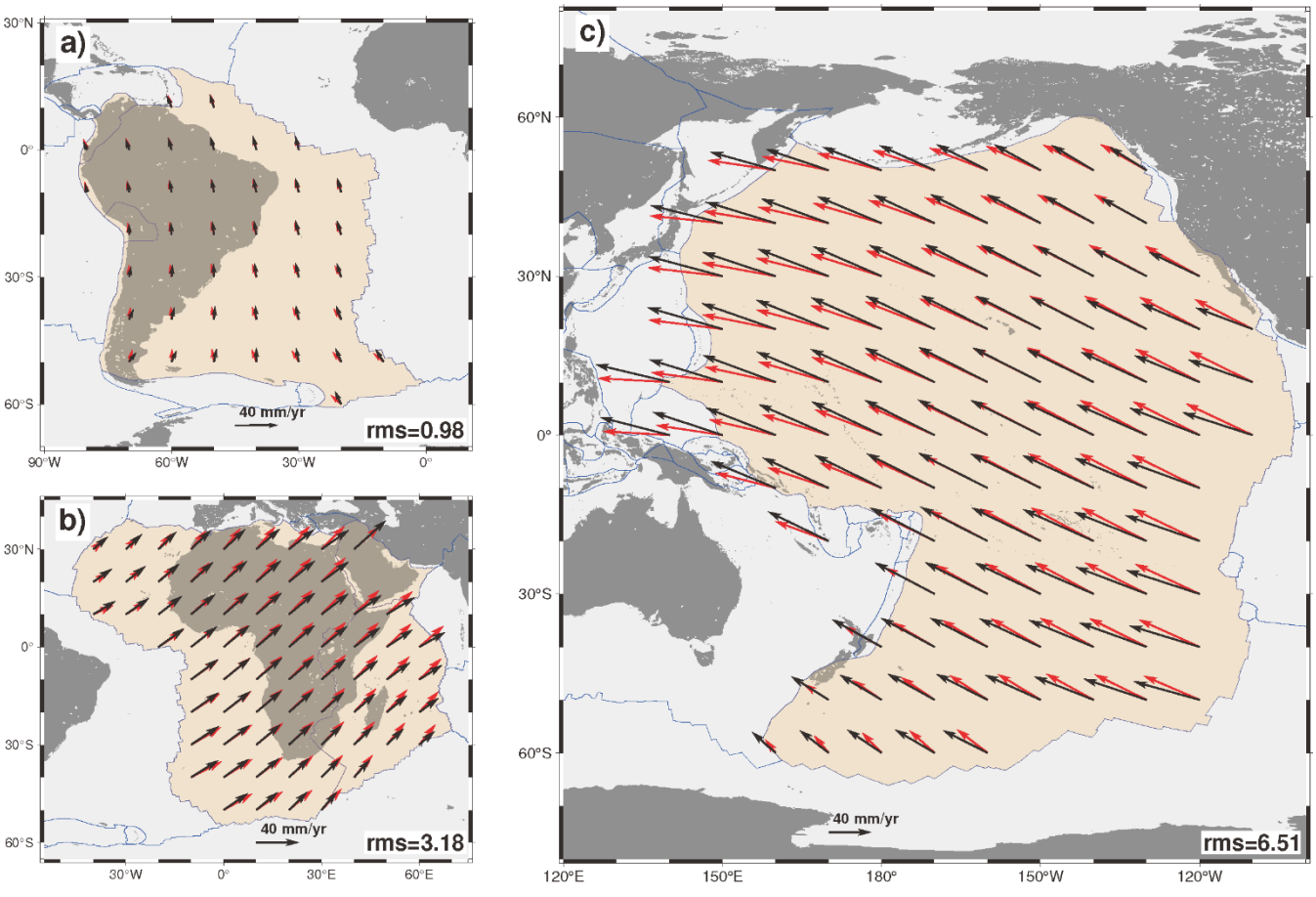

Figure 9: The reproduced movements from GSRM v.2.1 (black arrows) verse the calculated movements from our model (red arrows) in the method II. a), b), and c) are the South American, African, and African plates, respectively.

https://doi.org/10.5194/egusphere-2023-1458
Preprint. Discussion started: 3 August 2023

3.3 Resultant stress

As mentioned in section 2.2, the observed stresses are mostly concentrated on the uppermost part of the lithosphere (Zoback, 1992; Zoback et al., 1989; Zoback & Magee, 1991), whereas our modeling analysis suggests that the stress caused by the existing forces (i.e., the ridge push, basal friction, and collisional) are mainly concentrated on the lower part of the lithosphere. This discrepancy indicates that other force may be responsible for the observed stresses. Ocean water is loaded on the top of the lithosphere, this allows to create a stress field associated with the upper part of the lithosphere.

To examine this expectation, we add the ocean-generated force onto the model that is exhibited in Figure 2 (top). The final model is shown in Figure 10 (top left). The inputs include the vertical pressure caused by the rock's weight and the lateral pressures caused by these loads (i.e., F_{RW}, F_{LW}, F_{RP}, F_b, and F_c). F_{RW} and F_{LW} are the ocean-generated forces, they correspond to a result of 5 km water depth at the right and 3 km water depth at the left, respectively, and $F_{RW}=0.12\times10^{12}$ N m^{-1}, $F_{LW}=0.04\times10^{12}$ N m^{-1}. The outputs include the stress produced by the vertical pressure alone and the stress produced by a combination of the vertical and lateral pressures. Similarly, we will only discuss the horizontal stress (i.e., S11) in the following section. At this time, we first use these loads to yield Set A data and Set B data. The stress clouds of the area *GHIJ* are compared in Figure 10 (middle left). To realize a visual impression, we magnify these loads 50 times, which yields Set A' data and Set B' data. We find that the horizontal stress caused by these loads is compressional and tends to distribute across the middle part of section *GHIJ*. We then minify F_{RP} and F_b 100 times, remain F_{RW} and F_{LW} stable, and adjust F_c properly so as to sustain the horizontal force balance, this yields Set C data and Set D data. To realize a visual impression, we again magnify these revised loads 50 times, which yields Set C' data and Set D' data. A more detailed description of these loads for different sets is exhibited in Figure 10 (top right). It can be found that, after F_{RP} and F_b are reduced, the horizontal stress caused by these loads are mainly concentrated on the upper part of section *GHIJ*.

The stress diagrams for three sections (i.e., M_1N_1, M_2N_2, and M_3N_3) are also collected and compared in Figure 11. When we subtract the stress caused by the rock's weight from the stress caused by the rock's weight and these loads (i.e., F_{RW}, F_{LW}, F_{RP}, F_b, and F_c), we obtain the stress caused by these loads, which are expressed with Set A/B/C/D - Set I. We find that the result of the stress diagrams agrees that of the stress clouds. The continental plates are not only rigid but also curved, this allows the ocean-generated forces (i.e., the horizontal forces) to laterally penetrate across the plate. Our modeling analysis suggests that the stress caused by a combination of the ocean-generated force, ridge push force, collisional force, and basal friction force may be in accordance with the observed stresses.

https://doi.org/10.5194/egusphere-2023-1458
Preprint. Discussion started: 3 August 2023

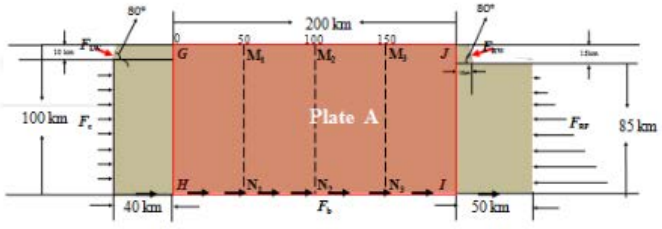

No.	Loads (*10^{12} N/m)				
	F_{RP}	F_b	F_c	F_{RW}	F_{LW}
Set A	4.00	3.20	0.87	0.12	0.04
Set B	4.00	2.00	2.08	0.12	0.04
Set C	0.04	0.03	0.09	0.12	0.04
Set D	0.04	0.02	0.10	0.12	0.04
Set A'	200.00	160.00	43.74	6.13	2.21
Set B'	200.00	100.00	103.92	6.13	2.21
Set C'	2.00	1.60	4.32	6.13	2.21
Set D'	2.00	1.00	4.92	6.13	2.21

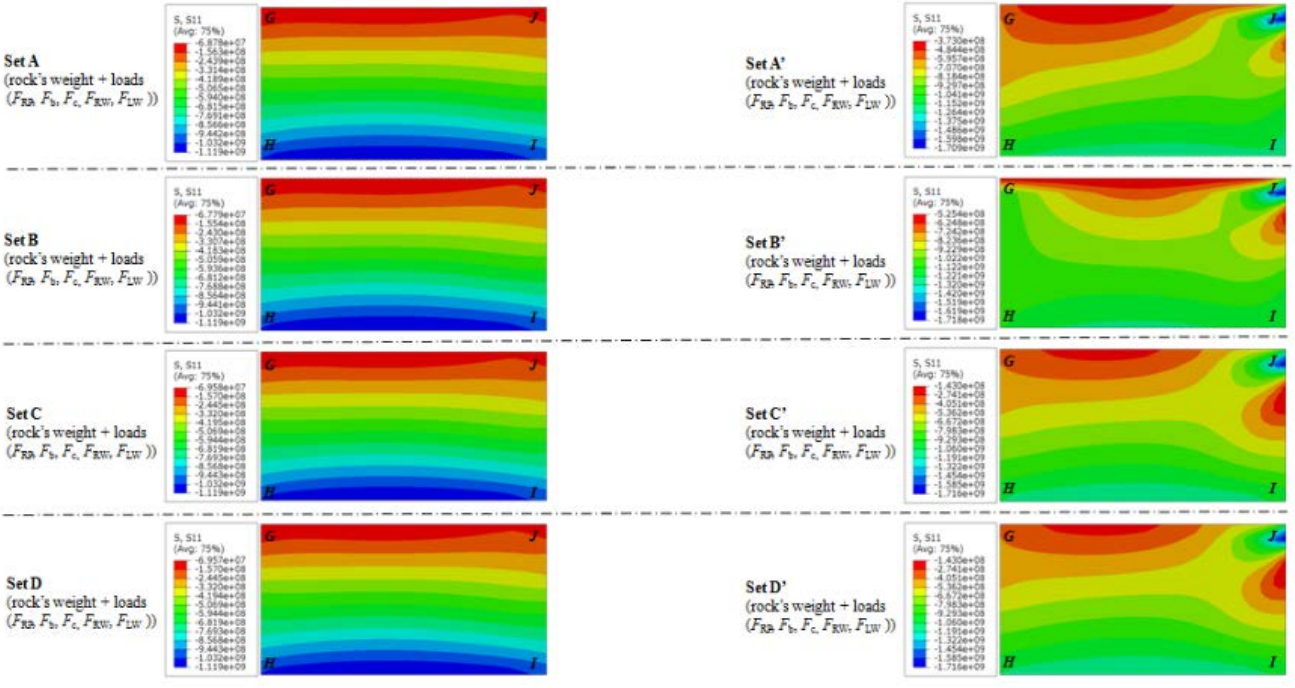

Figure 10: Stress cloud comparison. F_{RW} and F_{LW} denote the ocean-generated forces, respectively. F_{RP}, F_b, and F_c denote the ridge push force, the basal friction force, and the collisional force.

https://doi.org/10.5194/egusphere-2023-1458
Preprint. Discussion started: 3 August 2023

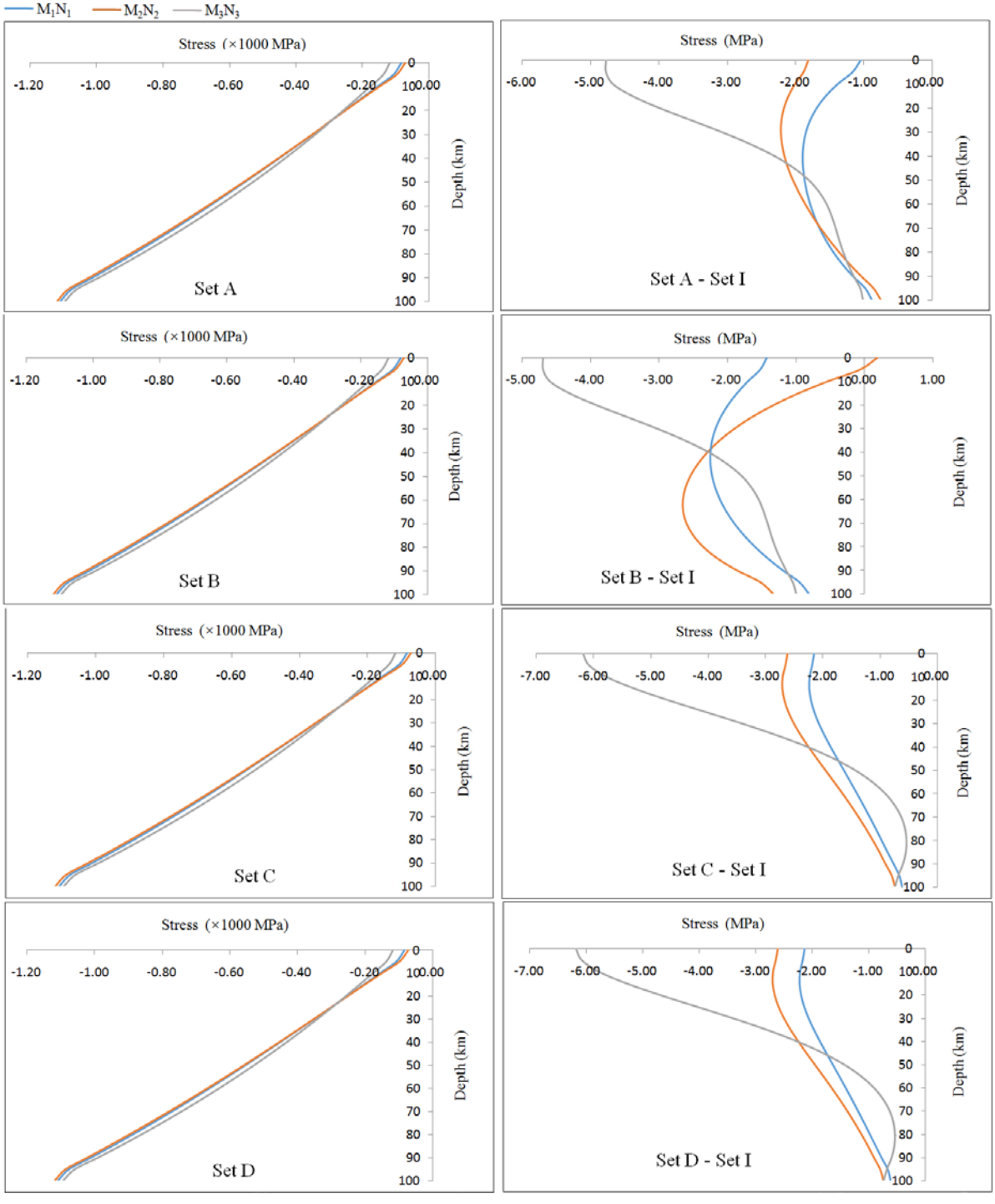

Figure 11: Stress diagram comparison.

https://doi.org/10.5194/egusphere-2023-1458
Preprint. Discussion started: 3 August 2023

The lithospheric plates are curved, the rocks within them are not homogeneous and isotropic, and their thickness and density also vary spatially; in addition, as seen in Figure 4, the directions of the ocean-generated force are various. We expect that the stresses caused by a combination of the ocean-generated force and all of these factors may realize a better match with the observed stresses in the WSM, and this will be included in the following research.

4 Discussion

4.1 Why may ocean-generated force drive plate motion?

Although we have demonstrated that the movements estimated from ocean-generated force are consistent with observations, many people still refuse this force to be a plate driving force for the following reasons: 1) The ocean constitutes just another deviation from the true radial density distribution of the Earth. Any “lateral” density heterogeneity creates stresses that in turn lead to deformation, and their extent is controlled by the rheological properties of the involved materials. 2) Plate motion determines the shape of the ocean basin; as a result, ocean water cannot contribute to plate motion. 3) Ocean loading on top of the lithosphere does not allow ocean-generated force to drive the lithospheric plates to move along the asthenosphere, this is similar to that the water held in a container standing on the ground cannot drive the container to move along the ground. 4) Ocean-generated force is too small to drive plate motion. These issues need to be clarified here. First, the view that any “lateral” density heterogeneity would lead denser materials (i.e., rocks) to flow toward lighter materials (i.e., air or water) is rather idealized. The Himalayas are denser than the surrounding air and water, but this density heterogeneity does not allow the mountains to reduce their height; instead, they increasingly rise up. The continents are also denser than the oceans, and if they flow toward the oceans, the ocean basin will be filled by the continent's rock substances. Then, the sea level would rise, causing water to submerge the coast. This would result in a decrease in the landmass area. Given the continent's volume is constant, then, the continent's height would reduce. This is evidently contrary to the continental accretion that is widely accepted by the geophysical community. The continental accretion indicates that the continents have been growing since the Archean. A further review of this topic can be found in this recent research (Zhu, et al., 2021). The examples of the Himalayas and continents suggest that a system composed of ocean water and the crust is permanently disturbed by the hydrostatic pressure force and tides; As a result, it is difficult for the continents to follow the principle of “lateral” density heterogeneity to flow toward the oceans. It is an opinion of this author that ocean water compresses the crust, the elasticity of the crust's rock allows the crust to deform as a response to the hydrostatic pressure force. With the passage of time, the ocean basin expands gradually, and then the water in the seas flows toward the ocean basin, and the sea level decreases to cause part of the seafloor to expose and become landmass. In addition, the continent's height increases relative to the sea level. This process simply accords with the continental accretion. Indeed, plate motion may reshape ocean basin, but ocean water is not passive, it may provide feedback through energy dissipation on the plate, and as a result, affect plate motion. Ocean loading on the lithosphere is far different from water loading in a container. Since the lithosphere has been broken into individual plates and these plates are attached to

https://doi.org/10.5194/egusphere-2023-1458
Preprint. Discussion started: 3 August 2023

the underlying viscous asthenosphere, this situation allows ocean-generated force to interact with the basal friction exerted by the asthenosphere on the plate. In contrast, a container is perfect, and the force produced by water pressure within the container is balanced out by the container itself and cannot interact with the basal friction exerted by the ground on the container. In physics, the interaction of a driving force and a resistive force is a precondition for an object to move.

Figure 12 outlines how force balances may be created for the plates. Three plates are totally designed in the model; along the vertical direction, the weight of each plate is balanced out by the support from the asthenosphere; thus, we will only consider the force along the horizontal direction. F_{AR}, F_{AL}, F_{CL}, and F_{CR} are the horizontal forces, F_{RL} and F_{RR} are the ridge push forces, F_{BA}, F_{AB}, F_{CB}, and F_{BC} are the collisional forces, f_A, f_B, and f_C are the basal friction forces. Slab pull and trench suction are neglected. Each of these forces can yield a torque relative to the Earth's center, because torque is a product of force and lever arm, and here the lever arm may be represented with the Earth's radius since plate is too thin relative to the Earth's radius, the lever arm length of one plate is approximately equal to that of another plate. This situation allows to simplify torque balance into force balance for the following discussion. We assume that Plate A rotates counterclockwise and Plate C rotates clockwise. For Plate A, we set F_{RL}= 4.0×10^{12} N m^{-1}, this magnitude is presently accepted by geophysical community (Turcotte and Schubert, 2004). We assume the ocean depth to be 5.00 km at the right and 3.00 km at the left, respectively. These two depths correspond to F_{AR}= 0.245×10^{12} N m^{-1} and F_{AL}= 0.0882×10^{12} N m^{-1}, the final horizontal force of these two forces would be F_{AR}-F_{AL} = 0.1568×10^{12} N m^{-1}. We set F_{BA}= 4.05×10^{12} N m^{-1}, and use F_{RL} = 4.0×10^{12} N m^{-1} and a little portion of the final horizontal force, which is represented by F_{ARL} = 0.05×10^{12} N m^{-1}, to balance out F_{BA}, and use the remaining final horizontal force F_{RARL}= 0.1068×10^{12} N m^{-1} to balance out the basal friction force f_A. The force balances for this plate would be F_{BA}- F_{RL}- F_{ARL}= 0 and F_{RARL}-f_A=0.

For Plate B, we set F_{CB}=4.0×10^{12} N m^{-1}, due to F_{BA}= F_{AB}= 4.05×10^{12} N m^{-1}, thus, F_{BA}- F_{CB} =0.05×10^{12} N m^{-1}. We use this net force to balance out the basal friction force f_B. The force balance for this plate would be F_{BA}- F_{CB} -f_B=0.

For Plate C, we set F_{RR}= 3.95×10^{12} N m^{-1}, and assume the ocean depth to be 4 km at the left and 6 km at the right, respectively. These two depths correspond to F_{CR}= 0.1568×10^{12} N m^{-1} and F_{CL} = 0.3528×10^{12} N m^{-1}, the final horizontal force of these two forces would be F_{CL} - F_{CR}=0.196×10^{12} N m^{-1}. Due to F_{CB} = F_{BC} =4.0×10^{12} N m^{-1}, we set F_{RR}= 3.95×10^{12} Nm^{-1} and use a little portion of the final horizontal force, which is represented by F_{CLR} = 0.05×10^{12} N m^{-1}, to balance out F_{BC}, and use the remaining final horizontal force F_{RCLR} = 0.146×10^{12} N m^{-1} to balance out the basal friction force f_C. The force balances for this plate would be F_{BC}- F_{RR}-F_{CLR} = 0 and F_{RCLR}-f_C=0.

These force balances allow three plates to be steadily rotated. We find, even if the ridge push force F_{RL} (F_{RR}) is given a smaller amplitude (~ 10^{10} N m^{-1}, for example), so long as the collisional force F_{BA} (F_{AB}, F_{CB}, and F_{BC}) is properly valued, these force balances can always be created. Nevertheless, as demonstrated in section 3.3, a ridge push force of 4.0×10^{12} N m^{-1} would result in a horizontal stress that is mostly concentrated on the lower part of the lithosphere, which is not in accordance with observation. Hence, we prefer to accept the ridge push force to be smaller than ocean-generated force.

https://doi.org/10.5194/egusphere-2023-1458
Preprint. Discussion started: 3 August 2023

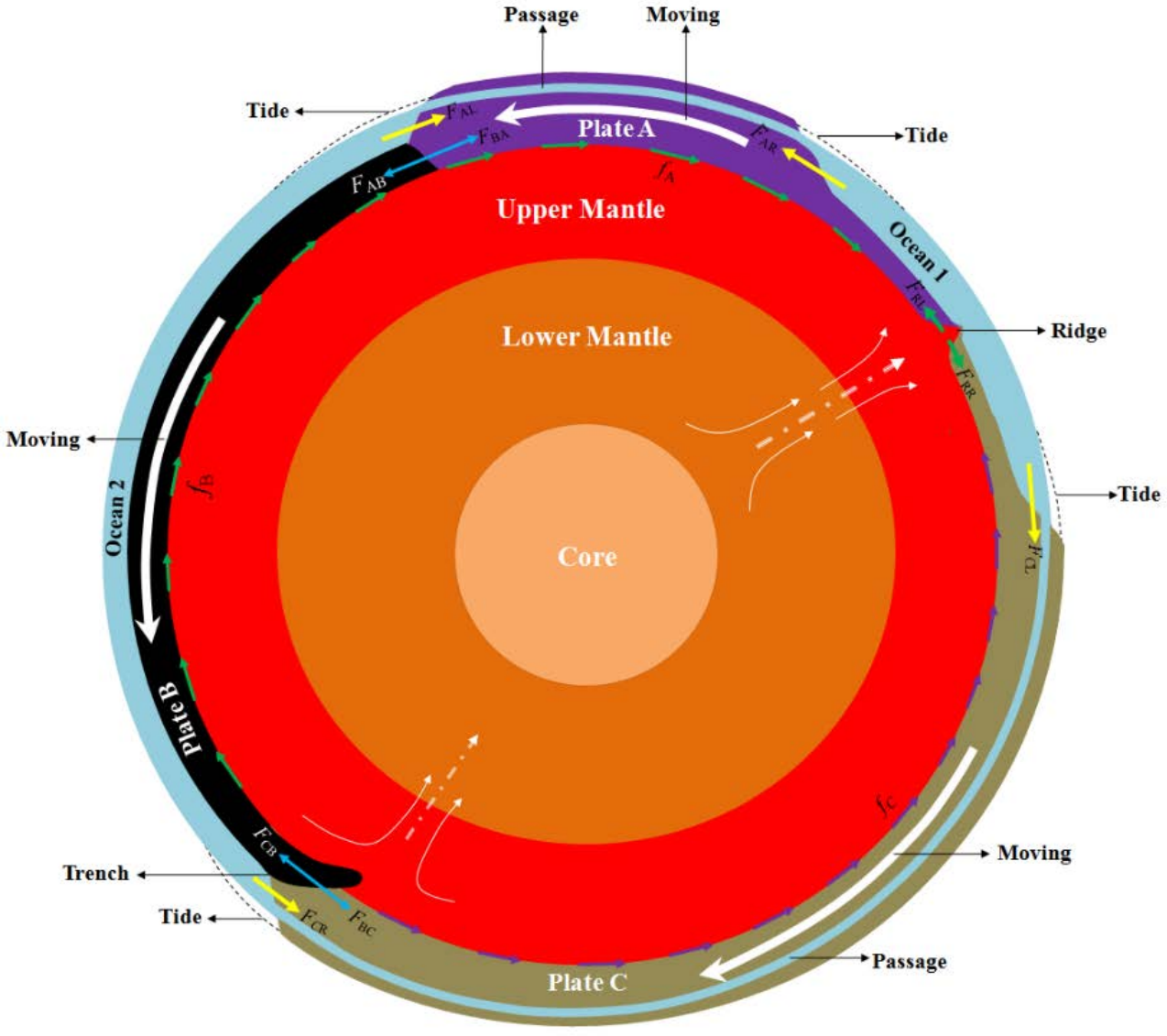

725 **Figure 12: Modeling the dynamics of the lithospheric plates.** Blue passages denote water compensation from one ocean to another. Note that the ocean depth, tide, plate's thickness, mantle, and core are highly exaggerated.

https://doi.org/10.5194/egusphere-2023-1458
Preprint. Discussion started: 3 August 2023

4.2 How does plate motion realize mechanically?

Thus far, we have concluded that ocean-generated force is able to combine the ridge push force, the collisional force, and the shearing force to satisfy the kinematics and geometry of plate motion. Now, let us discuss how plate motion can be mechanically realized. As shown in Figure 12, it is assumed that the depth of Ocean 1 is greater than that of Ocean 2. If we use a part of Ocean 2 that connects to Plate A, which is equal in length to Ocean 1, to do comparison, the depth difference between this part of Ocean 2 and Ocean 1 creates a net gravitational potential energy relative to the asthenosphere reference level. As Plate A and Plate B move away from each other, this separation would require the Ocean 1 depth to decrease as the basin elongates horizontally, and require the Ocean 2 depth to increase as the basin shortens horizontally. Consequently, the net gravitational potential energy decreases. Therefore, if there were no external energy inputs to compensate, the net gravitational potential energy would eventually disappear, terminating plate motion. Tides may be supplying this energy. Tides represent the regular alternations of high and low water on Earth; when high water falls, the gravitational potential energy converts into kinetic energy, then, ocean water obtains movement. As all oceans are physically connected, part of the water in Ocean 2 may travel via passages to compensate the decreasing ocean depth of Ocean 1, thus sustaining the net gravitational potential energy. Given the basal friction force f_{basal} = 1.62×10^{18} N and the movement distance u=3 cm/yr for the lithosphere, an energy of $Q_1=f_{basal}\times u=4.86\times10^{16}$ J/yr is required to satisfy this movement distance. This energy also represents the net gravitational potential energy. The ocean water level often increases twice a day due to tides, and the resultant height is assumed to be h=0.3 m. Given the gravitational acceleration g=9.8 m/s, the volume v=1.35×10^9 km^3 and density ρ=1000 kg/m^3 for the whole ocean, and consequently, the gravitational potential energy obtained by ocean water due to tides during a year would be $Q_2=2*365*\rho vgh=2.9\times10^{21}$ J/yr. The transformation from gravitational potential energy to kinetic energy within ocean water and the energy transition between oceans must be complicated, and we believe that a small part of this tidal energy is enough to supply the net gravitational potential energy. In fact, the impact of tidal energy on plate motion has long been discussed. Wegener (1924) proposed that tides cause a slight progressive displacement of the crust. Rochester (1973) showed that the total energy released due to tidal friction exceeds $5*10^{19}$ ergs/s. Several authors (e.g., Miller, 1966; Munk, 1968) concluded that the dissipation in both shallow seas and on the solid Earth is approximately $2*10^{19}$ ergs/s, and this amount of energy exceeds the lower bound set by seismic energy release by 2 orders of magnitude (Gutenberg, 1956) and might be driving the plate motion. Other authors (e.g., Riguzzi et al., 2010; Egbert and Ray, 2000) reevaluated the energy budget and found that the total energy released by tidal friction may reach up to $1.2*10^{20}$J/yr, and approximately $0.8*10^{20}$J/yr is dissipated in the oceans, shallow seas, and mantle, and the remaining energy is enough to maintain the lithosphere's rotation, estimated at approximately $1.27*10^{19}$J/yr. In contrast to these studies, we provide another insight: the tidal energy obtained by ocean water may feed plate motion.

https://doi.org/10.5194/egusphere-2023-1458
Preprint. Discussion started: 3 August 2023

4.3 Does the tidal forcing relate to plate motion or seismicity?

4.3.1 Tidal force versus plate motion

The impact of tidal drag on plate motion has been debated for many years. Wegener (1915) attributed the continent's drift to tidal drag and centrifugal forces, but these forces were shortly found to be too weak to work. Jeffreys (1929) claimed that the mean tidal friction corresponds to a westward stress of the order of only 10-4 dyn/cm^2 over the earth's surface, this stress is too small to maintain the drift. The notion of tidal drag revived after the discovery of a net rotation or westward drift of the lithosphere relative to the mantle (Le Pichon, 1968; Knopoff and Leeds, 1972). Another argument in favor of this notion stems from the assessment of energy budget, as discussed in section 4.2, it shows that tides are energetically enough for feeding plate motion. However, a satisfaction in energy cannot shield the notion of tidal drag anymore. Jordan (1974) and Jeffreys (1975) attached the theoretical basis of tidal drag, they claimed that the viscosity both related to tidal drag and necessary to allow decoupling between lithosphere and mantle (~10^{11} Pas) is far less than the present-day asthenosphere viscosity. Ranalli (2000) also showed that any non-zero torque due to difference in angular velocity between the mantle shell and lithosphere shell would be extremely transient, and cannot be a factor in the origin of the westward drift of the lithosphere. Despite these fierce objections, the advocators of tidal drag didn't give up. Scoppola et al. (2006) proposed the westward rotation of the lithosphere as a consequence of the combined effect of tidal torque, downwelling of the denser material into the mantle, and thin layers of very low viscosity hydrate channels in the asthenosphere. Several authors (e.g., Riguzzi et al., 2012; Doglioni and Panza, 2015) had suggested that, if an ultra-low viscosity layer exists in the upper asthenosphere, the horizontal component of the tidal oscillation and torque may be able to move the lithosphere. As demonstrated in section 3.2, laboratory experiments tend to support this possibility (Bercovici et al., 2015; Mei et al., 2002; Hirth and Kohlstedt, 1996; Scoppola et al., 2006; Doglioni et al., 2011). The asthenosphere's effective viscosity can be lowered to 10^{15} Pas if the water content in the case of both diffusion and dislocation creep is included (Korenaga and Karato, 2008). A "superweak", low-viscosity asthenosphere is being accepted by the geophysical community (Kawakatsu et al., 2009; Hawley et al., 2016; Holtzman, 2016; Naif et al., 2013; Freed et al., 2017; Hu et al., 2016; Stern et al., 2015; Bercker, 2017). Zaccagino et al. (2020) recently investigated a 20-year series of plate motion to conclude that plate motion relates to tidal drag in some way. For example, the lithospheric plates retain a non-zero horizontal component of the solid Earth tidal waves, and they move faster with frequencies of 8.8 and 18.6 years that correlate to lunar apsides migration and nodal precession.

We provide a few points to respond to the notion of tidal drag. First of all, the lithosphere's net rotation or westward drift is different from plate motion. The former indicates that the lithosphere is moving in a single direction, while the latter indicates that the lithospheric plates are moving in different directions. Second, it is already established in the astronomical field that tidal drag is operated through the tractive force. This force is geometrically decomposed from a tide-generating force, and its direction always follows the Earth's surface. Apparently, this force may be divided into two symmetric fields that are aligned with the Earth-Moon system. In each field the force vector is uniformly directed to the sub-lunar points, which are projections

https://doi.org/10.5194/egusphere-2023-1458
Preprint. Discussion started: 3 August 2023

of the Moon on the Earth's surface. Two patterns are expected for the lithospheric plates under the tractive force. One is that, as the Earth rotates around its axis, all the plates are continuously swept from east to west. Another is that parts of the lithosphere, which are located at middle and high latitudes, would be dragged toward lower latitudes. Nevertheless, upon comparison with the plate motion vector (Figure 13), it becomes evident that the tractive force is not in accordance with the plate motion. The Pacific Plate, for instance, moves northwest, the Eurasian Plate rotates clockwise, the North American Plate rotates counterclockwise, the African and Indian-Australian Plates move northeast. Moreover, the movements of the Pacific, Eurasian, and Indian-Australian plates intersect with each other. The diversity of plate motion implies that each plate is being operated by a set of independent forces, with a leading force controlling the direction of plate motion. Third, it has been found that the plates performed a cycle of dispersal and aggregation during a geological timescale, and that three supercontinents (i.e., Pangaea, Rodinia and Columbia) occurred over the past 2 billion years (Mitchell et al., 2021). This cycle of dispersal and aggregation is a manifestation of plate motion. When projected on the Earth's surface, the Moon's position is mostly between 18° N and 18° S (Pugh and Woodworth, 2014), which means that the tractive force on the Earth's surface remains relatively steady. Consequently, a relatively steady tractive force is not compatible with a secular cycle of plate motions. Last, we agree with Zaccagino et al. (2020) that tidal drag contributes to plate tectonics. Although there is a difference in tidal amplitude/direction between the plates, tidal drag permanently imparts energy into the system of plates, thereby allows for a modulation of plate tectonics.

https://doi.org/10.5194/egusphere-2023-1458
Preprint. Discussion started: 3 August 2023

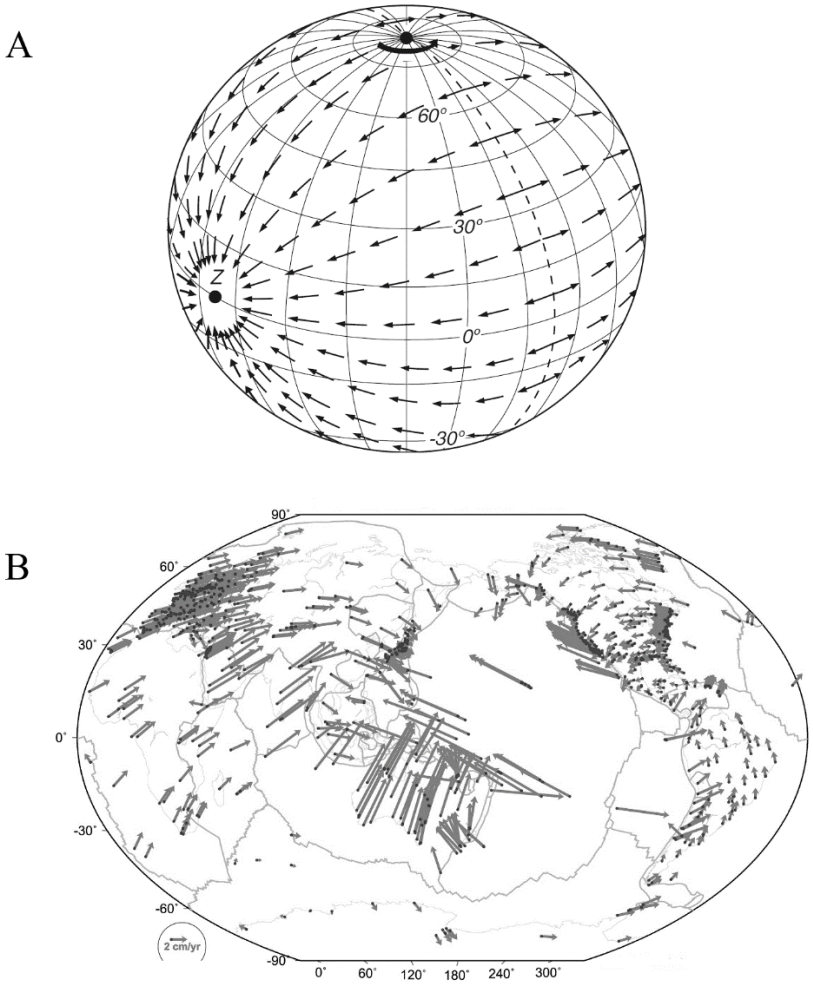

Figure 13: The tidal tractive force (A) versus plate motion (B). The tractive force on Earth is the situation when the Moon is above the Equator at Z (Robert, 2008). ITRF2014 horizontal velocity field of plate motion is from Altamimin et al. (2016).

4.3.2 Tidal force versus seismicity

Whether the tidal forcing relates to earthquake occurrence is a considerably hot topic. Most studies with global earthquake catalogs tend to show no correlation between the two (e.g., Schuster, 1897; Morgan et al., 1961; Hartzell and Heaton, 1989). Some of regional earthquake catalogs reveal a significant correlation (e,g., Young and Zurn, 1979; Ulbrich et al., 1987; Shirley, 1988), but others also revealed no correlation (Knopoff, 1964; Shlien, 1972; Shudde and Barr, 1977; Vidale et al., 1998). Nevertheless, these studies explored only the effect that is caused by solid Earth tide, the effect caused by ocean tide (i.e., the loading) is commonly ignored. By adding ocean tide to solid Earth tide, Tsuruoka et al. (1995) reached a point that a decrease in the confining pressure due to the tidal forcing is responsible for triggering earthquake occurrence. Tanaka et al.

https://doi.org/10.5194/egusphere-2023-1458
Preprint. Discussion started: 3 August 2023

(2002) expanded the method taken by Tsuruoka et al. (1995), they investigated 9350 globally distributed earthquakes with magnitude 5.5 or larger to conclude that a small stress change due to the tidal forcing encourages earthquake occurrence. The results of these studies (e.g., Tsuruoka et al., 1995; Tanaka et al., 2002) suggest that ocean tide plays a crucial role in determining the correlation.

If ocean tide really relates to earthquake occurrence, then it must depend on ocean water exerting its impact. For example, when a tide is added to the ocean, the ocean water depth will vary, the ocean water pressure will also vary. Ocean water pressure variation is not only vertically applied to the oceanic crust that is below the ocean, but also horizontally applied to the continental crust that connects to the ocean. Guillas et al. (2010) presented a link between the El Niño-Southern Oscillation (ENSO) and earthquake occurrences on the East Pacific Rise (EPR), and proposed that a reduction in ocean-bottom pressure over the EPR may encourage seismicity. A recent study found that sea level changes affect seismicity rates in a hydrothermal system near Istanbul (Martínez-Garzón et al., 2023). As pointed out by Tanaka et al. (2002), the most likely component to control the earthquake occurrence is the stress. Since tide represents a periodic oscillation, it should be expected that the stress produced by ocean water will behave periodically. In these studies (e.g., Tsuruoka et al., 1995; Tanaka et al., 2002; Martínez-Garzón et al., 2023), the tidal stress is theoretically estimated, but there is no modelling or experimental evidence for the tidal stress. In section 3.3, we have modelled the crust's stress through a combination of various forces (i.e., the ocean-generated force, the ridge push force, the collisional force, and the basal drag force), in which the ocean-generated force is constant. Below, we explore the stress when the ocean-generated force varies due to tide, in order to provide support for past and future studies.

The model (Figure 14) is based on that of Figure 10 (top left). The inputs include the hourly vertical pressure caused by the rock's weight and the hourly lateral pressures caused by these loads (i.e., F_{RW}, F_{LW}, F_{RP}, F_b, and F_c). Note, the solid body tide is neglected. F_{RW} and F_{LW} are the ocean-generated forces that assimilate the effect of tides. We here design a water level variation of totally 12 hours, which corresponds to a semidiurnal tide. The information of tidal height and loads is listed in Table 6. The outputs include the hourly stress produced by the vertical pressure alone and the hourly stress produced by a combination of the vertical and lateral pressures. Using the latter to subtract the former, we obtain the hourly stress produced by the lateral pressures. Similarly, we only discuss the horizontal stress (i.e., S11). At this time, we collect the results of 6 locations (i.e., ①, ②, ③, ④, ⑤, and ⑥) to do comparison. These locations belong to the 30 km depth and 60 km depth of three sections (i.e., M_1N_1, M_2N_2, and M_3N_3).

The stress diagrams for these locations are compared in Figure 15. We find that the stress oscillation due to ocean tide has laterally penetrated the crust's rock. This study has not yet considered the stress in the oceanic crust, but the result is expected. For example, ocean water exerts pressure on the oceanic crust, which produces stress for the oceanic crust; when tide is added to the ocean, the stress is mechanically entrained to oscillate. As depicted in Set C(D) - Set I of Figure 11, the stress generated over a depth of 50 km is approximately 2.0 to 6.0 Mpa. This magnitude has fallen within the range of earthquake stress drops (1~30 Mpa) (Kanamori, 1994), indicating that the ocean-generated force may closely relate to

https://doi.org/10.5194/egusphere-2023-1458
Preprint. Discussion started: 3 August 2023

earthquake occurrence. Please be aware of that our model is straight, the rock's materials within it are assumed to be homogeneous and isotropic. In practice, the Earth's surface is curved, the rock's materials are not only inhomogeneous but also anisotropic. The oceans circle the continents, which leads to the continents being laterally compressed inward. All of these factors allow the ocean water pressure to be amplified in the crust, resulting in a higher stress level.

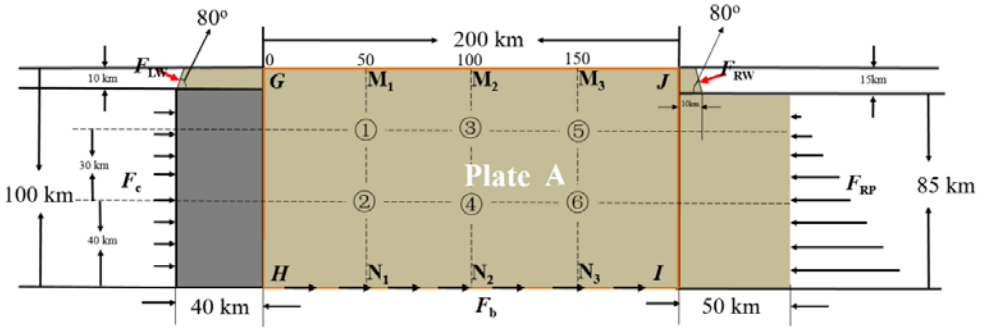

Figure 14: Model for oscillating ocean water.

Table 6. Information of tidal height and loads

Time (h)	Tidal height (m)	Loads (*10^{11}N/m)				
		F_{LW}	F_{RW}	F_{RP}	F_b	F_c
0	0.0	0.4410000000	1.2250000000	0.4000000000	0.2000000000	1.0000000000
1	0.4	0.4411176078	1.2251960078	0.4000000000	0.2000000000	1.0000000000
2	0.8	0.4412352314	1.2253920314	0.4000000000	0.2000000000	1.0000000000
3	1.2	0.4413528706	1.2255880706	0.4000000000	0.2000000000	1.0000000000
4	0.8	0.4412352314	1.2253920314	0.4000000000	0.2000000000	1.0000000000
5	0.4	0.4411176078	1.2251960078	0.4000000000	0.2000000000	1.0000000000
6	0.0	0.4410000000	1.2250000000	0.4000000000	0.2000000000	1.0000000000
7	-0.4	0.4408824078	1.2248040078	0.4000000000	0.2000000000	1.0000000000
8	-0.8	0.4407648314	1.2246080314	0.4000000000	0.2000000000	1.0000000000
9	-1.2	0.4406472706	1.2244120706	0.4000000000	0.2000000000	1.0000000000
10	-0.8	0.4407648314	1.2246080314	0.4000000000	0.2000000000	1.0000000000
11	-0.4	0.4408824078	1.2248040078	0.4000000000	0.2000000000	1.0000000000

https://doi.org/10.5194/egusphere-2023-1458
Preprint. Discussion started: 3 August 2023

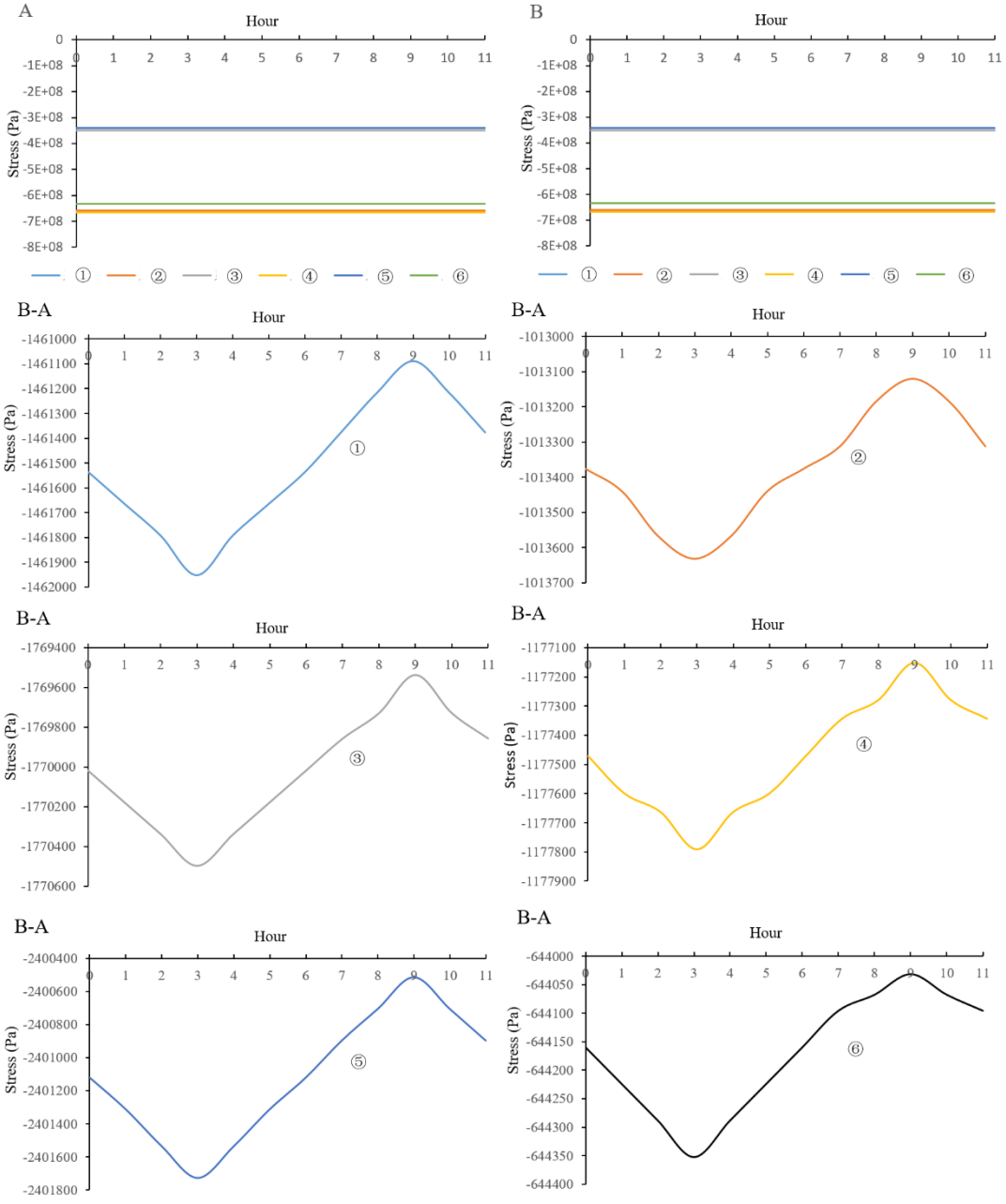

Figure 15: The stress variation out to time. Note, the stress variations in A and B are too small to be perceptible.

https://doi.org/10.5194/egusphere-2023-1458
Preprint. Discussion started: 3 August 2023

4.4 How may plate motion initiate and proceed?

The dispersal and aggregation of plates represent that the ocean basin had been periodically adjusted, and this change is often called the Wilson Cycle (Wilson, 1963). Figure 16 outlines how such a cycle may be realized. It is assumed that the left end of the model is connected to its right end and that the depth of Ocean 1 depth is greater than that of Ocean 2. The greater ocean depth corresponds to greater ocean-generated force. Slab pull and trench suction are neglected. The ocean-generated force, the collisional force, and the basal friction force combine to form force balances. For instance, the force balance for Plate A is F_{AL}-F_{AR}-F_{CA}-f_A=0, the force balance for Plate B is F_{BR}-F_{BL}-F_{CB}-f_B=0, and the force balance for Plate C is F_{AC}-F_{BC}-f_C=0. At time t_1 and t_2, these force balances allow Plate A and Plate B to move toward each other, Plate C is pushed to move. These movements make Ocean 2 basin shorten while make Ocean 1 basin elongate. Tides make ocean water move periodically, the passages between ocean basins allow water to travel and compensate. At time t_3, Plate A and Plate B meet, forming an aggregation. Meanwhile, Plate C sinks and becomes disappeared, Ocean 2 basin closes. Since plate motion stops, the forming oceanic crusts cannot spread away from the ridge, they gradually accumulate and plug up magma eruptions, and the ridge tends to die. Once the fractures of the lithosphere are repaired, the ocean-generated force cannot interact with the basal friction force, and then, these force balances terminate. After some time, a large asteroid violently collides with the aggregated plate, forming extensive fractures on the plate, and one of the fractures penetrates down to the lower part of the plate. At time t_4, the large fracture induces water entry, forming a large body of water that is deeper than Ocean 1. The deeper water body corresponds to greater ocean-generated force, this force may further expand the fracture. The large fracture also represents a mass loss of the upper part of the lithosphere; the isostasy would require the upper mantle to melt, the lower part of the aggregated plate is apparently broken. At time t_5, both the ocean-generated force and the molten material finally cut the plate into Plate D and Plate E. As the left end of the model is connected to its right end, the greater ocean-generated force would require the left part of Plate D to compress the right part of Plate E. Together with the basal friction exerted by the asthenosphere, the left part of Plate D is eventually detached from the plate, forming one subduction. Similarly, the right part of Plate E is detached from the plate, forming another subduction. These detachments and subductions allow to form a new oceanic plate--Plate F. At this moment, the ocean-generated forces may interact with the basal friction force, some new force balances are created. For instance, the force balance for Plate D is F_{DR}-F_{DL}-F_{FD}-f_D=0, the force balance for Plate E is F_{EL}-F_{ER}-F_{FE}-f_E=0, the force balance for Plate F is F_{DF}-F_{EF}-f_F=0. These force balances allow Plate D and Plate E to move away from each other. A new oceanic ridge gradually forms, and the increasing separation between the two plates results in a new Ocean 3 basin.

Ocean depth cannot be stable during a long geological timescale, it may change with the deepening/shallowing of basins. The ocean depth change in turn leads ocean-generated force to vary. We assume that, at time t_1, the Ocean 1 depth and the Ocean 2 depth are h_1=5,000 km and h_2=3,000 km, respectively, the length and width of Plate A are D=6,000 km and L=2,000 km, the water density is ρ=1000 kg/m^3, the gravitational acceleration is g=9.8 m/s. Then, the total ocean-generated force for Plate A would be F_{total}= F_{AL}-F_{AR}=0.5$\rho g L(h_1^2$-$h_2^2)$=1.5680×10^{17} N. We divide this total force into two exerting parts: one, as an opposing force, balances out the collisional force from Plate C, and the other, as a driving force, balances the basal friction

https://doi.org/10.5194/egusphere-2023-1458
Preprint. Discussion started: 3 August 2023

force. We also assume that half of the total force is used to act as the driving force, and then, according to Equation (2) exhibited in section 3, there would be 50%*F_{total}=$F_{driving}$=f_{basal}=μSu/y (where μ, S, u, and y are the viscosity of the asthenosphere, the area of Plate A, the speed of Plate A, and the thickness of the asthenosphere, respectively). Given μ=10^{18} Pas, S=DL=1.2×10^{13} m^2, and y=300 km, we get u=6.18 cm/yr. And now we assume that, at time t_2, which has passed 30,000,000 years since time t_1, the Ocean 1 depth reduces from 5,000 km to 4,500 km, the Ocean 2 depth increases from 3,000 km to 3,800 km, and that other parameters remain constant, and then, the speed of Plate A would be turned into u=2.24cm/yr. During a period of 30,000,000 years, the rate of Plate A is (6.18-2.24)/30000000=1.31×10^{-7} cm/yr. We again assume that, at time t_3, which has passed 50,000,000 years since time t_2, plate motion stops, and then, the speed of Plate A should be u=0.00 cm/yr. During a period of 50,000,000 years, the rate of Plate A is (2.24-0.00)/50000000=4.48×10^{-8} cm/yr. Figure 4 and Table 1 show that the ocean-generated forces around a continental plate are various in both magnitude and orientation, the ocean depth change would require these forces to vary. As a result, the final horizontal force varies, this leads plate motion to vary with time. Our calculation of the speed of Plate A suggests that the change of plate motion is considerably slow, thus, plate motion may be treated as near-steady.

Asteroid impacts are frequent events in the solar system, and it is widely believed that the initiation of plate motion relates to large asteroid impacts (Alvarez, et al., 1980; Rampino and Stothers, 1984; Prinn and Fegley, 1987; Marzoli, et al., 1999; Hames, et al., 2000; Condie, 2001; Wan, 2018), but the details of this coupling remain elusive. Our demonstration here provides the first insight into this issue: asteroid impact fractures the lithosphere, initiating plate motion; ocean water yields force to maintain plate motion; and tides provide energy for plate motion. Ocean depth cannot be stable during a long geological timescale, it may change with the deepening/shallowing of basins. The ocean depth change in turn leads ocean-generated force to vary. We assume that, at time t_1, the Ocean 1 depth and the Ocean 2 depth are h_1=5,000 km and h_2=3,000 km, respectively, the length and width of Plate A are D=6,000 km and L=2,000 km, the water density is ρ=1000 kg/m^3, the gravitational acceleration is g=9.8 m/s. Then, the total ocean-generated force for Plate A would be F_{total}= F_{AL}-F_{AR}=0.5ρgL(h_1^2-h_2^2)=1.5680×10^{17} N. We divide this total force into two exerting parts: one, as an opposing force, balances out the collisional force from Plate C, and the other, as a driving force, balances the basal friction force. We also assume that half of the total force is used to act as the driving force, and then, according to Equation (2) exhibited in section 3, there would be 50%*F_{total}=$F_{driving}$=f_{basal}=μSu/y (where μ, S, u, and y are the viscosity of the asthenosphere, the area of Plate A, the speed of Plate A, and the thickness of the asthenosphere, respectively). Given μ=10^{18} Pas, S=DL=1.2×10^{13} m^2, and y=300 km, we get u=6.18 cm/yr. And now we assume that, at time t_2, which has passed 30,000,000 years since time t_1, the Ocean 1 depth reduces from 5,000 km to 4,500 km, the Ocean 2 depth increases from 3,000 km to 3,800 km, and that other parameters remain constant, and then, the speed of Plate A would be turned into u=2.24cm/yr. During a period of 30,000,000 years, the rate of Plate A is (6.18-2.24)/30000000=1.31×10^{-7} cm/yr. We again assume that, at time t_3, which has passed 50,000,000 years since time t_2, plate motion stops, and then, the speed of Plate A should be u=0.00 cm/yr. During a period of 50,000,000 years, the rate of Plate A is (2.24-0.00)/50000000=4.48×10^{-8} cm/yr. Figure 4 and Table 1 show that the ocean-generated forces around a

https://doi.org/10.5194/egusphere-2023-1458
Preprint. Discussion started: 3 August 2023

continental plate are various in both magnitude and orientation, the ocean depth change would require these forces to vary. As a result, the final horizontal force varies, this leads plate motion to vary with time. Our calculation of the speed of Plate A suggests that the change of plate motion is considerably slow, thus, plate motion may be treated as near-steady.

Asteroid impacts are frequent events in the solar system, and it is widely believed that the initiation of plate motion relates to large asteroid impacts (Alvarez, et al., 1980; Rampino and Stothers, 1984; Prinn and Fegley, 1987; Marzoli, et al., 1999; Hames, et al., 2000; Condie, 2001; Wan, 2018), but the details of this coupling remain elusive. Our demonstration here provides the first insight into this issue: asteroid impact fractures the lithosphere, initiating plate motion; ocean water yields force to maintain plate motion; and tides provide energy for plate motion.

https://doi.org/10.5194/egusphere-2023-1458
Preprint. Discussion started: 3 August 2023

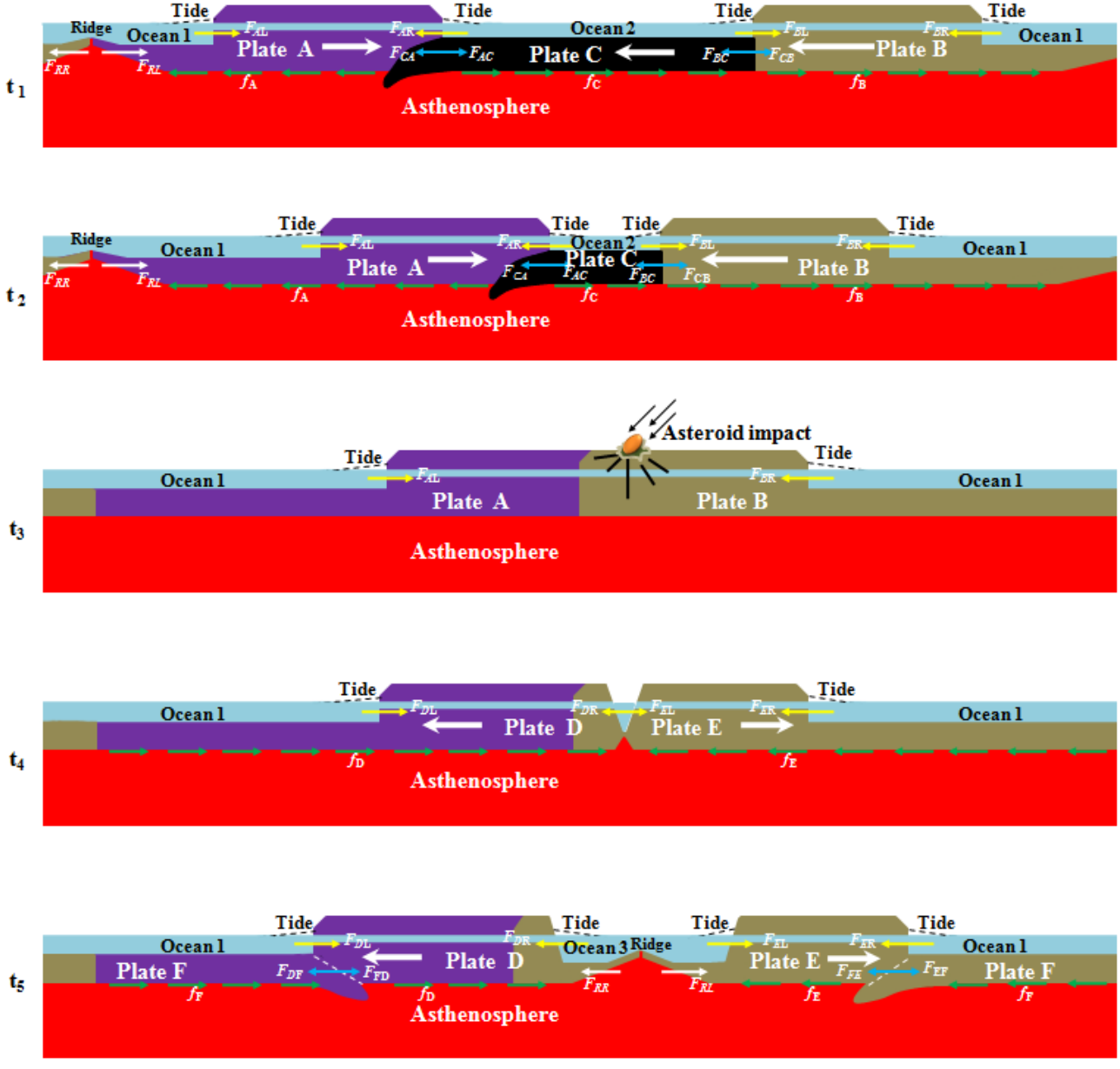

Figure 16: Modeling the dispersal and aggregation of plates. Large white arrows denote plate motion, small yellow arrows do ocean-generated forces, while small blue and green arrows do collisional and basal friction forces. Note that the ocean depth and the plate's thickness are highly exaggerated.

https://doi.org/10.5194/egusphere-2023-1458
Preprint. Discussion started: 3 August 2023

4.5 Why does ocean water contribute to tectonics?

All continents are surrounded by oceans, ocean-generated forces are extensively exerted on the sides of the continents that are fixed on top of the lithospheric plates, and all plates connect to each other; consequently, all the plates may interact with each other (Figure 17). Under the effect of ocean-generated force, a moving continental plate would ride on an oceanic plate, and the front part of the oceanic plate is forced to subduct, forming a sinking slab. Additionally, a moving plate would move away from another plate, and a gap would form between them. The gap allows magma to erupt, forming an MOR. From this point, the ridge push force may be treated as an auxiliary force for ocean-generated force. Since ocean-generated force is exerted on the continental wall (represented by coastline), and the oceanic crust is extensively connected to the continental crust, this allows ocean-generated force to be laterally transferred to the oceanic crust, and then, the continental crust drags the oceanic crust to move, causing the plate's boundary to follow the shape of coastline.

Many people are extraordinarily perplexed as to why the Earth owns plate tectonics whereas the Venus does not. Many studies have shown that water provides the right conditions (maintaining a cool surface, for example) for plate tectonics, while the absence of water on Venus prohibits plate formation (Driscoll and Bercovici, 2013; Hilairet et al., 2007; Lenardic et al., 2008; Korenaga, 2007; Tozer, 1985; Lenardic and Kaula, 1994; Hirth and Kohlstedt, 1996; Landuyt and Bercovici, 2009). Our understanding of ocean water provides a new perspective on this issue: no water on Venus means that there is no contribution of ocean-generated force and no further development of plate tectonics on that planet.

https://doi.org/10.5194/egusphere-2023-1458
Preprint. Discussion started: 3 August 2023

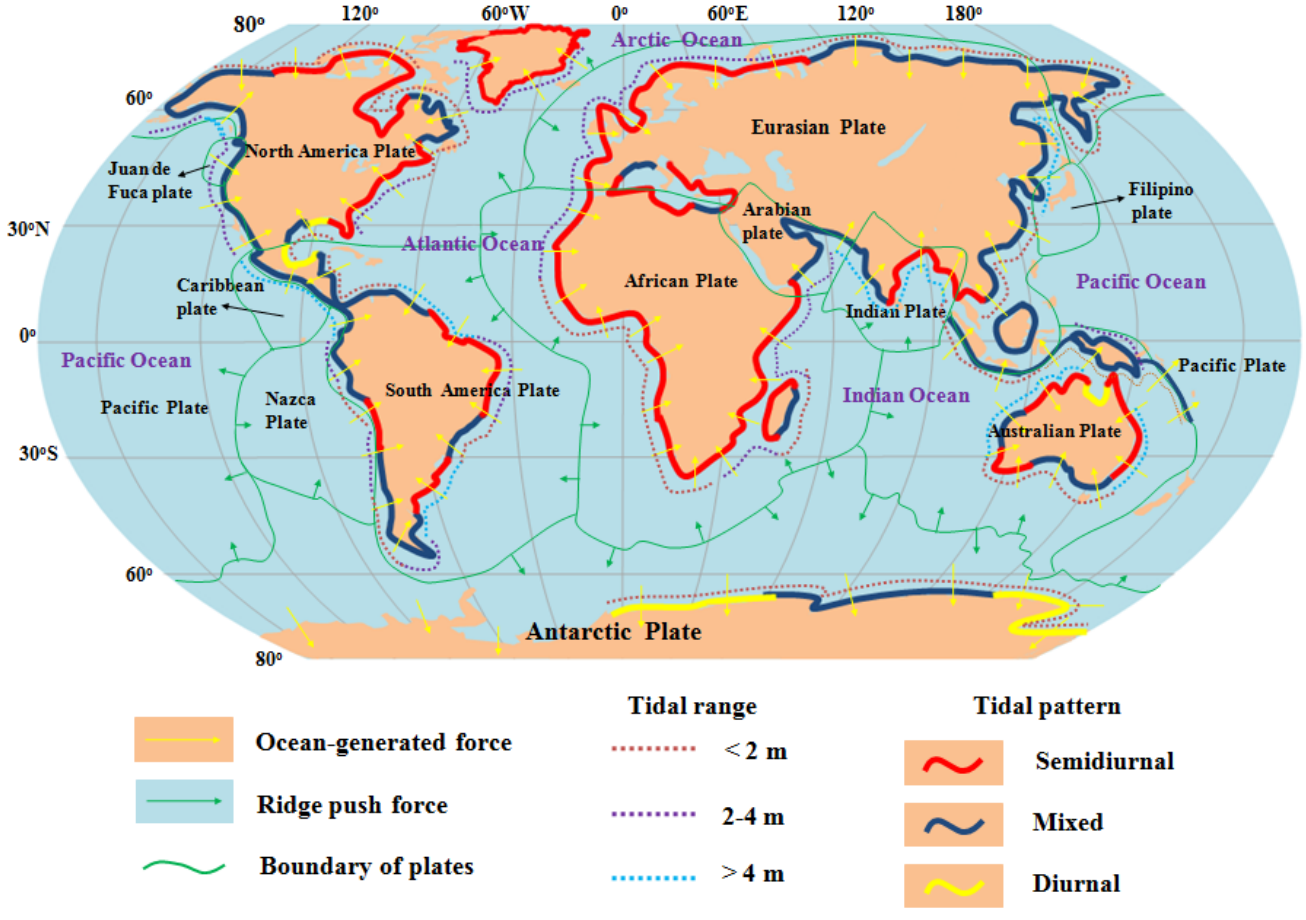

Figure 17: Global view of the distribution of ocean-generated forces (yellow arrows) and ridge push forces (green arrows). The supporting tidal data are mainly from the Global Sea Level Observing System (GLOSS) database (Caldwell et al., 2015).

4.6 What's the trouble with mantle convection?

Although mantle convection had been given up by most of geophysicists since the late 1990s, this cannot prevent it from becoming popular. We here restate how mantle convection cannot be realistic. The main problems with this paradigm include: 1) the convection cells proposed to exist in the asthenosphere require strong fitting to plate size. Seismic tomography shows that rising mantle material beneath ridges only extends down 200 to 400 km (Foulger, et al., 2001). This depth gives an upper limitation on the scale of the proposed cells. Most of plates (North American, Eurasian, and Pacific, for instance), however, are very wide, generally more than thousands of kilometers.

https://doi.org/10.5194/egusphere-2023-1458
Preprint. Discussion started: 3 August 2023

2) the movement of a large plate would yield a net mass flux in the asthenosphere to compensate the mass transport in the moving plate, this requires the plate to be treated as an integral part of the circulation (Forsyth & Uyeda, 1975). Richter (1973) employed a model to show that the asthenosphere exerts viscous resistive forces rather than driving forces on the plates, which actually opposes the mantle convection currents to act as the drivers.

3) in the scenario of mantle convection, poloidal motion involves vertical upwellings and downwellings, while toroidal motion undertakes horizontal rotation (Bercovic, et al., 2015). The generation of torioidal motion requires variable viscosity, but numerous studies of basic 3-D convection with temperature-dependent viscosity had failed to yield the requisite toroidal flow (Bercovic, 1993, 1995b; Cadek et al., 1993; Christensen and Harder, 1991; Stein et al., 2004; Tackley, 1998; Trompert and Hansen, 1998; Weinstein, 1998).

4) mantle convection models are unsuccessful in yielding plate motions, although some of them had yielded plate-like behavior and mathematically got solution for plate motion velocity by means of a non-Newtonian way, i.e., a balance relationship of buoyancy force and drag force (Bercovici, et al., 2015). Doglioni and Panza (2015) concluded that none of mantle convection models is really able to satisfy the constraints posed by the plate kinematics, the temperature, and the asymmetry of plate boundaries.

5) when mantle convection is treated as the plate driving force, it requires not only the mantle to couple the plates but also the movement of mantle currents to keep consistent with that of the plates. But reality is not so. The Pacific Plate is the fastest W-ward moving one relative to the mantle and is slipping over an Low Velocity Zone (LVZ) (Doglioni et al., 2005) with low viscosity (Pollitz et al., 1998). Evidently, the Pacific is the most decoupled plate, while mantle convection requires the faster moving plates to be more coupled (higher viscosity) with the mantle. The Hawaii hot spot volcanic chain represents that the underlying mantle is moving E-SE-ward. These authors (Hammond and Toomey, 2003; Doglioni et al., 2003) modeled, beneath the East Pacific Rise (EPR), an eastward-migrating mantle. The hot spot reference frame remains consistent with the existence of an eastward relative mantle flow beneath the South America plate (Van Hunen, van den Berg, & Vlaar, 2002). A relatively moving eastward mantle flow has been proposed also beneath North America (Silver & Holt, 2002) and beneath the Caribbean plate (Gonzalez, Alvarez, Moreno, & Panza, 2011; Negredo, Jiménez-Munt, & Villasenor, 2004). All these results indicate that the movements of the mantle currents are reverse to that of the plates, the opposed moving mantle currents provide resistive force rather than driving force for these plates.

6) our modeling analysis suggests that, if mantle convection were considered as a driving force, what it performs is a drag on the plate's base, more like the basal friction force F_b exhibited in Figure 1, and then, its resultant stress must be mainly concentrated on the lowermost part of the plate, which cannot be in accordance with observed stress.

Competing interests

The contact author declares no competing interests.

https://doi.org/10.5194/egusphere-2023-1458
Preprint. Discussion started: 3 August 2023

Acknowledgements

We express sincere thanks to Jinmin Chen for conducting the vector force analysis and to Bernhard Steinberger, Jeroen van Hunen, Maureen D. Long, and Thorsten Becker for their helpful comments on this research. The author declares that there is no conflict of interest. No funding was provided for this research.

Availability of data and material

The movement data of the 121 sample locations are extracted from GSRM v.2.1 (Kreemer et al., 2014) and are available through UNAVCO (https://www.unavco.org/software/geodetic-utilities/plate-motion-calculator/plate-motion-calculator.html). The latitude and longitude of the controlling sites on the continental plates in Figure 4 are determined through the ETOPO1 Global Relief Model (Amante and Eakins, 2009), and the ocean depths are artificially resolved through the NOAA Bathymetric Data Viewer (https://ngdc.noaa.gov/mgg/global/global.html). The tide data in Figure 14 are from the GLOSS database (Caldwell et al., 2015).

References

Alvarez, L. W., Alvarez, W., Asaro, F., and Michel, H. V.: Extraterrestrial cause for the Cretaceous-Tertiary extinction, *Science*, 208, 1095-1108, 1980.

Altamimin, Z., Rebischung, P., Métlvler, L., and Collilleux, X.: ITRF2014: A new release of the International Terrestrial Reference Frame modeling nonlinear station motions, *J. Geophys. Res.*, 121, 6109-6131, https://doi.org/10.1002/2016JB013098, 2016.

Amante, C., and Eakins, B. W.: ETOPO1 1 Arc-Minute Global Relief Model: Procedures, Data Sources and Analysis, NOAA Technical Memorandum NESDIS NGDC-24, National Geophysical Data Center, NOAA. doi:10.7289/V5C8276M, 2009.

Alisic, L., Gurnis, M., Stadler, G., Burstedde, C., and Ghattas, O.: Multi-scale dynamics and rheology of mantle flow with plates, *J. Geophys. Res.*, 117, B10402, doi:10.1029/2012JB009234, 2012.

Becker, T. W., Faccenna, C.: Mantle conveyor beneath the Tethyan collisional belt: Earth Planet, *Sci. Lett.*, 310, 453-461, 2011.

Becker, T. W., and O'Connell, R. J.: Predicting plate velocities with mantle circulation models, *Geochem. Geophys. Geosyst.*, 2, 2001GC000171, 2001.

Becker, T. W.: Superweak asthenosphere in light of upper mantle seismic anisotropy, *Geochem. Geophys. Geosyst.*, 18, doi:10.1002/ 2017GC006886, 2017.

Bercovici, D.: A simple model of plate generation from mantle flow, *Geophys. J. Int.*, 114, 635-650, 1993.

https://doi.org/10.5194/egusphere-2023-1458
Preprint. Discussion started: 3 August 2023

Bercovici, D.: A source-sink model of the generation of plate tectonics from non-Newtonian mantle flow, *J. Geophys. Res.*,100, 2013-2030, 1995.

Bercovici, D., Tackeley, P. J., and Ricard, Y. : The generation of plate tectonics from mantle dynamics: Reference Module in Earth Systems and Environmental Science, *Treatise on Geophysics (Second Edition)*, 7, 271-318, 2015.

Berner. R.: The Phanerozoic Carbon Cycle, Oxford University Press, 2004.

Bird, P., Liu, Z., Rucker, W. K. : Stresses that drive the plates from below: definitions, computational path, model optimization, and error analysis, *J. Geophys. Res*., 113, B11406, 2008.

Bokelmann, G. H. R.: Which forces drive North America?, *Geology*, 30, 1027-1030, 2002.

Bott, M. H. P.: Modeling the Plate-Driving Mechanism, *Journal of the Geological Society*, 150, 941-951, 1993.

Brandmayr, E., Marson, I., Romanelli, F., &Panza, G. F.: Lithosphere density model in Italy: no hint for slab pull, *Terra Nova*, 23, 292-299, 2011.

Cadek, O., Ricard, Y., Martinec, Z., and Matyska, C.: Comparison between Newtonian and non-Newtonian flow driven by internal loads, *Geophys. J. Int*., 112, 103-114, 1993.

Cande, S. C., LaBrecque, J. L., Larson, R. L., Pitman, W. C., III, Golovchenko, X., and Haxby,W. F.: Magnetic lineations of the world's ocean basins, Tulsa, Oklahoma, American Association of Petroleum Geologists, 1989.

Cande, S. C., Kent, D. V.: A new geomagnetic polarity time scale for the Late Cretaceous and Cenozoic, *J. Geophys. Res*., 97(10), 13917-13951, 1992.

Caldwell, P. C., Merrfield, M. A., Thompson, P. R.: Sea level measured by tide gauges from global oceans - the Joint Archive for Sea Level holdings (NCEI Accession 0019568), Version 5.5, NOAA National Centers for Environmental Information, Dataset, doi:10.7289/V5V40S7W, 2015.

Chapple, W. M., and Tullis, T. E.: Evaluation of the forces that drive the plates, *J. Geophys. Res*., 82, 1969-1984, 1977.

Christensen, U., Harder, H.: Three-dimensional convection with variable viscosity, *Geophys. J. Int*., 104, 213-226, 1991.

Cloetingh, S., and Wortel, R.: Stress in the Indo-Australian plate, *Tectonophysics*, 132, 49-67, 1986.

Coltice, N., Gerault, M., and Ulvrova, M.: A mantle convection perspective on global tectonics, *Earth-Science Reviews*, 165, 120-150, 2017.

Condie, K. C.: Mantle plumes and their record in Earth history, Cambridge University Press, Cambridge, 2001.

Conrad, C. P., Hager, B. H.: The effects of plate bending and fault strength at subduction zones on plate dynamics, *J. Geophys. Res*., 104, 17551-17571, 1999.

Conrad, C. P., Lithgow-Bertelloni, C.: How Mantle Slabs Drive Plate Tectonics, *Science*, 298 (5591), 207-09, 2002.

Conrad, C. P., & Lithgow-Bertelloni, C.: How mantle slabs drive plate tectonics, *Science*, 298, 207-209, 2003.

Cruciani, C., Carminati, E., &Doglioni, C.: Slab dip vs. lithosphere age: no direct function, Earth Planet, *Sci. Lett*., 238, 298-310, 2005.

Doglioni, C., Carminati, E., & Bonatti, E.: Rift asymmetry and continental uplift, *Tectonics*, 22, 1024-1037, 2003.

https://doi.org/10.5194/egusphere-2023-1458
Preprint. Discussion started: 3 August 2023

Doglioni, C., Green, D. H., & Mongelli, F.: On the shallow origin of hotspots and the westward drift of the lithosphere. In G. R. Foulger, J. H. Natland, D. C. Presnall, & D. L. Anderson (Eds.), Geological society of America special paper: Vol. 388. Plates, plumes, and paradigms (pp. 735e749), 2005.

Doglioni, C., Ismail-Zadeh, A., Panza, G., Riguzzi, F.: Lithosphere-asthenosphere viscosity contrast and decoupling, *Physics of the Earth and Planetary Interiors*, 189, 1-8, 2011.

Doglioni, C., and Panza, G.: Polarized Plate Tectonics, *Advances in Geophysics*, 56, 1-167, 2015.

Driscoll, P. and Bercovic, D.: Divergent evolution of Earth and Venus: Influence of degassing, tectonics, and magnetic fields, *Icarus*, 226, 1447-1464, 2013.

Egbert, G. D., Ray, R. D.: Significant dissipation of tidal energy in the deep ocean inferred from satellite altimeter data, *Nature*, 405, 775-778, 2000.

El Gabry, M. N., Panza, G. F., Badawy, A. A., &Korrat, I. M.: Imaging a relic of complex tectonics: the lithosphere-asthenosphere structure in the Eastern Mediterranean, *Terra Nova*, 25(2), 102-109, 2013.

Faccincani, L., Faccini, B., Casetta, F., Mazzucchelli, M., Nestola, F., Coltorti, M.: EoS of mantle minerals coupled with composition and thermal state of the lithosphere: Inferring the density structure of peridotitic systems, *Lithos*, 404-405, 106483, 2021.

Fleitout, L., Froidevaux, C.: Tectonic stresses in the lithosphere, *Tectonics*, 2(3), 315-324, 1983.

Forsyth, D. & Uyeda, S.: On the relative importance of the driving forces of plate motion, *Geophys. J. Int.*, 43, 163-200, 1975.

Foulger, G. R., et, al.: Seismic tomography shows that upwelling beneath Icealand is confined to the upper mantle, *Geophys. J. Int.*, 146, 504-530, 2001.

Freed, A., Hashima, A., Becker,T. W., Okaya,D. A., Sato,H., and Hatanaka, Y.: Resolving depth-dependent subduction zone viscosity and afterslip from postseismic displacements following the 2011 Tohoku-oki, Japan earthquake, *Earth Planet. Sci. Lett.*, 459, 279-290, 2017.

Frepoli, A., Selvaggi, G., Chiarabba, C., & Amato, A.: State of stress in the Southern Tyrrhenian subduction zone from fault-plane solutions, *Geophys. J. Int.*, 125, 879-891, 1996.

Ghosh, A., Becker, T. W., Humphreys, E. D.: Dynamics of the North American continent, *Geophys. J. Int.*, 194, 651-669, 2013.

Ghosh, A., and Holt, W. E.: Plate motions and stresses from global dynamic models, *Science*, 335, 839-843, 2012.

Gonzalez, O. F., Alvarez, J. L., Moreno, B., & Panza, G. F.: S-waves's velocities of the lithopshere-asthenosphere system in the Caribbean region, *Pure and Applied Geophysics*, 169(1-2), 101-122, 2011.

Gölke, M., and Coblentz, D.: Origins of the European regional stress field, *Tectonophysics*, 266, 11-24, 1996.

Gripp, A. E., & Gordon, R. G.: Young tracks of hotspots and current plate velocities, *Geophys. J. Int.*, 150, 321-361, 2002.

Grünthal, G., and Stromeyer, D.: The recent crustal stress field in central Europe: Trajectories and finite element modelling, *J. Geophys. Res.*, 97(B8), 11, 805-11, 820, 1992.

https://doi.org/10.5194/egusphere-2023-1458
Preprint. Discussion started: 3 August 2023

Guillas, S., Day, S. J., and McGuire, B.: Statistical analysis of the El Niño–Southern Oscillation and sea-floor seismicity in the eastern tropical Pacific, *Philos. Trans. A. Math. Phys. Eng. Sci.*, 368(1919), 2481-500, 2010.

Gutenberg, B.: The energy of Earthquakes, *Quart. J. Geol. Soc. London*, 112, 1-14, 1956.

Hager, B. H., and Richards, M. A.: Long-wavelength variations in Earth's geoid: Physical models and dynamical implications, *Philosophical Transactions of the Royal Society of London, Series A*, 328, 309-327, 1989.

Hales, A.: Convection currents in the Earth, *Monthly Notice of the Royal Astronomical Society, Geophysical Supplement*, 3, 372-379, 1936

Hames, W. E., Renne, P. R., Ruppel, C.: New evidence for geologically instantaneous emplacement of earliest Jurassic Central Atlantic magmatic province basalts on the North American margin, *Geology*, 28,859-862, 2000.

Hammond, W. C., & Toomey, D. R.: Seismic velocity anisotropy and heterogeneity beneath the mantle electromagnetic and tomography experiment (MELT) region of the East Pacific Rise from analysis of P and S body waves, *J. Geophys. Res.*,108, 2176, 2003.

Hartzell, S., and Heaton, T.: The fortnightly tide and the tidal triggering of earthquakes, *Bull. Seismol. Soc. Am.*, 79, 1282-1286, 1989.

Hawley, W. B., Allen,R., and Richards, M. A.: Tomography reveals buoyant asthenosphere accumulating beneath the Juan de Fuca plate, *Science*, 353, 1406-1408, 2016.

Heidbach, O., Rajabi, M., Cui , X. F., Fuchs,K., Müller, B., Reinecker, J., Reiter, K.,Tingay., M., Wenzel, F., Xie, F. R., Ziegler, M. O., Zoback, M., Zoback, M.: The World Stress Map database release 2016: Crustal stress pattern across scales, *Tectonophysics*, 744, 484-498, 2018.

Heidbach, O., Reinecker, J., Tingay, M., Müller, B., Sperner, B., Fuchs, K., Wenzel, F.: Plate boundary forces are not enough: Second- and third-order stress patterns highlighted in the World Stress Map database, *Tectonics*, 26, http://doi.org/10.1029/2007TC002133, 2007.

Heidbach, O., Tingay, M., Barth, A., Reinecker, J., Kurfeß, D., Müller, B.: Global crustal stress pattern based on the World Stress Map database release 2008, *Tectonophys*, 482, 3-15, 2010.

Heidbach, O., Rajabi, M., Reiter, K., Ziegler, M.: World Stress Map 2016, GFZ Data Services, http://doi.org/10.5880/WSM.2016.002, 2016

Hess, H. H.: History Of Ocean Basins, in Engel, A. E. J., James, H. L., & Leonard, B. F., eds. Petrologic Studies: A volume in honor of A. F. Buddington. Boulder, CO, *Geological Society of America*, 599-620, 1962.

Hibsch, C., Jarrige, J-J., Cushing, E. M., Mercier, J.: Paleostress analysis, a contribution to the understanding of basin tectonics and geodynamic evolution: example of the permian-cenozoic tectonics of Great Britain and geodynamic implications in Western Europe, Tectonophysics, 252, 103-136, 1995.

Hilairet, N., Reynard, B., Wang, Y., Daniel, I., Merkel, S., Nishiyama, N., and Petitgirard, S.: High-Pressure Creep of Serpentine, Interseismic Deformation, and Initiation of Subduction, Science, 318(5858), 1910-1913, 2007.

https://doi.org/10.5194/egusphere-2023-1458
Preprint. Discussion started: 3 August 2023

Hirth, G. and Kohlstedt, D.: Water in the oceanic upper mantle: Implications for rheology, melt extraction and the evolution of the lithosphere, Earth Planet, *Sci. Lett.*, 144, 93-108, 1996.

Holmes, A.: Radioactivity and Earth Movements, *Nature*, 128, 496-496, 1931.

Holtzman, B.: Questions on the existence, persistence, and mechanical effects of a very small melt fraction in the asthenosphere, *Geochem. Geophys. Geosyst.*, 17, 470-484, doi:10.1102/2015GC006102, 2016.

Hu, Y., Bürgmann, R., Banerjee, P., Feng, L. J., Hill, E. M., Ito, T., Tabei, T., Wang, K. L.: Asthenosphere rheology inferred from observations of the 2012 Indian Ocean earthquake, *Nature*, 538(7625), 368-372, 2016.

Isacks, B., & Molnar, P.: Distribution of stresses in the descending lithosphere from a global survey of focal-mechanism solutions of mantle earthquakes, *Reviews of Geophysics*, 9, 103-174, 1971.

James, T. S., Gowan, E. J., Wada, L., and Wang, K. L.: Viscosity of the asthenosphere from glacial isostatic adjustment and subduction dynamics at the northern Cascadia subduction zone, British Columbia, Canada, *Journal of Geophysical Research: Solid Earth*, 114(B4), CiteID B04405, 2009.

Jeffreys, H.: The Earth, 2 nde d., p. 304, Cambridge University Press, London, 1929.

Jeffreys, H.: The Earth, Cambridge, Cambridge University Press, London, 1975.

Jordan, T. H.: Some comments on tidal drag as a mechanism for driving plate motions, *J. Geophys. Res.*, 79, 2141-2142, 1974.

Kanamori, H.: Mechanics of Earthquakes, Annual Reviews of Earth and Planetary Sciences, 22, 207-237, 1994.

Kaufmann, G., and Lambeck, K.: Mantle dynamics, postglacial rebound and the radial viscosity profile, *Physics of the Earth and Planetary Interiors*, 121, 301-324, 2000.

Kawakatsu, H., Kumar,P., Takei,Y., Shinohara,M., Kanazawa,T., Araki,E., and Suyehiro, K.: Seismic evidence for sharp lithosphere asthenosphere boundaries of oceanic plates, *Science*, 324, 499-502, 2009.

Kido, M., Yuen, D. A., Cadek, O., and Nakakuki, T.: Mantle viscosity derived by genetic algorithm using oceanic geoid and seismic tomography for whole mantle versus blocked-flow situations, *Physics of the Earth and Planetary Interiors*, 107, 307-326, 1998.

King, S. D.: The viscosity structure of the mantle, In Reviews of Geophysics (Supplement) U.S. *Quadrennial Report to the IUGG* 1991-1994, 11-17, 1995.

Knopoff, L.: Earth tides as a triggering mechanism for earthquakes, *Bull. Seismol. Soc. Am.*, 54, 1865-1870, 1964.

Knopoff, L., Leeds, A.: Lithospheric momenta and the deceleration of the Earth, *Nature*, 237(12), 93-95, 1972.

Korenaga, J.: Thermal cracking and the deep hydration of oceanic lithosphere: A key to the generation of plate tectonics?, *J. Geophys. Res.*, 112(B5), DOI: 10.1029/2006JB004502, 2007.

Korenaga, J., Karato, S.-I.: A new analysis of experimental data on olivine rheology, *J. Geophys. Res.*, 113, B02403, 2008.

Kreemer, C., Blewitt, G., and Klein, E.C.: A geodetic plate motion and Global Strain Rate Model, *Geochem. Geophys. Geosyst.*, 15, 3849-3889, 2014.

https://doi.org/10.5194/egusphere-2023-1458
Preprint. Discussion started: 3 August 2023

Kreemer, C., Holt, W. E., & Haines, A. J.: The global moment rate distribution within plate boundary zones, *American Geophysical Union Geodynamics Series*, 30, 173-189, 2002.

Kusznir, N. J., &Bott, M. H. P.: Stress concentration in the upper lithosphere caused by underlying visco-elastic creep, *Tectonophysics*, 43, 247-256, 1977.

Landuyt, W. and Bercovici, D.: Variations in planetary convection via the effect of climate on damage, Earth Planet, *Sci. Lett*., 277, 29-37, 2009.

Lenardic, A., Jellinek, M., and Moresi, L-N.: A climate change induced transition in the tectonic style of a terrestrial planet, Earth Planet, *Sci. Lett*., 271, 34-42, 2008.

Lenardic, A. and Kaula, W.: Self-lubricated mantle convection: Two-dimensional models, *Geophys. Res. Lett*., 21, 1707-1710, 1994.

Le Pichon, X.: Sea-floor spreading and continental drift, *J. Geophys. Res*., 73(12), 3661-3697, 1968.

Lithgow-Bertelloni, C., Richards, M. A.: Cenozoic plate driving forces, *Geophys. Res. Lett*., 22, 1317-1320, 1995.

Lithgow-Bertelloni, C.: Driving Forces: Slab Pull, Ridge Push, Encyclopedia of Marine Geosciences, 2014.

Ma, Z. J., Li, C. D., Gao, X. L.: General characteristics of global tectonics in the Mesozoic and Cenozoic (in Chinese), *Geological Science and Technology Information*, 15(4), 21-25, 1996.

Martínez-Garzón, P., Beroza, G. C., Bocchini, G. M., & Bohnhoff, M.: Sea level changes affect seismicity rates in a hydrothermal system near Istanbul, *Geophys. Res. Lett*., 50, e2022GL101258, https://doi.org/10.1029/2022GL101258, 2023.

Marzoli, A., Renne, P. R., Piccirillo, E. M., Ernesto, M., Bellieni, G., de Min, A.: Extensive 200-million-year-old continental flood basalts of the Central Atlantic magmatic province, *Science*, 284(5414), 616-618, 1999.

McKenzie, D. P.: The Influence of the Boundary Conditions and Rotation on Convection in the Earth's Mantle, *The Geophysical Journal*, 15, 457-500, 1968.

McKenzie, D. P.: Speculations on the Consequences and Causes of Plate Motions, *The Geophysical Journal*, 18, 1-32, 1969.

Mei, S., Bai, W., Hiraga, T., and Kohlstedt, D. L.: Influence of melt on the creep behavior of olivine basalt aggregates under hydrous conditions, Earth Planet, *Sci. Lett*., 201, 491-507, 2002.

Middleton, G. V., Wilcock, P. R.: Mechanics in the Earth and Environmental Sciences, Cambridge University Press, Australia, 1996.

Miller, G. R.: The flux of tidal energy out of the deep oceans, *J. Geophys. Res*., 71, 2485-2489, 1966.

Mitchell, R. N., Zhang, N., Salminen, J., Liu, Y. B., Spencer, C. J., Steinberger, B., Murphy, J. B., & Li, Z. X.: The supercontinent cycle, *Nature Reviews Earth & Environment*, 2, 358-374, 2021.

Mitrovica, J. X.: Haskell (1935) revisited, *J. Geophys. Res*., 101, 555-569, 1996.

Mojzsis, S. J., Harrison, T. M., and Pidgeon, R. T.: Oxygen-isotope evidence from ancient zircons for liquid water at the Earth's surface 4,300 Myr ago, *Nature*, 409(6817), 178-181, 2001.

https://doi.org/10.5194/egusphere-2023-1458
Preprint. Discussion started: 3 August 2023

Morgan, W. J., Stoner, J. O., and Dicke, R. H.: Periodicity of earthquakes and the invariance of the gravitational constant, *J. Geophys. Res.*, 66, 3831–3843, 1961.

Morgan, W. J.: Deep mantle convection plumes and plate motions, *Bull. A. Pet. Geol*., 56, 203-213, 1972.

Müller, B., Zoback, M. L., Fuchs, K., Mastin, L., Gregersen, S., Pavoni, N., Stephansson, O., Ljunggren, C.: Regional patterns of tectonic stress in Europe, *J. Geophys. Res.*, 97(B8), 11,783-11, 803, 1992.

Munk, W.: Once again-tidal friction, *Quarterly Journal of the Royal Astronomical Society*, 9, 352-375, 1968.

Naif, S., Key, K., Constable,S., and Evans, R. L.: Melt-rich channel observed at the lithosphere-asthenosphere boundary, *Nature*, 495, 356-359, 2013.

Naliboff, J. B., Lithgow-Bertelloni, C., Ruff, L. J., de Koker, N.: The effects of lithospheric thickness and density structure on Earth's stress field, *Geophys. J. Int*., 188, 1-17, 2012.

Negredo, A. M., Jiménez-Munt, I., & Villasenor, A.: Evidence for eastward mantle flow beneath the Caribbean plate from neotectonic modelling, *Geophys. Res. Lett*., 31, L06615, 2004.

Oxburgh, E. and Turcotte, D.: Mechanisms of continental drift, *Reports on Progress in Physics*, 41, 1249-1312, 1978.

Panza, G. F., Peccerillo, A., Aoudia, A., & Farina, B.: Geophysical and petrological modeling of the structure and composition of the crust and upper mantle in complex geodynamic settings: the Tyrrhenian Sea and surroundings, *Earth-Science Reviews*, 80, 1-46, 2007.

Parsons, B., Richter, F. M.: A relation between the driving force and geoid anomaly associated with mid-ocean ridges, Earth Planet, *Sci. Lett*., 51, 445-450, 1980.

Perkeris, C.: Thermal convection in the interior of the Earth, *Monthly Notices of the Royal Astronomical Society, Geophysical Supplement*, 3, 343-367, 1935.

Pollitz, F. F., Bürgmann, R., & Romanowicz, B.: Viscosity of oceanic asthenosphere inferred from remote triggering of earthquakes, *Science*, 280, 1245-1249, 1998.

Prinn, R. G., Fegley, B.: Bolide impacts, acid rain, and biospheric traumas at the Cretaceous-Tertiary boundary, Earth Planet, *Sci. Lett*., 83,1-15, 1987.

Rampino, M. R., Stothers, R. B.: Geological rhythm and cometary impacts, Sciences, 226(4681),1427-1431, 1984.

Ranalli, G.: Westward drift of the lithosphere: not a result of rotation drag, *Geophys. J. Int.*, 141, 535-537, 2000.

Raymond, C. A., Stock, J, M., Cande, S. C.: Fast Paleogene motion of the Pacific hotspots from revised global plate circuit constraints, *Geophysical Monography*, 121, 359-375, 2000.

Reynard, B., Hilairet, N., Wang, Y., Daniel, I.,Merkel, S.,Petitgirard, S., Nishiyama, N.: High-pressure creep of serpentine, interseismic deformation, and initiation of subduction, *Science*, 318(5858), 1910-1913, 2007.

Ricard, Y., Fleitout, L., Froidevaux. C.: Geoid heights and lithospheric stresses for a dynamic earth, *Ann. Geophys*, 2, 267-286, 1984.

https://doi.org/10.5194/egusphere-2023-1458
Preprint. Discussion started: 3 August 2023

Richardson, R. M.: Ridge Forces, Absolute Plate Motions, and the Intraplate Stress Field, *J. Geophys. Res*., 97, 11739-11748, 1992.

Richardson, R. M., and Cox, B. L.: Evolution of oceanic lithosphere: A driving force study of the Nazca Plate, *Journal of Geophysical Research: Solid Earth*, 89 (B12), 10043-10052, 1984.

Richardson, R. M., and Reding, L.: North American plate dynamics, *J. Geophys. Res*., 96, 12201-12223, 1991.

Richardson, R. M., Solomon, S. C., and Sleep, N. H.: Tectonic stress in the plates, *Rev. Geophys*., 17, 981-1019, 1979.

Richter, F.: Dynamical models for sea-floor spreading, *Rev. Geophys. Space Phys*., 11, 223-287, 1973.

Riguzzi, F., Panza, G., Varga, P., Doglioni, C.: Can Earth's rotation and tidal despinning drive plate tectonics?, *Tectonophysics*, 484, 60-73, 2012.

Robert, H. S.: Introduction to physical oceanography, Texas A & M University, 2008.

Rochester, M. G.: The Earth's rotation, *EOS, T rans. Am. geophys. Un.*, 54, 769-780, 1973.

Runcorn, S.: Towards a theory of continental drift, *Nature*, 193, 311-314, 1962a.

Runcorn, S.: Convection currents in the Earth's mantle, *Nature*, 195, 1248-1249, 1962b.

Russo, R. M., & Silver, P. G.: Trench-parallel flow beneath the Nazca plate from seismic anisotropy, *Science*, 263, 1105-1111, 1994.

Schuster, A.: On lunar and solar periodicities of earthquakes, *Proc. R. Soc. London*, 61, 455-465, 1897.

Scoppola, B., Boccaletti, D., Bevis, M., Carminati, E., Doglioni, C.: The westward drift of the lithosphere: A rotational drag?, *GSA Bulletin*, 118, 199-209, 2006.

Shirley, J. H.: Lunar and solar periodicities in large earthquakes: Southern California and the Alaska-Aleutian Islands seismic region, *Geophys. J. Int*., 92, 403-420, 1988.

Shlien, S.: Earthquake-tide correlation, *Geophys. J. R. Astron. Soc*., 28, 27-34, 1972.

Shudde, R. H., and Barr, D. R.: An analysis of earthquake frequency data, *Bull. Seismol. Soc. Am*., 67, 1379-1386, 1977.

Silver, P. G., & Holt, W. E.: The mantle flow field beneath western North America, *Science*, 295, 1054-1057, 2002.

Slomon, S. C., Sleep, N. H., and Richardson, R. M.: On the forces driving plate tectonics: Inferences from absolute plate velocities and intraplate stress, *Geophys. J. R. Astron. Soc*., 42, 769-801, 1975.

Spence, W.: Slab pull and the seismotectonics of subducting lithosphere, *Reviews of Geophysics*, 25 (1), 55-69, 1987.

Sperner, B., Müller, B., Heidbach, O., Delvaux, D., Reinecker, J., Fuchs, K.: Tectonic stress in the Earth's crust: advances in the World Stress Map project, in New insights in structural interpretation and modelling, edited by D. A. Nieuwland, Special Publication 212, 101-116, Geol. Soc. Spec. Pub., London, 2003.

Stadler, G., Gurnis, M., Burstedde, C., Wilcox, L. C., Alisic, L., Ghattas, O.: The dynamics of plate tectonics and mantle flow: from local to global scales, *Science*, 329, 1033-1038, 2010.

Stefanick, M., and Jurdy, D. M.: Stress observations and driving force models for the South American plate, *J. Geophys. Res*., 97, 11905-11913, 1992.

https://doi.org/10.5194/egusphere-2023-1458
Preprint. Discussion started: 3 August 2023

Stern, T. A., Henrys, S. A., Okaya, D., Louie, J. N., Savage, M. K., Lamb, S., Sato, H., Sutherland, R., and Iwasak, T.: A seismic reflection image for the base of a tectonic plate, *Nature*, 518, 85-88, 2015.

Steinberger, B., Schmeling, H., Marquart, G.: Large-scale lithospheric stress field and topography induced by global mantle circulation, *Earth Planet. Sci. Lett.*, 186, 75-91, doi:10.1016/S0012-821X(01)00229-1, 2001.

Steinberger, B.: Topography caused by mantle density variations: observation-based estimates and models derived from tomography and lithosphere thickness, *Geophys. J. Int.*, 205, 604-621, 2016.

Stein, C., Schmalzl, J., Hansen, U.: The effect of rheological parameters on plate behavior in a self-consistent model of mantle convection, *Physics of the Earth and Planetary Interiors*, 142, 225-255, 2004.

Squyres, S.W., Grotzinger, J. P., Arvidson, R. E., Bell III, J. F., Calvin, W., Christensen, P. R., Clark, B. C., Crisp, J. A., Farrand, W. H., Herkenhoff, K. E., Hohnson, J. R., Klingelhöfer, J., Knoll, A. H., Mclennan, S. M., Mcsween JR, H. Y., Morris, R. V., Rice JR, J. W., Rieder, R., and Soderblom, L. A.: In situ evidence for an ancientaqueous environment at MeridianiPlanum, Mars, *Science*, 306(5702), 1709-1714, 2004.

Tackley, P.: Self-consistent generation of tectonic plates in three-dimensional mantle convection, Earth Planet, *Sci. Lett.*, 157, 9-22, 1998.

Tanaka, S., Ohtake, M., and Sato, H.: Evidence for tidal triggering of earthquakes as revealed from statistical analysis of global data, *J. Geophys. Res.*, 107, NO. B10, 2211, doi:10.1029/2001JB001577, 2002.

Tanimoto, T., Lay, T.: Mantle dynamics and seismic tomography, *Proceedings of the National Academy of Sciences*, 97 (23), 12409-12410, 2000.

Tozer, D.: Heat transfer and planetary evolution, *Geophysical Surveys*, 7, 213-246, 1985.

Trompert, R., Hansen, U.: Mantle convection simulations with reheologies that generate plate-like behaviour, *Nature*, 395, 686-689, 1998.

Tsuruoka, H., Ohtake, M., and Sato, H.: Statistical test of the tidal triggering of earthquakes: contribution of the ocean tide loading effect, *Geophys. J. Int.*, 122, 183-194, 1995.

Turcotte, D. L., and Oxburgh, E.: Mantle convection and the new global tectonics, *Annual Review of Fluid Mechanics*, 4, 33-66, 1972.

Turcotte, D. L., & Schubert, G.: Geodynamics, Cambridge University Press, Cambridge, 2002.

Turcotte, D. L., Schubert, G.: Geodynamics (Third Edition), Cambridge University Press, Cambridge, 2014.

Tutu, A. O., Steinberger, B., Sobolev, S. V., Rogozhina, I., Popov, A. A.: Effect of upper mantle heterogeneities on lithospheric stress field and dynamic topography, *Solid Earth*, 9, 649-668, doi:10.5194/se-9-649-2018, 2018.

Ulbrich, U., Ahorner, L., and Ebel, A.: Statistical investigations on diurnal and annual periodicity and on tidal triggering of local earthquakes in central Europe, *J. Geophys.*, 61, 150-157, 1987.

Ulmer, P., &Trommsdorff, V.: Serpentine stability to mantle depths and subduction related magmatism, *Science*, 268, 858-861, 1995.

https://doi.org/10.5194/egusphere-2023-1458
Preprint. Discussion started: 3 August 2023

Valley, J. W., Peck, W. H., King, E. M., and Wilde, S. A.: A cool early earth. *Geology*, 30(4): 351-354, 2002.

Van Hunen, J., van den Berg, A. P., & Vlaar, N. J.: The impact of the South American plate motion and the Nazca Ridge subduction on the flat subduction below South Peru, *Geophys. Res. Lett*., 29, 14, 2002.

Vidale, J. E., Agnew, D. C., Johnston, M. J. S., and Oppenheimer, D. H.: Absence of earthquake correlation with Earth tides: An indication of high preseismic fault stress rate, *J. Geophys. Res.*, 103, 24,567-24,572, 1998.

Vigny, C., Ricard, Y., Froidevaux, C.: The Driving Mechanism of Plate Tectonics, *Tectonophysics*, 187, 345-360, 1991.

Vine, F. J., & Matthews, D. H.: Magnetic Anomalies Over Oceanic Ridges, *Nature*, 199, 947-949, 1963.

Walker, J., Hays, J., and Kasting, J.: A negative feedback mechanism for the long-term stabilization of Earth's surface temperature, *J. Geophys. Res*., 86, 9776-9782, 1981.

Wan, T. F.: Tectonic stress field and its application to the intraplate in Eastern China (in Chinese), Beijing, Geological Publishing Company, 1-103, 1993.

Wan, T. F.: On the dynamic mechanics of global lithosphere plate tectonics (In Chinese), *Earth Science Frontiers*, 25, DOI:10.13745/j.esf.sf.2018.1.1, 2018.

Wegener, A.: The Origin of Continents and Oceans, New York, NY, Courier Dover Publications, 1915.

Wegener, A.: The origin of continents and oceans (Entstehung der Kontinente und Ozeane), Methuen & Co, 1924.

Weinstein, S.: The effect of convection planform on the toroidal-poloidal energy ratio, Earth Planet, *Sci. Lett*., 155, 87-95, 1998.

White, R., McKenzie, D.: Magmatism at rift zones: The generation of volcanic continental margins and flood basalts, *J. Geophys. Res*., 94, 7685-7729, 1989.

Wilson, J. T.: A possible origin of the Hawaiian Island, *Canada Journal of Physics*, 41, 863-868, 1963.

Wortel, R., and Cloetingh, S.: On the origin of the Cocos-Nazca spreading center, *Geology*, 9, 425-430, 1981.

Young, D., and Zurn, W.: Tidal triggering of earthquakes in the Swabian Jura?, *J. Geophys.*, 45, 171-182, 1979.

Zaccagnino, D., Vespe, F., Doglioni, C.: Tidal modulation of plate motions, *Earth-Science Reviews*, 205, https://doi.org/10.1016/j.earscirev. 2020.103179, 2020.

Zhong, S.: Role of ocean-continent contrast and continental keels on plate motion, net rotation of lithosphere, and the geoid, J. Geophys. Res., 106, 703-712, 2001.

Zhu, R., Zhao, G., Xiao, W., Chen, L., & Tang, Y.: Origin, accretion, and reworking of continents, Reviews of Geophysics, 59, e2019RG000689. https://doi.org/10.1029/2019RG000689, 2021.

Zoback, M. L., and Burke, K. : Lithospheric stress patterns: A global view, Eos Trans. AGU, 74, 609-618, 1993.

Zoback, M. L., Zoback, M. D., Adams, J., Assumpção, M., Bell, S., Bergman, E. A., Blümling, P., Brereton, N. R., Denham, D., Ding, J., Fuchs, K., Gay, N., Gregersen, S., Gupta, H. K., Gvishiani, A., Jacob, K., Klein, R., Knoll, P., Magee, M., Mercier, J. L., Müller, B. C., Paquin, C., Rajendran, K., Stephansson, O., Suarez, G., Suter, M., Duias, A., Xu, Z. H., Zhi, Z. M.: Global patterns of tectonic stress, *Nature*, 341, 91-298, 1989.

https://doi.org/10.5194/egusphere-2023-1458
Preprint. Discussion started: 3 August 2023

Zoback, M. L., Magee, M.: Stress magnitudes in the crust: constraints from stress orientation and relative magnitude data, *Philosophical Transactions of the Royal Society, London*, A337(1645), 181-194, 1991.

Zoback, M. L.: First- and Second-Order Patterns of Stress in the Lithosphere: The World Stress Map Project, *J. Geophys. Res*., 97(B8), 11703-11728, 1992.

Zoback, M. D., and Zoback, M. L.: Tectonic stress field of North America and relative plate motions, In Neotectonics of North America, Decade Map vol. I, edited by D. B. Slemmons et al., 339-366, Geol. Soc. of Am., Boulder, Colo, 1991.